ENERGY, ENVIRONMENT & STORAGE

AN INTERNATIONAL JOURNAL

Volume-3
Issue-3
September, 2023
ISSN: 2791-6197

Editor in Chief
Dr. Selahaddin Orhan AKANSU

ENERGY, ENVIRONMENT AND STORAGE

EES JOURNAL

Founded and Published by Erciyes Energy Association

Energy, Environment and Storage Journal is indexed in Crossref

Copyright © 2023

Printed in Turkey

ISSN-2791-6197

EES- EDITORIAL BOARD

BOARD MEMBER

VOLUME 3, ISSUE 3, REVIEWER BOARD

EDITORIAL OFFICE

AIM AND SCOPE

Energy, Environment and Storage papers consider the prospects of energy technologies, environment, materials, process control and industrial systems. The Energy, Environment and Storage will be published 3 times per year.

Contributions describe novel and significant applications to the fields of:

- Hydrogen Fuels
- Hydrogen and Fuel Cell
- Hydrogen Economic
- Biomass
- Solar PV Technology
- Solar Thermal Applications
- Wind Energy
- Materials for Energy
- Drones and Energy Applications
- Nuclear Energy and Applications
- Hydro Power
- Fuel Technologies (CNG, LNG, LPG, Diesel, Gasoline, Ethanol, etc.)
- Numerical Modelling
- Energy Storage and Systems
- Battery Technologies
- Energy Management
- Heat and Mass Transfer
- Aerodynamics
- Aerospace and Energy Applications
- Combustion
- Electric Vehicle Transportation
- Off-grid Energy Systems
- Environment Management
- Air Pollution
- Water and Wastewater Pollution
- Water and Wastewater Management
- Waste Management
- Global Warming and Climate Change
- Environmental Ecosystem
- Environmental System Modelling and Optimization
- Ecological Applications or Conservation

VOLUME 3, ISSUE 3

SEPTEMBER 2023

CONTENTS

Energy, Environment and Storage

Journal Homepage: www.enenstrg.com

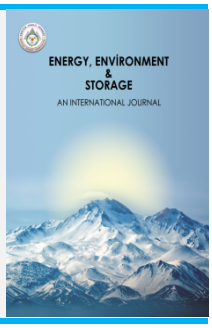

Investigation of Solid Waste Management (SWM) in Coastal Settlement: Makassar City, Indonesia

Nani Anggraini[1*], Ramdiana Muis [1], Reza Darma Al Fariz[1], Sattar Yunus[2], Indriyani Rachman [1,3], Toru Matsumoto[1,4]

[1]*Graduate Programs in Environmental Systems, Graduate School of Environmental Engineering, The University of Kitakyushu, Kitakyushu, 808-0135, Japan*

[2]*Department of Environmental Engineering, Faculty of Engineering, Universitas Muslim Indonesia, Makassar, 90231, Indonesia*

[3]*Department of Natural Science Education, School of Postgraduate Studies, Universitas Pakuan Bogor, 16143, Indonesia*

[4]*Research Center for Urban Energy Management, Institute of Environmental Science and Technology, The University of Kitakyushu, Kitakyushu, 808-0135, Japan*

ABSTRACT. Solid waste management is among the most popular urban environmental problems in many developing countries due to increasing urban, economic, and industrial activities. Indonesia is a developing country with many coastal settlements, such as Makassar City. This study aims to determine Waste Management on the coast of Makassar City, namely the "Kawasan Pelabuhan", a slum settlement. An investigation was carried out regarding waste generation, storage, and collection. The population of this study was 119 houses/households consisting of permanent and semi-permanent houses partially built over the sea on the coast. The method used in this research is quantitative and qualitative. The analysis results show that the volume of waste generated is around 58% organic and 42% inorganic, with an average of 1.8 kg per household for organic waste and 1.31 kg for inorganic waste. Most houses use individual bins; only houses on the main road get communal collection and storage services.

Keywords: Solid Waste, Waste Management, Waste Generated, Coastal Settlement

Article History: Received:01.08.2023; Accepted: 22.08.2023; Available online:30.09.2023
Doi : https://doi.org/1052924/XFBP5264

1. INTRODUCTION

Solid Waste Management (SWM) is a scientific discipline related to the control of generation, storage, collection, transfer, transportation of waste, and waste treatment [1]. Currently, SWM is one of the most popular urban environmental problems in many developing countries due to the increasing urban, economic, and industrial activities [2] [3]. Poor municipal waste management practices can result in soil, water, and air pollution [4].

The problem of waste management is also a problem that Indonesia faces as a developing country. Countries with long coastlines are highly prioritized regarding coastal waste and public participation issues [5]. Indonesia is the largest archipelagic country; most of its main cities are in coastal areas, and one is Makassar City. Makassar City is the gateway to Eastern Indonesia, a dynamic metropolis [6] with a population of 1.5 million [7] and the densest population concentration in coastal areas, including along rivers and canals. The coast of Makassar City has experienced drastic urbanization, so it has transformed become a metropolis in the last 15 years [8].

The ever-increasing population will go hand in hand with production waste generation, so this condition must be balanced with waste management. Without adequate waste management, an estimated 80% of the land will end up in the sea [9], [10]. Based on observations from slum area data in Makassar City (Mayor Decree No. 1301/050.13/2021), coastal areas are mostly dominated by slum areas with mild, moderate, and severe levels [6]. Waste management facilities are only 8% of slum settlements [6]. The "Kawasan Pelabuhan" slum area is one of the slum areas on the north coast of Makassar City, which is the research location.

*Corresponding author: nanianggraini.jp@gmail.com

This study aims to determine the Solid Waste Management activities that occur in the slum area "Kawasan Pelabuhan", including characteristics of generation, storage, and collection. This research will provide insight into SWM that applies in coastal areas of developing countries and will become the basis for stakeholders in managing SWM.

2. MATERIALS AND METHODS

2.1 Location of Study

The study is in "Kawasan Pelabuhan", located in the north part of Makassar. **Fig. 1** shows a map of Indonesia, and the arrow points to the study area's location (5.110958 E,119.4248602 S).

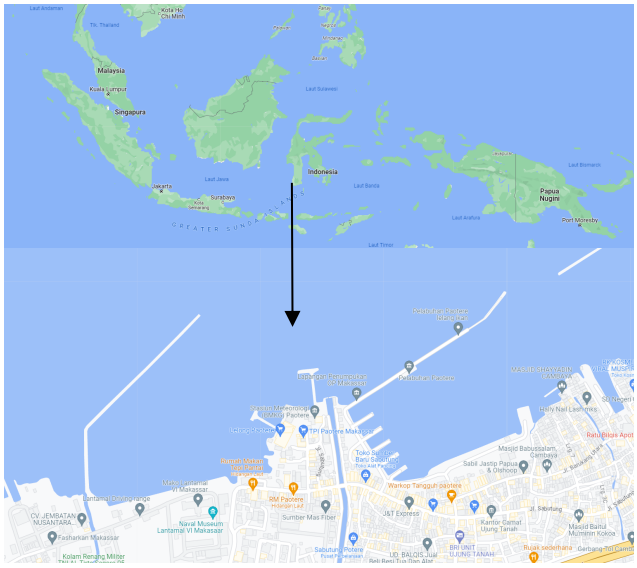

Fig. 1. Location of study

Fig. 2. The condition of the Kawasan Pelabuhan coastal area

The slum settlement in the New Port area is in Cambayya Village in **Fig 2**, with a population of 6,428 people, a total of 1,267 families, and a population density of 12,128 people/km2.

2.2 Characteristics of Settlement

The city keeps experiencing rapid economic development, population, urbanisation, and expansion of residential areas. Those who choose to live in slum areas are mostly urbanites who want to be close to workplaces in the city but cannot buy decent land [7].

The high price of land in the city centre makes some of them occupy vacant public lands such as road shoulders, riparian areas, riverbanks, and canal banks. This settlement is generally semi-permanent housing, which continues to grow with the inadequate physical condition of the building and the environment; this is known as the slum area [3]. This phenomenon occurs in Makassar City, Indonesia.

The Mayor's Decree on Slums of 2021 has designated 20 urban areas as slums with a total area of 428 hectares, most of which are in riparian and coasts. The coastal settlement in Makassar City was originally formed from a fisherman settlement [6]. The history of Makassar City was developed from the coastal area by fishermen who utilised marine resources as the source of life [6]. However, a vast city development transforms this settlement into a slum with limited facilities for life. One of their big problems is waste management. "Kawasan Pelabuhan" is one of the coastal settlements in North Makassar, also located at the edge of the big canal. Most of the people built their wooden houses over the sea. This settlement included part of its low-income class area. The areas with poor social services and amenities are shown in Fig 3.

Fig. 3 Settlement conditions

Buildings Characteristics in the "Kawasan Pelabuhan" settlement are divided into two types, including permanent and semi-permanent buildings shown in **Fig 3**. Most of the semi-permanent (red colour) buildings were built over the sea. The building was built over the land boundary. Moreover, the street in this settlement is a narrow alley about 50 cm in width or less, making it difficult to do several activities, including waste management.

2.3 Material

The tools and materials used in the waste generation survey process as shown in **Fig 4** are:

a. The digital scales used are hand digital scales with accurate, fast, and efficient measurement results to carry anywhere. Each surveyor is equipped with a digital scale.
b. The volume measuring tool is a box that has a volume value description.

c. Plastic bags are given to residents as containers to facilitate the process of weighing waste.
d. Masks and gloves are additional tools used by surveyors in carrying out the weighing process because of the unpleasant odour and the condition of the organic waste, which is sometimes watery.
e. The camera is used for documentation and recording all ongoing activities.
f. As a tool for recording survey results, smartphones use Google Forms to make data collection more efficient.

Fig. 4. Materials and tools

2.4 Method

This research uses SNI 19-3964-1994 as a standard issued by the Indonesian government to take and measure sample generation and composition of urban waste. This method aims to get the amount of waste generation used in waste planning and management.
Sampling locations for waste generation are divided into 2 main groups, namely:
1) Housing consisting of:
(1) permanent high income;
(2) moderate-income semi-permanent;
(3) non-permanent low income
2) non-housing consisting of:
(1) shops;
(2) office;
(3) school;
(4) market;
(5) roads;
(6) hotels;
(7) restaurants, eating houses;
(8) other public facilities.

In this study, we limit ourselves by taking a special sample of residential areas. Permanent housing represents high-income settlements, semi-permanent settlements represent moderate income, and non-permanent settlements represent low incomes.

The condition of a permanent house is made of concrete or bricks that stand firmly, and a semi-permanent building is an independent building, such as a hut or cottage, built with locally available materials. For example, such as wooden planks, sun-dried bricks, straw or other vegetable materials for the purpose of private residence. Non-permanent buildings are temporary buildings, materials that last only a short time or can mean buildings that can be moved, and their useful life is not more than 10 years.

In this research area, there are no non-permanent buildings, and there are only two types of buildings: permanent and semi-permanent as shown in **Fig.6.**
Total population (housing units) = 119 housing units consisting of 57 units of permanent houses; and 62 units of semi-permanent houses.
(S1) = proportion of the number of permanent housing/ high-income households = 48%
(S2) = proportion of the number of semi-permanent housing/ moderate-income households = 52%

This research was conducted through several activities:
2.4.1 The questionnaire survey
This activity was carried out to discover people's lifestyle in "Kawasan Pelabuhan". Questionnaires were distributed to 119 respondents living in two types of houses (permanent and semi-permanent). The questionnaire asks about the resident's environmental characteristics in waste management (storage, sorting, collecting, transportation) and their current behaviour.

Fig. 5. Waste generation survey process

2.4.2 Field observation of waste generation
Each household is given labelled waste plastic. Each household that became the research sample was asked to fill a garbage bag and sort organic and inorganic waste. This process lasts for 8 consecutive days. Every day a surveyor will come to weigh the waste in each sack, measure the volume, and keep records shown in **Fig.5**. In addition to measuring waste generation, at the same time a questionnaire survey was conducted regarding the characteristics of the local community from the aspects of education, economy, employment, and family structure. The housewife or the head of the household was selected as the person who was the respondent to the questionnaire. The questionnaire was made as an open question on Google form, and the surveyor read the question and filled in the answer column according to the answer given by the respondent.

2.4.3 Direct interview
In-depth interviews with key informants were required in this study. Key informants are considered capable of providing information about the object of research. In-depth interviews are open-ended questions and answers to obtain data about participants' intentions – how to describe their world and explain or express their feelings about important life events [11].

This interview was conducted to explore the waste generated every day by households. A total of 5 homemakers who are female leaders in the community were selected to be interview subjects as respondents. In

addition, interviews were also conducted with village heads as respondents who were considered to know the activities of their residents.

Examples of questions given in general regarding how the local community behaves in disposing of garbage, what is the system for collecting and transporting waste (waste collection equipment, collection frequency, collection organisers, transportation routes), and container systems.

In-depth interviews are very important because local people with secondary and lower education levels need more knowledge about waste management. It is common for some residents to be less open in providing information because they fear various things, so this approach is considered better for gathering information.

2.4.4 Mapping

A mapping process is carried out to report collection services and routes.

2.5 Sample

The population in the solid waste survey is housing units living in the coastal settlement area of "Kawasan Pelabuhan". The research population was determined, considering the location in the coastal area and the mouth of the canal so that it has more urgency than the other locations.

The research location is the "Kawasan Pelabuhan", one of the coastal slum settlements in Makassar City with an area of around 1.97 Ha in 2021. Then 119 houses were selected as the study population located at the mouth of the canal with the characteristics of permanent and semi-permanent buildings.

Determination of waste generation samples follows the provisions of the Indonesian National Standard (INS) 19-3964-1994 (Measurement Method of Collection and Composition of Municipal Solid Waste Samples).

The sample size is determined using the formula from SNI 19-3964-1994 as in Equations (1) and (2):

$$S=Cd\sqrt{PS} \quad (1)$$

Cd is the domestic coefficient (0.5 for average/small city), and Ps is the total population. The sample size (S) is divided by the number of household members (n) to count the number of household samples.

$$K=\frac{S}{n} \quad (2)$$

Furthermore, the house chosen as the sample was taken randomly according to the agreement that the family was willing to participate in the waste collection process. This survey has challenges due to the habits of some residents who sometimes immediately throw the trash into the sea. Besides, residents are not accustomed to sorting trash and need help understanding the differences between organic and inorganic waste.

2.6 Analysis

Waste generation data from recording primary data in the field are inputted and analysed statistically. Likewise, the data from the questionnaire results were then analysed using statistical primary data tabulations. A descriptive analysis was performed for in-depth interviews to check the answers and incorporate them into the report. Finally, an overlay map is used to determine the service area for waste collection and waste storage.

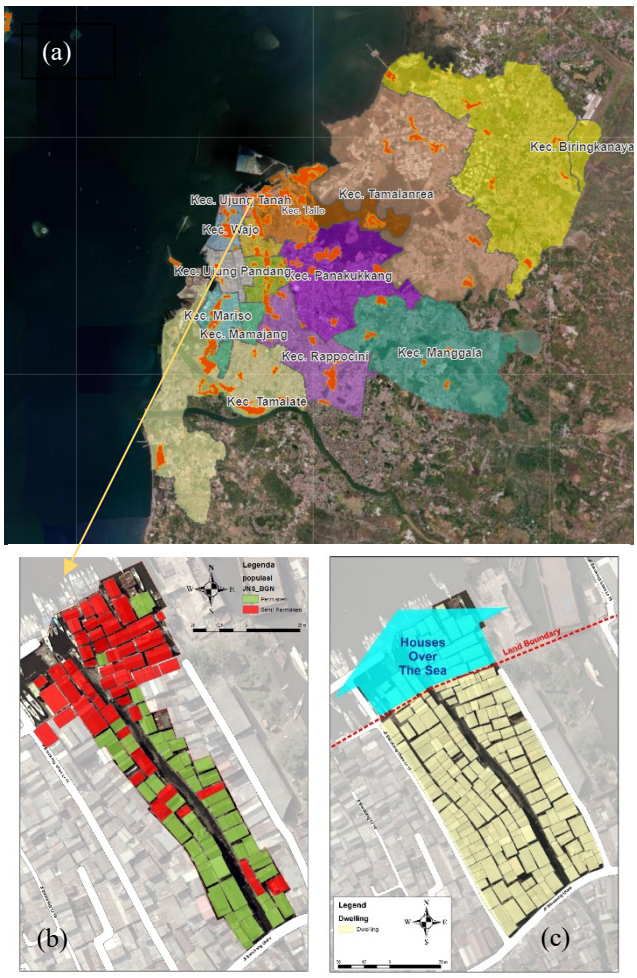

Fig. 6 (a) Distribution of slum settlements in Makassar City (b) Location of survey (c) Orientation of the building towards the sea

3. RESULT AND DISCUSSION

3.1 Characteristics of Respondents

Of the total respondents were 119 households, 35% were male, and the remaining 65% were female. Most of the respondents were female, as solid waste management encourages the participation of females. The average age of the respondents is above 40 years. Five people and 4 people dominate each house, but up to 12 occupied houses.

Based on the level of education, most of the respondents (34%) did not receive a formal education, this was quite related to their livelihood, which was dominated by the informal sector, and 66% of the respondents had several levels of formal education such as only graduating from elementary school (19.1%), (17.2%) graduating from high school, (11.3%) diploma, and (18.3%) undergraduate.

Regarding the job category, (71%) are self-employed, and (29%) of respondents are government employees. The livelihoods of the head of the family are daily labourers

(41%) and fishermen (35%). This condition is supported by the coastal area near the sea and the port area, allowing them to work in the informal sector as casual daily labourers at the port. The average earner (50%) has 66 USD/month earnings, up to 132 USD/month, and only a small percentage earn above 199 USD/month.

3.2 Waste Generation Result

Fig 7. describes the result of the waste generation survey of waste weight from 34 research samples of 34 houses. From this survey, the average waste generation was 1.8 kg of Organic Waste per day per house and inorganic waste 1.31 per day per house.

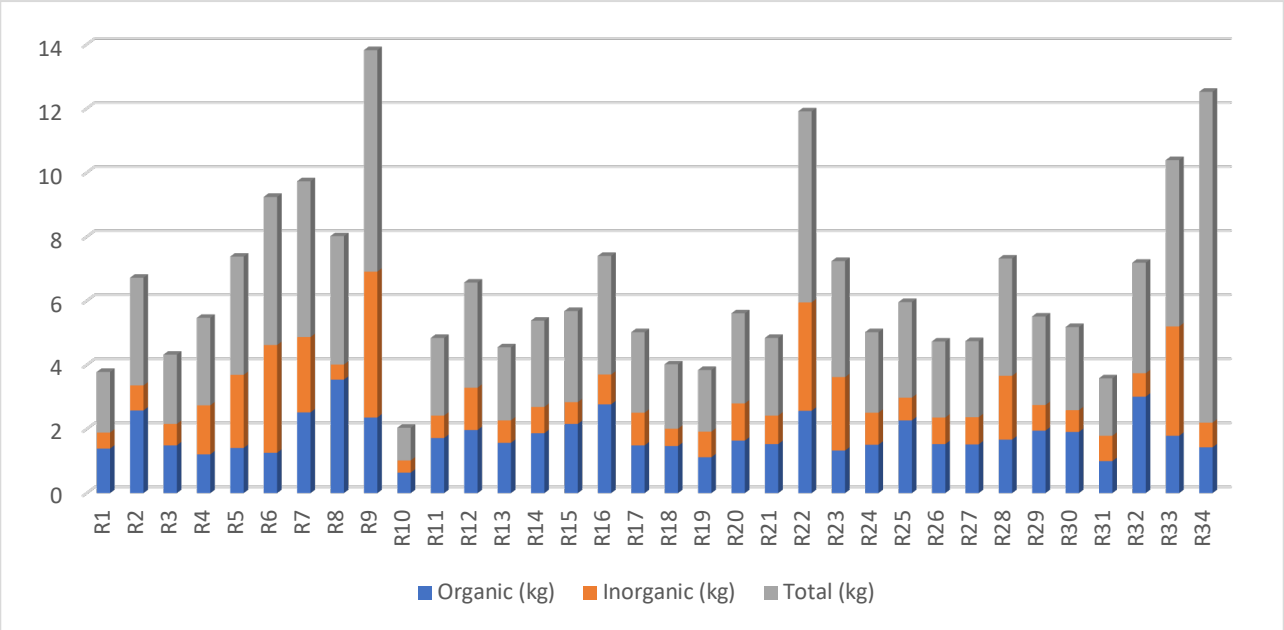

Fig. 7 Waste generation based on the waste weight in kg (R1-R34 as sample code).

Table 1 Survey results of the average volume of organic and inorganic waste generation

Sample Code	Average volume of organic waste generation/house (liter/house)			Sample Code	Average volume of organic waste generation/house (liter/house)		
	Organic	Inorganic	Total		Organic	Inorganic	Total
R1	3.83	5.00	9	R18	4.00	5.33	9
R2	4.50	7.00	12	R19	1.33	7.83	9
R3	2.83	7.17	10	R20	3.67	8.83	13
R4	2.17	9.83	12	R21	4.17	9.00	13
R5	2.67	17.33	20	R22	7.83	16.00	24
R6	2.00	20.83	23	R23	3.33	13.33	17
R7	8.33	14.83	23	R24	3.67	8.50	12
R8	9.67	2.83	13	R25	7.83	7.50	15
R9	5.67	12.17	18	R26	4.50	8.33	13
R10	2.83	4.17	7	R27	4.67	8.67	13
R11	3.17	3.17	6	R28	5.50	14.67	20
R12	5.83	2.00	8	R29	6.50	8.00	15
R13	3.83	4.17	8	R30	6.17	7.00	13
R14	5.17	4.83	10	R31	2.17	8.00	10
R15	6.33	5.50	12	R32	9.33	7.00	16
R16	9.00	5.50	15	R33	5.17	22.00	27
R17	3.83	8.17	12	R34	3.67	7.33	11

The volume of waste generated in the "Kawasan Pelabuhan" coastal area was dominated by 58% organic waste and 42% inorganic waste as shown in **Fig. 8**. This waste was potentially thrown into the water bodies without proper waste management. Compared to other big cities in Indonesia, biodegradable organics were 68% in Jakarta and 72.41% in Surabaya [12]. The values for the cities of Jakarta and Surabaya differ higher because the data from the two cities is a total of one city and does not specifically describe coastal areas. There is also another cause where the people who live in the "Kawasan

Pelabuhan" are middle to lower-class people who are economically difficult, so they have a limited variety of food and do not have food waste behavior. Refers to other developing countries in Asia, shown the same existing conditions, the solid waste generation was high because of the population, and the main component of SW is decomposable [12], Whereas, in Asian developed countries, such as Japan, Singapore, Taiwan, and South Korea, these values were generally less than 45% [13].

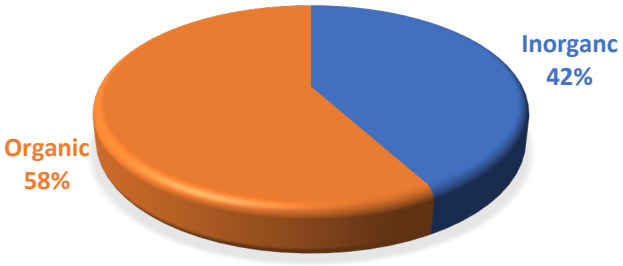

Fig. 8. Average percentage of weight of organic and inorganic (waste/house/kg)

Solid waste generation depends on lifestyle, habits, food, living standards, season, and commercial activities degree [14]. The highest fraction of organic waste is in the low-class area [15]. However, managing waste is a complex activity that requires appropriate technical solutions, cooperation between all stakeholders, and sufficient organization capacity [16]. Furthermore, the urban waste composition is changing recently with the increasing single use of packing materials and plastics [3], [17].

3.3 Storage System

The existing container system was used as an individual and communal system. Each family collected waste from individual containers and brought it to a communal container located on the main road in a residential area. Some families potentially directly throw their waste into the water bodies, especially those who live over the sea or in front of the canal.

The survey results show that 80% of the community did not yet separate their waste because of a lack of materials, knowledge, and motivation. Citizens need to be educated to keep bins for waste storage at the source and stop littering on the water bodies and streets.

Waste disposal has become a serious problem worldwide, especially in developing countries [18]. Problems such as ecological imbalances and certain diseases have taken over the world, causing damage to the natural environment and its resources [19]. Many biological species are on the verge of extinction due to a worsening ecological imbalance. This condition is due to the widespread use of non-biodegradable waste, such as plastic and the hazardous chemicals used to synthesise it. It can also cause soil, water, and air pollution, harming human health [20] [21]. This condition certainly requires serious and continuous efforts to overcome it. On the other hand, organic waste can also pollute water bodies by increasing BOD and COD [22].

3.4 Collection System

Transportation is important to SWM because waste not collected and transported will cause environmental problems [1]. The collection in the location of the study is carried out frequently, almost every day, and a cleaning fee is charged to the people.

Fig. 9. Visualization of collection service and route.

However, not all households receive good collection services. The type of collection vehicle is a three-wheeled motor. Visualization of the collection service and route is shown in **Fig. 9.**

The challenge in the waste collection process in this area is the narrow roads that are difficult for waste transport vehicles to pass. In some slum areas, families still lack access to waste collection sites [6]. Cleaning costs are also considered to be a burden for the middle to lower-economic communities who live there.

Based on **Fig. 9**, a collection route by vehicle was shown in the dotted red line so that most of the settlements do not get a collection service (shown in the light-yellow area).

Community participation has a direct bearing on the efficiency of SWM. Without a basic facility for storing and collecting waste from sources, communities are prone to dumping waste on the streets, open spaces, drains, and water bodies in the vicinity creating unsanitary situations [17] [3].

4. CONCLUSION

In general, waste management in the "Kawasan Pelabuhan" Coastal Settlement has not gone well due to the characteristics of the settlements, the characteristics of

the residents, and the lack of MSW facilities. The waste generated in the "Kawasan Pelabuhan" is dominated by 58% organic and 42% inorganic waste, and most residents do not have access to waste collection points. Hence, domestic waste has the potential to enter water bodies. Serious attention is needed in implementing SWM in coastal areas by adding facilities that are by the characteristics of the local area and community development activities to improve the local community's lifestyle. Additional research is needed to calculate the type of waste and the potential amount of waste that enters the water bodies.

Acknowledgments

We thank the Matsumoto Laboratory, Graduate Programs in Environmental Systems, Graduate School of Environmental Engineering, and The University of Kitakyushu, Japan, for support so that this research can be carried out. We also remember to thank all those who have supported the implementation of this research.

REFERENCES

[1] F. Kreith and G. Tchobanoglous, Eds., *Handbook of solid waste management*, 2nd ed. in McGraw-Hill handbooks. New York: McGraw-Hill, 2002.

[2] J. B. Nyakaana, "Solid Waste Management in Urban Centers: The Case of Kampala City—Uganda," *East Afr. Geogr. Rev.*, vol. 19, no. 1, pp. 33–43, Mar. 1997, doi: 10.1080/00707961.1997.9756235.

[3] N. Anggraini, R. Muis, F. Ariani, S. Yunus, and . S., "Model of Solid Waste Management (SWM) in Coastal Slum Settlement: Evidence for Makassar City," *Nat. Environ. Pollut. Technol.*, vol. 20, no. 2, Jun. 2021, doi: 10.46488/NEPT.2021.v20i02.002.

[4] S. Raharjo, V. S. Bachtiar, Y. Ruslinda, T. Matsumoto, and I. Rachman, "Improvement of recycling-based municipal solid waste management in Padang City, West Sumatera, Indonesia," *IOP Conf. Ser. Earth Environ. Sci.*, vol. 245, p. 012007, Mar. 2019, doi: 10.1088/1755-1315/245/1/012007.

[5] H. Herdiansyah, H. G. Saiya, K. I. I. Afkarina, and T. L. Indra, "Coastal Community Perspective, Waste Density, and Spatial Area toward Sustainable Waste Management (Case Study: Ambon Bay, Indonesia)," *Sustainability*, vol. 13, no. 19, p. 10947, Oct. 2021, doi: 10.3390/su131910947.

[6] Asian Development Bank, "Slum Assement for Makassar City," Dec. 2021.

[7] T. Arifin *et al.*, "Forecasting land-use changes due to coastal city development on the peri-urban area in Makassar City, Indonesia," *Egypt. J. Remote Sens. Space Sci.*, vol. 26, no. 1, pp. 197–206, Feb. 2023, doi: 10.1016/j.ejrs.2023.02.002.

[8] C. Niles, "Makassar Livable City Plan: Situation Assessment Report".

[9] P. R. Pawar, S. S. Shirgaonkar, and R. B. Patil, "Plastic marine debris: Sources, distribution and impacts on coastal and ocean biodiversity," 2016.

[10] D. Wulandari *et al.*, "Solid waste management in a coastal area (Study Case: Sukolilo Sub-district, Surabaya)," *IOP Conf. Ser. Earth Environ. Sci.*, vol. 799, no. 1, p. 012030, Jun. 2021, doi: 10.1088/1755-1315/799/1/012030.

[11] J. H. McMillan and S. Schumacher, *Research in education: a conceptual introduction*, 5th ed. New York: Longman, 2001.

[12] Y. Dhokhikah and Y. Trihadiningrum, "Solid Waste Management in Asian Developing Countries: Challenges and Opportunities," 2012.

[13] A. V. Shekdar, "Sustainable solid waste management: An integrated approach for Asian countries," *Waste Manag.*, vol. 29, no. 4, pp. 1438–1448, Apr. 2009, doi: 10.1016/j.wasman.2008.08.025.

[14] W. A. S. Moftah, D. Marković, O. A. S. Moftah, and L. Nesseef, "Characterization of Household Solid Waste and Management in Tripoli City—Libya," *Open J. Ecol.*, vol. 06, no. 07, pp. 435–442, 2016, doi: 10.4236/oje.2016.67041.

[15] K. Miezah, K. Obiri-Danso, Z. Kádár, B. Fei-Baffoe, and M. Y. Mensah, "Municipal solid waste characterization and quantification as a measure towards effective waste management in Ghana," *Waste Manag.*, vol. 46, pp. 15–27, Dec. 2015, doi: 10.1016/j.wasman.2015.09.009.

[16] A. Perteghella, G. Gilioli, T. Tudor, and M. Vaccari, "Utilizing an integrated assessment scheme for sustainable waste management in low and middle-income countries: Case studies from Bosnia-Herzegovina and Mozambique," *Waste Manag.*, vol. 113, pp. 176–185, Jul. 2020, doi: 10.1016/j.wasman.2020.05.051.

[17] P. U. Asnani, "India Infrastructure Report 2006: Urban Infrastructure," New Deihi, India, 2006.

[18] N. Ferronato and V. Torretta, "Waste Mismanagement in Developing Countries: A Review of Global Issues," *Int. J. Environ. Res. Public. Health*, vol. 16, no. 6, p. 1060, Mar. 2019, doi: 10.3390/ijerph16061060.

[19] A. J. McMichael, S. Friel, A. Nyong, and C. Corvalan, "Global environmental change and health: impacts, inequalities, and the health sector," *BMJ*, vol. 336, no. 7637, pp. 191–194, Jan. 2008, doi: 10.1136/bmj.39392.473727.AD.

[20] M. Rashid, S. Yunus, R. Mat, S. Baharun, and P. Lestari, "PM 10 black carbon and ionic species concentration of urban atmosphere in Makassar of South Sulawesi Province, Indonesia," *Atmospheric Pollut. Res.*, vol. 5, no. 4, pp. 610–615, Oct. 2014, doi: 10.5094/APR.2014.070.

[21] S. Yunus, M. Rashid, R. Mat, S. Baharun, and C. M. Hasfalina, "Characteristic of The Pm10 in Urban Environment of Makassar," *J. Urban Environ. Eng.*, pp. 198–207, Oct. 2019, doi: 10.4090/juee.2019.v13n1.198-207.

[22] Y. Wen, G. Schoups, and N. Van De Giesen, "Organic pollution of rivers: Combined threats of urbanization, livestock farming and global climate change," *Sci. Rep.*, vol. 7, no. 1, p. 43289, Feb. 2017, doi: 10.1038/srep43289.

Energy, Environment and Storage

Journal Homepage: www.enenstrg.com

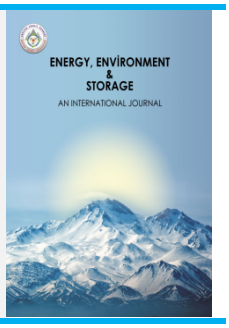

Numerical Analysis of The Multilayer Structures Melting with Different Hole Network with Phase Change Material

Elanur Baki Sezgin[1], Mustafa Yasin Gökaslan [2*], İrfan Uçkan [3]

[1]*Department of Mechanical Engineering, Institute of Natural and Applied Sciences,Yüzüncü Yıl University,Van,Turkey 0000-0001-7982-371X*

[2]*Department of Mechanical Engineering, Faculty of Engineering, Yüzüncü Yıl University, Van, Turkey 0000-0003-3859-8485*

[3]*Department of Mechanical Engineering, Faculty of Engineering, Yüzüncü Yıl University, Van, Turkey 0000-0003-3679-5661*

ABSTRACT. Phase change materials (PCM) are used with different geometries increase thermal performance. The thermal performance of the geometries on phase change materials have been investigated. For thermal energy storage systems (TES), porous structures are widely used to increase the thermal performance of the PCM. In addition, geometric parameters affect heat transfer, flow and melting solidification. In this work, the thermal performance of multilayer structure with different surface geometries and the control of the melt fraction of the PCM was investigated in terms of energy efficiency. The results were obtained by modeling the studies in the Computational Fluid Dynamics (CFD) program. The physical model was obtained by creating a multi-layer porous structure with different surface geometries in each layer, thanks to the additive system. Modeling was carried out for natural convection depending on time. Paraffin was used as the PCM. The melting temperature of the paraffin used is 41 °C and the latent heat of fusion is 165 kJ/kg. In the present work, the distribution of melting isotherms gives more homogeneous results for the selected geometry. The results of PCM multilayer structure and other geometries were compared under the same conditions and it was seen that the multilayer structure improved the thermal performance. All melting graphs range from 0-1 (0: solid, 1: liquid). The results obtained for the selected geometry show that the melting value is between 0.8-0.9. In addition, the proposed physical model is a subject that can be encountered in engineering applications, thermal design engineering. In this respect, it is thought that the results obtained from the study, especially in the field of energy storage, will fill an important gap.

Keywords: Energy storage, Phase change material, Numerical analysis, Multi-layer structure.

Article History: Received 18.07.2023; Accepted: 29.08.2023; Available online:30.09.2023
Doi : https://doi.org/1052924/ZBHA5406

1. INTRODUCTION

Energy storage has gained a lot of importance in the world in recent years. Phase change materials (PCM), on the other hand, have an important property due to their thermal energy storage (TES) properties. Metal foams, porous medium or solid geometry, which are used in TES systems due to their important properties, are widely preferred to enhance the thermal performance of the PCM. The effects of porosity geometry, and porosity on the phase change material performance of porous domain have been investigated. Lattice structures or foams are used to create spaces in cellular structures [1]. During the recent years, porous domain ordered according to foam models due to its adjustable property, it creates a new potential heat transfer media. The additive manufacturing promotes the customization of these structures [2-3]. With this method, the production of parts in large geometric structures has become easier [4]. The use of heatsinks in electronic cooling systems has been studied in the studies of Qureshi et al. [5]. They found that the structure of triply periodic minimal surfaces (TPMS) fitted by additive manufacturing can reduce the temperature under high-temperature conditions for different pore geometries, heat fluxes, and PCMs. Fan et al. [6] aimed to enhance the efficiency of the battery by using paraffin wax combined with a battery thermal energy system (BTES) with TPMS of different geometric structures. With the system they used, they increased the efficiency of the battery by reducing the temperature increase. Three new porous TPMS heat sinks with computational fluid mechanics (CFD) have been modeled by Baobaid et al. [7]. TPMS-based heatsinks outperform conventional heatsinks in packing density and random distribution of flow. They found that porous

*Corresponding author: my.gokaslan@yyu.edu.tr

heatsinks are more promising. Catchpole-Smith et al. [8] and Qureshi et al. [9] obtained the same results in their numerical studies in TPMS, which they modeled, and in their experimental studies in PCM and embedded TPMS cages, respectively, and determine that the thermal conductivity of TPMS cages depends not only porosity but also on the structure of the TPMS cages. For increasing thermal performance, Hu et al. [10] designed a porous material as a heatsink, thermal conductivity enhancer and produced it with 3D printing. They shortened the operating time of the PCM by applying power to the systems they created with different porosity ratios with various heaters Hu et al. [10]. The development of 3D printing has led to its development, allowing porous media to be produced accurately and quickly [11,12]. Hasan and Tbena [13], studied a micro-channel heat sink (MCHS) with a PCM inside. They concluded that the cooling performance of PCMs was improved by using air first and then four different PCMs for cooling. Arshad et al. [14] carried out studies by examining the fins on electronic devices for the safer operation of electronic devices at low temperatures and prolonging their operating times. In other studies, Arshad et al. [15] stated that the use of PCM in cooling of electronic devices would be more efficient since phase change takes a long time. Gu et al. [16] studied the use of lattice structures showing that 2D lattice sandwich panels with continuous cross-section could be optimized for combined thermo-mechanical performance. The thermal performance and fabricated topology of PCM-optimized heat sinks were studied by Iradukunda et al [17]. As a result of their studies, they expressed that the heat sink they designed importantly increased PCM performance over a plate fin heat sink they selected as reference. The effect of porosity on periodic minimal surfaces (TPMS) with 3D printable geometrically complex structures was investigated by CFD modeling in the study of Hassan Ali et al. [18] convection coefficient, temperature and pressure drop values were estimated by CFD method using natural and forced convection effects in TPMS. Gopalan and Eswaran [19] used both PCM and porous structure to further increase conductivity in heat exchangers. In their results, they determined that the performance of the heat exchanger completely depends on the conductivity, and they found that the use of PCM together with the porous structure improves the conductivity.

The aim of the study is to increase energy savings and control the melting time thanks to a new multilayer hole network structures design using CFD. Then novelty of this study is that it is important in terms of its effects on the melt fraction and time of multilayer hole network structures with different surface geometries including PCM. Also, to show that this system can achieve some advantages without requiring additional energy.

2. PHYSICAL MODEL

The PCM was investigated by integrating it into the multi-layer structure as in Fig.1. Each layer is shown separately in Fig. 2. The geometric structure consists of three separate parts. There are cells of different diameter and number in each unit. The heat transfer performance of these cells of different diameters and their control over the PCM melt fraction are observed in terms of energy efficiency. Each layer has a 9 mm height and the height of the heater is 1 mm. The diameters of the holes and void volume in the structures are given in Table 1.

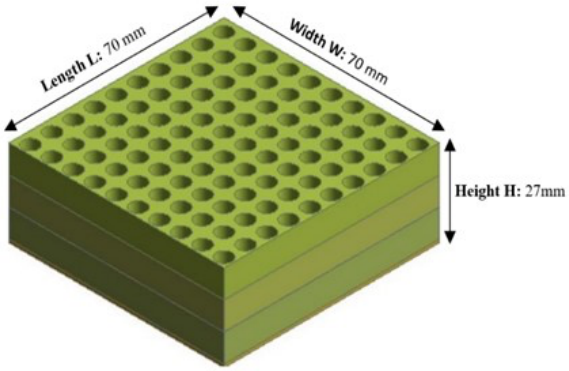

Figure 1. Multi-layer structure.

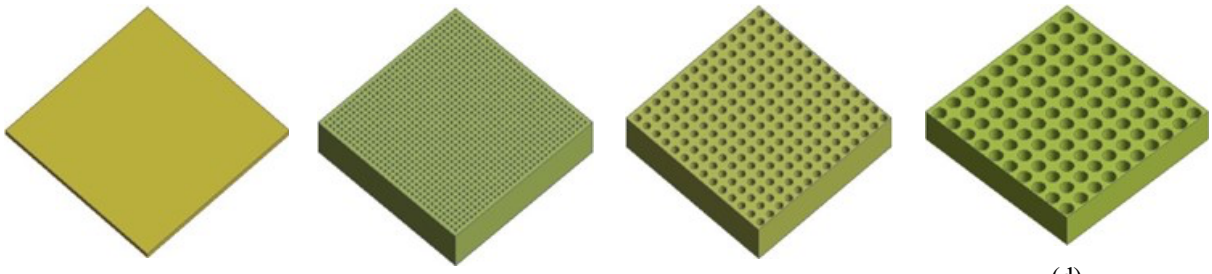

Figure 2. Parts of the physical model. (a) Heater, (b) Model 1, (c) Model 2, (d) Model 3.

Model 1 with a diameter of 5 mm, there are 10 cylindrical spaces on the horizontal axis, while there is solid geometry with a total length of 20 mm. In addition, there is solid geometry with a total length of 28 mm in Model 2 and 36 mm in Model 3. As the hole diameter increases, the void volume also increases. The void volume of the multilayer structures is 38311.7 mm^3.

Table 1 Cell diameters of physical model parts

Physical model	Cell diameter (mm)	Void volume (mm^3)
Model 1	5	17671.5
Model 2	3	12469.0
Model 3	1	8171.3

The initial and boundary conditions of this numerical study are below,

- The upper surface is fixed constant temperature which is 344 K,
- The side surfaces are fixed constant at isothermal boundary conditions,
- Constant heat flux is applied to base of the system which its value is 100 kW/m^2.
- The initial temperature is accepted 300 K.

Nazir et al. [20] studied the use of PCM, especially paraffin wax, in TES due to its advantages such as non-toxicity, latent heat of fusion and the fact that this heat does not deteriorate over time. The use of paraffin with metal foams to increase thermal performance which is melting time and melt fraction. The use of low-conductivity PCM in combination with a high-conductivity metal foam was explored by Rehman et al. [21]. The properties of PCM and metal used in the system were obtained by ref. [22], [23-25] and are summarized in Table 2. In this study, Organic paraffin was chosen as PCM. While selecting this organic paraffin, this choice was decided depending on the temperature required by the system. This selected PCM is defined as a new fluid in ANSYS.

Table 2 Thermophysical properties of the PCM and the material used in the study.

Material	Paraffin	AlSi10Mg
k (W/m^2)	0.2	175
ρ (kg/m^3)	880	2670
$\mathbf{c_p}$ (J/kgK)	2000	900
μ (kg/ms)	0.00365	-
β (1/K)	0.001	-
L (J/kg)	165000	-
$\mathbf{T_m}$ (K)	314	

3. GOVERNING EQUATIONS

The Boussinesq approach is used to model the melting of the PCM [26-27]. In addition, the continuity, momentum and conservation of energy equations for PCM are expressed as [28-29]:

Continuity equations

$$\nabla . u = 0 \tag{1}$$

Momentum equations

$$\rho_{PCM}\frac{\partial u}{\partial t} + \rho_{PCM}(u.\nabla)\mathrm{u} = -\nabla \mathrm{P} + \mu_{PCM}\nabla^2 u + \rho_{PCM} g\beta(T_{PCM} - T_m) - Au \tag{2}$$

where u, $\boldsymbol{\mu_{PCM}}$, $\boldsymbol{\rho_{PCM}}$ and $\mathrm{T_{PCM}}$ are the velocity, dynamic viscosity, density and temperature of the PCM. $\mathrm{T_m}$ is the PCM melting temperature, β is the volume expansion coefficient, g is the gravity acceleration, respectively. A is the source term by Eq. (3)

$$A = \frac{C_{mush}(1 - f_{PCM})^2}{\delta + f^3{}_{PCM}} \tag{3}$$

where f_{PCM} represent indicates the liquid fraction of PCM and it ranges from 0 to 1. 0 is the solid phase and 1 is the liquid phase, $\mathrm{C_{mush}}$ is the mushy zone parameter. It is defined as 10^5 based on ANSYS Fluent User's Guide [30].

Energy equations

$$\rho_{PCM} c_{p,PCM}\frac{\partial T_{PCM}}{\partial t} + \rho_{PCM} c_{p,PCM} u.\nabla T_{PCM} = \nabla.(k_{PCM}\nabla T_{PCM}) - \rho_{PCM} L\frac{\partial f_{PCM}}{\partial t} \tag{4}$$

where L, $\boldsymbol{k_{PCM}}$, $\boldsymbol{c_{p,PCM}}$ are the denotes the latent heat, thermal conductivity, specific heat capacity of the PCM, respectively. The $\boldsymbol{f_{PCM}}$ term is expressed in Eq. (5), depending on the temperature of the PCM:

$$f_{PCM} = \begin{cases} 0 & T_{PCM} \le T_{solid} \\ \dfrac{T_{PCM} - T_{solid}}{T_{liquid} - T_{solid}} & T_{solid} \le T_{PCM} \le T_{liquid} \\ 1 & T_{PCM} \ge T_{liquid} \end{cases} \tag{5}$$

where $\boldsymbol{T_{PCM}}$, T_{solid} and T_{liquid} are the PCM, the solid and liquid temperatures of the PCM, respectively. Heat transfer in metals (for aluminium) in Eq. (6):

$$\rho_s c_{p,s}\frac{\partial T_s}{\partial t} = \nabla.(k_s \nabla T_s) \tag{6}$$

where $\mathrm{T_s}$, $\mathrm{k_s}$, $\mathrm{c_{p,s}}$, and ρ_s, are thermophysical properties of solid which is aluminium. These terms represent temperature, thermal conductivity, specific heat capacity, and density, respectively.

Finally, the structure-PCM interface relation are given in Eq. (7) and Eq. (8)

$$T_f = T_s \tag{7}$$

$$k_f \frac{\partial T_f}{\partial n} = k_s \frac{\partial T_s}{\partial n} \tag{8}$$

4. NUMERICAL ANALYSIS

Commercial software ANSYS -Fluent was used to solve the governing equations. The finite volume method was used for the model's governing equations. In addition, for the thermophysical properties of paraffin and the solid are included in the model by writing a User Defined Function (UDF). The UDF used was obtained to be valid for the SI unit system. The SIMPLE algorithm was used for the solution of the equations. The residuals were set to 10^{-6}. The solutions were built using a 6-core processing unit. In addition, time step sensitivity analysis was taken into account in the analyses and was defined as 0.05 s for this analysis. Some assumptions made for PCM phase change to occur are given below:

• By ignoring the volume expansion of the PCM, the "Boussinesq" approach, which is embedded in the package program, is used in the density change of the fluid to perform the melting analysis.

• Flow; incompressible, laminar and Newtonian.

• The thermophysical properties of the metal and PCM are considered constant.

• The region where the PCM is neither liquid nor solid is considered mushy.

• Radiation and magnetic field are neglected.

Grid distribution

In this work, since the geometries obtained to determine the melting analyses in porous structures are not complex, network structures can be easily obtained. In Table 3, the properties of the meshes obtained for the layers of the physical model are given as nodes elements and average orthogonal quality values.

Table 3. Mesh parameters.

Physical model layers	Nodes	Elements	Average orthogonal quality
Model 1	988944	862564	0.94
Model 2	286566	237430	0.92
Model 3	150118	113554	0.96
Multi-layer structure	506557	414862	0.92

High orthogonal quality meshes were created. The average orthogonal quality values obtained by the appropriate meshing method show that those with results between 0.7-0.95 are in very good condition, and those with results between 0.95-1.00 are in excellent condition. As indicated in Table 4, the mesh structure converges after the certain value of the element size. The mesh sensitivity is applied for all cases.

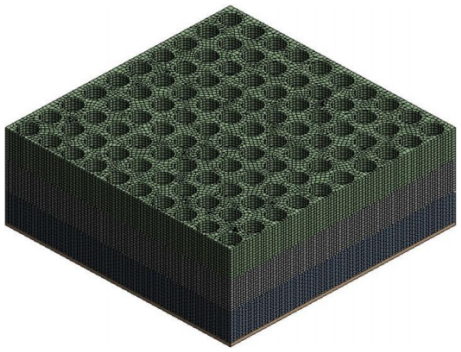

Figure 3. Mesh for the Multi-layer structure

The mesh sensitivity study was carried out to examine the variation of the converged solutions in each mesh with the solutions obtained using the mesh structures at different element size values of the same simulations. As it can be seen from the values in Table 4, the validity of the network structures formed as a result of the change in the absolute differences of the results obtained with this mesh sensitivity study at similar rates is proven. The element size value used for physical multi-layer structure is 70.

Table 4. Mesh sensitivity study for multi-layer structure.

Physical model	Element Size	Melt Fraction
Multi-layer structure	50	0.843
	55	0.847
	60	0.849
	65	0.853
	70	0.858

5. RESULT and DISCUSSION

In this section, the results obtained from the numerical simulations are explained and discussed. The results obtained separately for each layer were compared with the results of multi-layer structure obtained by combining all layers. The effects of the obtained results on the melting time are discussed. Melting curves and graphs for multi-layer structure are shown in Fig. 4-7. As seen in Fig. 4-5, the different axis states of the geometries, the transferred heat has positive effects on the melt fraction and the process by providing melting at the PCM and hole network structure interface.

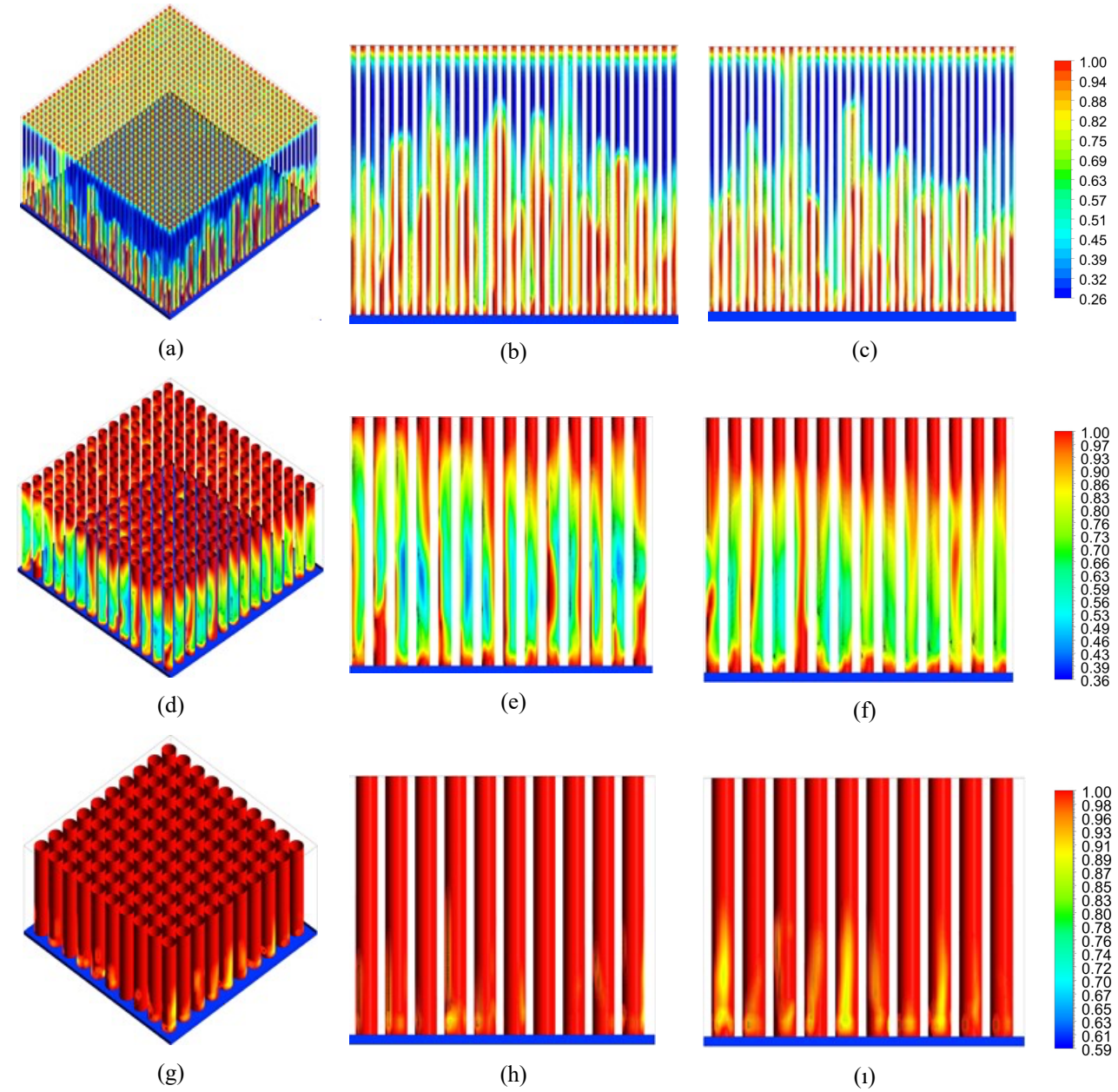

Figure 4. Liquid fraction of physical model layers at 500 s. (a) Model 1 view, (b) x-y axis view of Model 1, (c) y-z axis view of Model 1, (d) Model 2 view, (e) x-y axis view of Model 2, (f) y-z axis view of Model 2, (g) Model 3 view, (h) x-y axis view of Model 3, (ı) y-z axis view of Model 3.

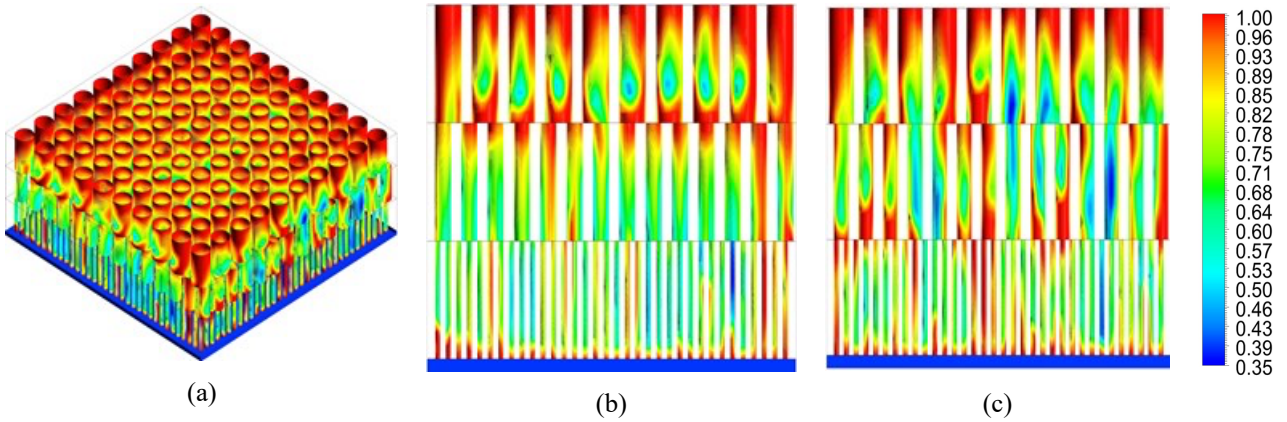

Figure 5. Liquid fraction of physical multi-layer structure at 500 s. (a) Multi-layer structure view, (b) x-y axis view, (c) y-z axis view

The presence of hole network structure for all cases improved melting. PCM properties are very important for melting time as most of the geometry volume is used by PCM. All melting graphs vary between 0-1. This means that the value of 0 is completely solid and the value of 1 is completely liquid.

The melting graphs of each layer at 500 s. are given in Fig. 4. Among the parameters affecting the melt fractions is the geometry of the structure, depending on the hole diameter. As shown in Fig. 6., when the layers of the physical model are examined separately, it is seen that the melt fraction in the Model 3 is closer to 1 than in the other physical models. This depends on the nature of the geometry in the Model 3. Under the same initial and boundary conditions, the melt fraction decreased as the hole diameter decreased. At the 300. s, the melt fraction of the geometry with the highest hole diameter is approximately 0.8, while the geometry with the lowest hole diameter is 0.6.

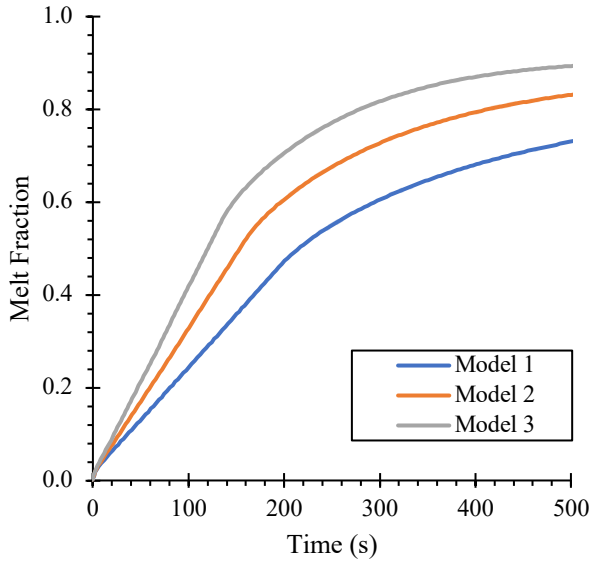

Figure 6. Melt fraction for different layers.

As can be seen in Fig. 5, the multi-layered hole network structure provided a proportionally more regular spread of the distribution of the melting contours over the geometry. It should be noted here that since each layer is placed on top of each other, the height is 27 mm and therefore the volume is equal to the sum of these three geometry volumes. The void volume is the geometry with the highest value.

Figure 7 shows relation the melt fraction of the multilayer structure between time. Also, the melt fractions of each layer are also given for comparison. The melt fraction of the multilayer structure shows closer to the Model 2 and between the melting fractions of the Model 3 and Model 2 structure. However, the void volume of the Model 2 is 12469 mm^3, while the void volume of the multi-layer structure is 38311.7 mm^3. It is determined that the phase change material with approximately three times higher volume provides better thermal performance under the same initial and boundary conditions. As indicated in the graph in Fig. 7., At 500 s., the melt fractions are between 0.8-0.9 for multi-layer structure, between 0.9-1.0 for the Model 3, between 0.8-0.9 for the Model 2, and between 0.8-0.9 for the Model 1.

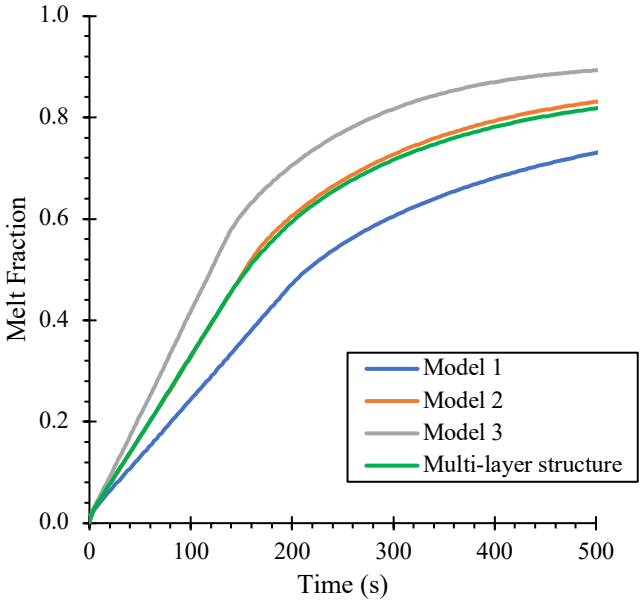

Figure 7. Comparison of melt fraction.

It is expected that the multi-layered structure may have a positive effect on the melting performance. However, although the analyzes are performed under the same conditions, the void volumes of each layer and multi-layer structures are not the same. The multi-layer structures exhibited better thermal performance despite having five times the void volume than the Model 1. When multi-layer structure and the Model 3 structure are compared, it is seen that the thermal performance of the Model 3 structure is better. However, the structure on the Model 3 has almost half the void volume compared to the other. This is the most important factor affecting the melt fraction and time.

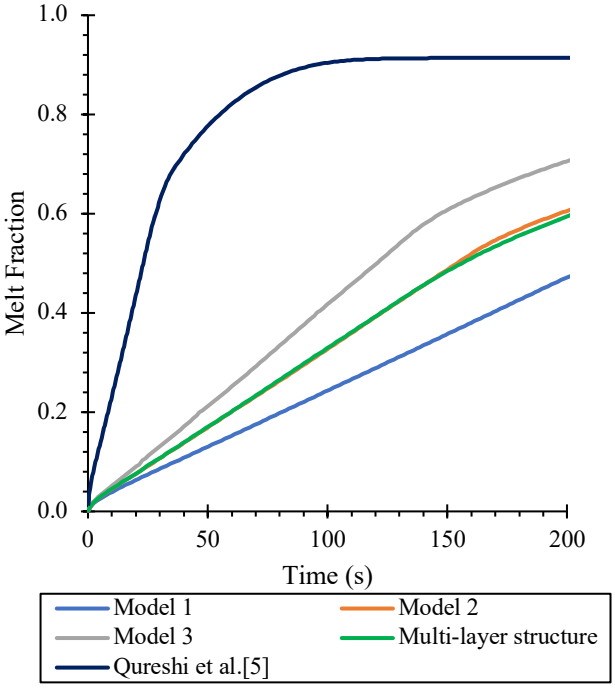

Figure 8. Validation of the study with literature.

Qureshi et al. [5, 28] carried out melting analysis using dimensions and materials with similar properties in their numerical studies. The validity of this study, Qureshi et al. [5] was chosen for comparison. The melting data obtained as indicated as seen in in Fig. 8. Using the same heat flux in their work, Qureshi et al. [5] determined that the melt fraction was approximately 0.9 in the Kelvin model at 200 s. Aluminum was used as solid material and docosane which is an organic PCM was used as phase change material in their study. In this study, the melting rate in the 200 s. multi-layer model is approximately 0.6. Compared to this study, the Authors's [5] work had a melting rate of 0.9 in 100 s., while the melt fraction in the multi-layer is about 0.35 at this time. This difference in comparison also depends on the mass of the phase change material in the models. In this numerical study, the melting time is longer and the melt fraction curve is linear. This may provide an advantage according to the usage area of these models.

6. CONCLUSION

The effects of PCM melt fraction and melting time on the hole network structures design obtained by combining multilayer hole network structures with different diameters were investigated. Thus, 3D analyses were conducted for each layer separately and for the geometry obtained by combining all layers. Initial and boundary conditions are equal for all cases. The results show that the melting time of the multilayer structure showed approximately close results with other layered structures. However, the melting formed in the multi-layered structure reveals a more regular distribution compared to other structures, in this case, it states that the study can provide an advantage for melting. The melting time and rate of the multi-layer structure are very similar to the Model 2 structure, but the distribution of the melting contours is more even and regular in all regions.

In the analyses performed for the PCM selected in the study and the initial temperature, the melt fractions vary between 0.8-0.9 values. This situation shows that %80 melting occurred in the analysed geometries. Studies can be improved to increase the melt fraction. In future studies, the melting temperature of the selected PCM can be selected differently or the initial temperature can be changed in order to obtain analyses where the melt fraction is 1 and 100% melting is achieved. There are two recommendations for the geometries in this study, either the PCM used should be replaced with a PCM with a lower melting temperature or the initial temperature should be increased without changing the PCM. Thus, the melt fraction will be improved for the work done.

The void volumes of the analysed geometries are different from each other as shown in Table1. The melting performance is better in the multi-layer structure with the void volume higher in the Model 1 and Model 2. However, the melt fraction of the multilayer structure is worse than the Model 3. The reason for this is that the void volume of the multi-layer structure is higher, and therefore the phase change material is more. In order to see the thermal performance difference between these two geometries more clearly, the analyses should be repeated when the void volumes are the same.

As a future study, heat flux power, solid material, PCM material, geometry dimensions and layer locations can be modified to better understand the thermal performance and effects of parameters which is effects of design variables. In addition, in order to better comparison of results, the geometric heights of each model can be adjusted so that the void volume is the same and they can be compared.

REFERENCES

[1] Mazur, M., Leary, M., McMillan, M., Sun, S., Shidid, D., Brandt, M. 2016. Mechanical properties of Ti6Al4 and AlSi12Mg lattice structures manufactured by Selective Laser Melting (SLM), *Elsevier Science & Technology*, 1 (5):119-161.

[2] Yang, L., Harrysson, O., Cormier, D., West, H., Gong, H., Stucker, B. 2015. Additive manufacturing of metal cellular structures: Design and Fabrication, *The Minerals, Metals & Materials Society*, 3 (67):608-615.

[3] Thompson, M., K., Moroni, G., Vaneker, T., Fadel, G., Ian Campbell, R., Ian, G., Bernard, A., Scuhulz, J., Graf, P., Ahuja, B., Martina, F. 2016. Design for additive manufacturing: Trends, opportunities, considerations and constraints*, CIRP Annals*, 2 (65):737-760.

[4] Al-Ketan, O., Rowshan, R., Al-Rub, R., K., A. 2018. Topology-mechanical property relationship of 3D printed strut, skeletal and sheet based periodic metallic cellular materials, *Additive Manufacturing*, 19:167-183.

[5] Qureshi, Z., A., Elnajjar, E., Al-Ketan, O., Al-Rub, R., A., Al-Omari, S., B. 2021. Heat transfer performance of a finned metal foam-phase change material (FMF-PCM) system incorporating triply periodic minimal surfaces (TPMS), *International Journal of Heat and Mass Transfer*, 170:121-001.

[6] Fan, Z., Fu, Y., Gao, R., Liu, S. 2023. Investigation on heat transfer enhancement of phase change material for battery thermal energy storage system based on composite triply periodic minimal surface, *Journal of Energy Storage*, 57 (14):106-222.

[7] Baobaid, N., Ali, M., I., Khan, K., A., Al-Rub, R., K., A.. 2022. Fluid flow and heat transfer of porous TPMS architected heat sinks in free convection environment, *Case Studied in Thermal Engineering*, 33:101-944.

[8] Catchpole-Smith, S., Sélo, R., R., J., Davis, A., W., Ashcroft, I., A., Tuck, C., J., Clare, A. 2019. Thermal conductivity of TPMS lattice structures manufactured via laser powder bed fusion, *Additive Manufacturing*, 30:100-846.

[9] Qureshi, Z., A., Al Omari, S., A., B., Elnajjar, E., Mahmoud, F., Al-Ketan, O., Al-Rub, R., A. 2021. Thermal characterization of 3D-Printed lattices based on triply periodic minimal surfaces embedded with organic phase change material, *Case Studies in Thermal Engineering*, 27 (3):101-315.

[10] Hu, X., Gong, X. 2021. Experimental study on the thermal response of PCM- based heat sink using structured porous material fabricated by 3D printing*, Case Studies in Thermal Engineering*, 24:100-844.

[11] Ngo, T., D., Kashani, A., Imbalzono, G., Nguyen, K., T., Q., Huis, D. 2018. Additive manufacturing (3D printing): A review of materials, methods, applications and challenges, *Composites Part B Engineering*, 143:172-196.

[12] Maiti, A., Small, W., Lewicki, J., P., Weisgraber, T., H., Duoss, E., B., Chinn, S., C., Pearson, M., A., Spadaccini, C., M., Maxwell, R., S., Wilson, T., S. 2016. 3D printed cellular solid outperforms traditional stochastic foam in long-term mechanical response, *Scientific Reports*, 25 (6):24871.

[13] Hasan, M., I., Tbena, H., L. 2018. Using of phase change materials to enhance the thermal performance of micro channel heat sink, *Engineering Science and Technology an International Journal*, 3 (21):517-526.

[14] Arshad, A., Ali, H., M., Ali, M., Manzoor, S. 2017. Thermal performance of phase change material (PCM) based pin-finned heat sinks for electronics devices: Effect of pin thickness and PCM volume fraction, *Applied Thermal Engineering*, 112:143-155.

[15] Arshad, A., Ali, H., M., Khushnood, S., Jabbal, M. 2018. Experimental investigation of PCM based round pin-fin heat sinks for thermal management of electronics: Effect of pin-fin diameter*, International Journal of Heat and Mass Transfer*, 117:861-872.

[16] Gu, S., Lu, T., J., Evans, A., G. 2001. On the design of two-dimensional cellular metals for combined heat dissipation and structural load capacity, *International Journal of Heat and Mass Transfer*, 11 (44):2163-2175.

[17] Irandukunda, A., C., Vargas, A., Huiting, D., Lohan, D. 2020. Transient thermal performance using phase change material integrated topology optimized heat sink, *Applied Thermal Engineering*, 2 (179):115-723.

[18] Ali, M., I., H., Al-Keetan, O., Khalil, M., Baobaid, N. 2020. 3D printed architected heat sinks cooling performance in free and forced convection environments, Proceedings of the ASME 2020 Heat Transfer Summer Conference, HT2020-9067.

[19] Gopalan, K., S., Eswaran, V. 2016. Numerical investigation of the thermal performance of PCM based heat sink using structured porous media as thermal conductivity enhancers, *International Journal of Thermal Sciences*, 104:266-280.

[20] Nazir, H., Batool, M., Osorio, F., J., B., Isaza-Ruiz, M., Xu, X., Vignarooban, K., Phela, P., Inamuddin, Kannan, A., M. 2019. Recent developments in phase change materials for energy storage applications: A review, *International Journal of Heat and Mass Transfer*, 129:491-523.

[21] ur-Rehman, T., Ali, H., M., Janjua, M., M., Sajjad, U., Yan, W-M. 2019. A critical review on heat transfer augmentation of phase change materials embedded with porous materials/foams, *International Journal of Heat and Mass Transfer*, 135:649-673.

[22] RT-42, data sheet https://www.rubitherm.eu/media/products/datasheets/Techdata_-RT42_EN_09102020.PDF (Accessed on July 12, 2023)

[23] Zhang, Z., He, X. 2016. Three-dimensional numerical study on solid-liquid phase change within open-celled aluminium foam with porosity gradient, *Applied Thermal Engineering*, 113:9-10.

[24] Zhu, F., Zhang, C., Gong X. 2017. Numerical analysis on the energy storage efficiency of phase change material embedded in finned metal foam with graded porosity, *Applied Thermal Engineering*, 123:256–265.

[25] AlSi10Mg, data sheet https://software.xactmetal.com/md/datasheets/Material%20Data%20Sheet%20-%20AlSi10Mg.pdf (Accessed on July 12, 2023)

[26] Brent, A., D., Voller, V., R., Reid, K., J. 2007. Enthalpy-porosity technique for modelling convection-diffusion phase change: Application to the melting of a pure metal, *Numerical Heat Transfer*, 3 (13):297–318.

[27] Mahdi, M., Khadom, A., A., Mahood, H., B., Yaqup, M., A., R., Hussain, J., M., Salih, K., I., Kazem, H., A. 2019. Effect of fin geometry on natural convection heat transfer in electrical distribution transformer: Numerical study and experimental validation, *Thermal Science and Engineering Progress*, 4 (14):100–414.

[28] Qureshi, Z., A., Al-Omari, S., A., B., Elnajjar, E., Al-Ketan, O., Al-Rub, R., A. 2022. Architected lattices embedded with phase change materials for thermal management of high-power electronics: A numerical study, *Applied Thermal Engineering*, 22:01350–3.

[29] Moon, C., Kim, H., D., Kim, K., C. 2018. Kelvin-cell-based metal foam heat exchanger with elliptical struts for low energy consumption, *Applied Thermal Engineering*, 144:540-550.

[30] ANSYS 18 Fluent User's Guide 2018

Energy, Environment and Storage

Journal Homepage: www.enenstrg.com

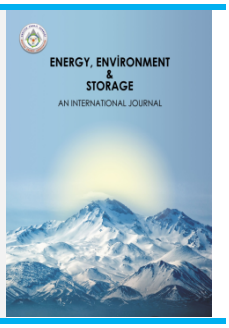

Experimental thermal performance investigation of double pipe heat exchanger using MWCNT/water nanofluid

Sajjad Porgar[1*], Orhan Keklikcioglu [2], Nese Keklikcioglu Cakmak[3]

[1]Department of Chemical Engineering, South Tehran Branch, Islamic Azad University, Tehran, Iran, 0000-0002-7910-6531

[2]Department of Mechanical Engineering, Faculty of Engineering, Erciyes University, Kayseri, 38039, Turkey, 0000-0002-6227-3130

[3]Department of Chemical Engineering, Faculty of Engineering, Sivas Cumhuriyet University, Sivas 58140, Turkey, 0000-0002-8634-9232

ABSTRACT. This paper presents an experimental study investigating the thermal performance of multiwall carbon nanotubes in a twin pipe heat exchanger using a water-based fluid. The research followed a two-step method, where a concentration of 0.01 weight percent of SDS surfactant was utilized to prepare the carbon nanotubes. The heat transfer coefficient, friction coefficient, and overall heat transfer coefficient of the nanofluid were compared to those of the base fluid. The results revealed that the addition of a small amount of multiwall carbon nanotubes significantly enhanced the thermal conductivity and heat transfer coefficient of the water-based fluid. Moreover, the heat transfer coefficient exhibited an increase with higher Reynolds numbers. When the nanofluid flowed counter currently and was in the outer tube, the highest values for the overall heat transfer coefficient and the heat transfer coefficient were determined as 2864 and 7655.7 W/m2K, respectively. The findings indicate notable improvements in the thermophysical and thermal characteristics of the nanofluid.

Keywords: CNT, Water-base fluid, Heat Transfer Coefficient, Heat exchanger, Thermal properties

Article History: Received:26.07.2023; Accepted:25.08.2023; Available online: 30.09.2023
Doi : https://doi.org/1052924/MAUS1078

1. INTRODUCTION

Nanofluids, a novel class of adaptable fluids, are produced as a result of nanoparticles dispersing in common fluids. These particles are composed of metal fragments such as copper, silver, or metal oxides like aluminium and copper oxide. The dispersion of nanoparticles in common fluids improves their capacity to conduct heat by increasing their thermal conductivity. Micrometer-sized particles were previously added to the fluids to enhance their thermal conductivity; however, these particles lacked the necessary stability in suspension and precipitated too quickly, leading to rapid obstruction of the fluid passageway. In contrast, nanosized particles pose less of a problem as they form considerably more stable suspensions and have slower settling rates. Agglomeration or aggregation is one of the factors affecting the stability of nanofluids. This phenomenon is influenced by several variables, including particle size, particle composition, base fluid properties, and nanofluid preparation.

Carbon nanotubes (CNTs) have recently received attention as nanomaterials with distinctive thermal characteristics. Table 1 lists some works that aim to improve CNT nanofluids' thermal conductivity at room temperature. As determining a nanofluid's thermal conductivity during the preclinical stage is an expensive and time-consuming process, several academics have proposed that we anticipate better conductivity in nanofluids for this purpose.

Water is commonly used in heat transfer due to its high heat capacity and availability. However, water has a low thermal conductivity, and researchers have suggested that incorporating nanoparticles into water at the nanoscale, known as water-based nanofluids, can enhance its thermal properties. Aminian [9] evaluated and tested his neural network model using a total of 1273 experimental results.

*Corresponding author: sajjad.porgar@gmail.com

Table 1- Enhancement of CNT nanofluids' thermal conductivity

Ref.	Basefluid	Nanoparticle	Max.Improvement
[1]	Water	MWCNT	38.0%
[2]	Water	CNT	27.3%
[3]	Water	Graphene/MXene	65.34%
[4]	Oil	CNT	138%
[5]	Water	Aluminium Oxide	7.8%
[6]	$CaCO_3$	Y_2O_3	29.18 %
[7]	EG+ Water	CuO Al_2O_3 TiO_2	6.34% 4.87% 3.59%
[8]	EG	SWCNT	14.8%

Table 2- Experimental equations proposed for nanofluid thermal conductivity

Correlations	*Nanofluids*	*Ref.*
$\frac{k_{eff}}{k_f} = 1 + 64.7\varphi^{0.746}(\frac{d_r}{d_p})^{0.369}(\frac{k_p}{k_f})^{0.747} * Pr^{0.9955} * Re^{1.2321}$	*Al_2O_3/Water*	*[13]*
$\frac{(k_{af}-k_{bf})}{k_{bf}} = 0.764\varphi + 0.0186T - 0.46$	*Al_2O_3/Water*	*[14]*
$\frac{(k_{af}-k_{bf})}{k_{bf}} = 3.761088\varphi + 0.017924T - 0.30734$	*CuO/Water*	
$\frac{k_{eff}}{k_f} = A + B\varphi$	*TiO_2/Water*	*[15]*
$\frac{k_{eff}}{k_f} = 0.99 + 0.25(100\varphi) - 0.001T - 0.002d_p - 0.18(100\varphi)^2 + 0.619 * 10^{-5}T^2 + 1.31 * 10^{-5}{d_p}^2 + 0.049(100\varphi)^3 - 7.66 * 10^{-7}T^3$	*Al_2O_3/Water*	*[16]*
$\frac{k_{eff}}{k_f} = 1 + 3.5\varphi + 2.5\varphi^2$	*Al_2O_3/Water*	*[17]*
$\frac{k_{eff}}{k_f} = \frac{\varphi}{0.17581 - 0.0003692(T - 273)} + 1.0026$	*CNT/Water*	*[18]*
$\frac{k_{eff}}{k_f} = \frac{(360.69 + T)}{(455.59 - 11080\varphi)}$	*CNT/Water*	*[19]*
$k_{nf} = k_{bf}(1 + 7.74\varphi)$	Al_2O_3 / SiO_2	*[20]*
$\frac{k_{nf}}{k_f} = 0.9472 - 0.052\varphi + 0.001482T + 0.00663(\varphi * T)$	TiO_2-Ag/ Water	*[21]*
$\frac{k_{nf}}{k_f} = 1 + 6.2299\,(\frac{\varphi}{100})^{0.9371} + (\frac{T}{333})^{10.2685}$	TiO_2-CuO/C/ EG	*[22]*
$\frac{K_{nf}}{K_{bf}} = \frac{\alpha(1+\beta T)}{1+\exp\left(\frac{\delta-\varphi}{\theta}\right)} + \gamma T$	MWCNT/Oil	*[23]*

The key physical characteristics of nanofluids include temperature, thermal conductivity of the base fluids, solid particles, and nanoparticle volume fraction. A total of 26 different types of nanofluids were tested, including Al2O3-water/EG, CuO-water/TO/EG/MEG/paraffin, Al-water/EG/EO/TO, TiO2-water/EG, ZnO-water/EG, SiO2-water/EG/oil, MWCNT-water/EG/oil/R113, and Ag-water. The particle diameter used ranged from 10 to 150 nm.

Lotfi et al. [10] conducted a study on the enhancement of heat transfer using multiwall carbon nanotubes in water within a shell and a metal horizontal heat exchanger. According to their findings, the addition of multilayer nanotubes improved heat transmission compared to the base fluid. Jafargholi et al. [11] examined the flow of nanofluids, including single-walled carbon nanotubes with a water-based fluid, in a double-pipe heat exchanger. The nanofluids circulated as internal cooling and hot water in the annular heat exchanger zone, with a Reynolds number of 8000. The results demonstrated a 25% increase in heat flux compared to pure water when utilizing single-walled carbon nanotubes. Hosseinian & Meghadadi [12] investigated the effects of introducing carbon nanoparticles (5-15 nm) on the heat transfer of a twin-pipe non-metallic PVDF heat exchanger. The findings showed that the heat transfer coefficient increased with increasing temperature, concentration, and flow rate. The most significant enhancement in heat transfer was observed with an increased flow rate. As the concentration and temperature increased, the heat transfer coefficient of the nanofluid improved compared to that of pure water, with the concentration having a greater influence than the temperature. The study also demonstrated that the utilization of carbon nanotubes could increase the heat transfer coefficient by up to 75%, which is a significant improvement compared to other types of nanofluids. Table 2 presents several modified equations developed by various researchers for calculating the thermal conductivity of nanofluids.

Table 3 provides an overview of research conducted on the utilization of nanoparticles in water-based fluids, including the operating conditions and the rate of improvement achieved with different nanoparticles

In an experiment, Balaga et al. investigated the thermal conductivity of f-MWCNT-Fe_2O_3 hybrid nanofluids at different individual component ratios of Fe_2O_3 and f-MWCNT as 4:1, 3:2, 1:1, 2:3, and 1:4 for total weight concentrations of 0.01%, 0.02%, and 0.03% in the range of temperatures from 30 °C to 60 °C. The experimental results showed that the thermal conductivity improved up to 2:3 and then decreased for all total concentrations when the weight ratio of MWCNTs in total weight rose due to the unfavorable effects of MWCNT aggregations. It follows the same pattern as the temperature and overall concentration rise. When comparing 60 °C to 30 °C, the greatest increase in thermal conductivity remained at 13.53% at 0.02% of total weight concentration. Eventually, a correlation based on the experimental findings was

developed to predict the thermal conductivity of f-MWCNT-Fe_2O_3/deionized water hybrid nanofluids [41].

Table 3- Thermal conductivity enhancement for water based nanofluid

Ref.	Nano particle	Size (nm)	Φ	Temp.	Enhancement (%)	Method
[23]	MWCNT	15-30	0.25-1	294–344 K	20	-
[24]	MWCNT	10-50	0.25–1	-	11.3	Two step
	SiO_2	12	-		3	
	CuO	33			5	
[25,26]	Ag	60, 63	1-4	323–363 K	125	Two step
[27]	MWCNT	-	0-1	-	19.6	Two step
[28]	MWCNT	100	0-0.6	298 K	38	Two step
[29]	MWCNT	-	0.01-3	15–75 °C	64	Two step
[30]	MWCNT -Ag	-	0-0.04	28-50 °C	37.3	Two step
[31]	Al_2O_3	-	0-0.4	20-50 °C	24	Two step
[32]	Al_2O_3	-	0.5- 6.0	15-40 °C	28	Two step
[33]	Al_2O_3	8–282	1.86-4	297-300 K	20	Two step
[34]	Al_2O_3	36,47	-	5- 40°C	31	-
[35]	Al_2O_3	43	0.33–5		10	-
[36]	ZnO	20-40	0.05-5.0	295-350 K	21	-
[37]	MgO	20,40,50, 60	0.005, 0.01, 0.015, 0.02	-	22	-
[38]	Al_2O_3-CuO	CuO: 29 Al_2O_3: 40 nm	0.5 – 2.0	23 – 25 °C	90–95	Two step Sonication time was 16 h
[39]	Al_2Cu	30,70,100	1-2	-	106	-
	Ag_2Al	-	1-2	-	150-210	-
[40]	MWCNT	-	0.01-0.1	25-60 °C	287	24 h sonication

Huang et al. created EG-water-based MCNT nanosuspensions using a two-step process. The rheological characteristics of prepared samples at various volume fractions and temperatures were examined through either experimental work or theoretical analysis. The findings demonstrated that, when the effective volume percentage of aggregations was taken into account, the experimental viscosity values might have effectively matched the modified K-D model. Additionally, this research revealed an intriguing pattern in the behavior of the viscosity vs. shear rate curve as temperature decreased. The association among MCNT aggregate conditions and temperature was

revealed, as well as the variety of shear behavior of nano-suspensions, using the particle aggregation transformation procedure [42].

Dalkilic et al.'s experimental investigation included a measurement of the thermal conductivity of CNT-SiO_2 hybrid nanofluids based on distilled water. Using a two-step process with three different CNT-SiO_2 concentrations and four different mass ranges, nanofluids were created. SiO_2 has a density of 2200 kg/m^3, a thermal conductivity of 1.4 W/mK, and an average particle size of 7 nm. CNT has a density of 2620 kg/m^3, a thermal conductivity of 25 W/mK, and an average particle size of 6–10 nm. Samples spent 3 hours in an ultrasonic homogenizer set at its highest power. In order to prevent changing the volumetric percentage of nanofluids, the temperature of the nanofluids was controlled throughout the sonication process. A thermal conductivity meter was used for all thermal conductivity measurements. Di-water was used to calibrate the thermal conductivity meter. Thermal conductivity was measured at temperatures ranging from 25 °C to 60 °C for every 5 °C. Using di-water, measurements have been validated, and the results were displayed as a thermal conductivity-temperature graph. Details of the minimum and maximum thermal conductivity improvements were published. It has been noted in the literature that thermal conductivity changes with temperature due to different volumetric fractions and that this definitely leads to an increase in thermal conductivity. Figures also showed improvements in the thermal conductivity of di-water at various temperatures and volume fractions. The literature provided almost well-known relationships along with their expected rates. Additionally, this study provided comparisons with other studies. For other researchers, a useful association was suggested [43]. Chandrasekar et al. report on experimental investigations and theoretical determinations of the efficient thermal conductivity and viscosity of Al_2O_3/H_2O nanofluid. In order to create the nanofluid, Al_2O_3 nanoparticles were first synthesized using a microwave-assisted chemical precipitation process, and then they were dispersed in distilled water using a sonicator. For the research, a room-temperature Al_2O_3/water nanofluid with a nominal diameter of 43 nm was used at various volume concentrations (0.3–3%). Measurements of the thermal conductivity and viscosity of nanofluids reveal that the viscosity increase is significantly greater than the thermal conductivity increase. With increasing nanoparticle volume concentrations, nanofluids become more viscous and thermally conductive. The well-known Maxwell and Einstein models are not used in the development of theoretical models to forecast the thermal conductivity and viscosity of nanofluids [44]. Nanofluids, which are a combination of conventional fluids with added nanoparticles of various types and volumes, represent a new class of fluids currently under investigation. The ability to manipulate or design the different thermo-physical properties of these fluids, both collectively and individually, holds significant potential for improving overall system performance. Of particular interest is the potential to enhance the thermal conductivity of these fluids by incorporating nanoparticles made of highly thermally conductive materials. Common base fluids include water, ethylene glycol, oil, and other fluids, while the nanoparticles can be composed of metals, metal oxides, carbon nanotubes, or graphene [45–54].

There is little research on the use of carbon nanotubes in different base fluids, and because carbon nanotubes have a very high thermal conductivity, they have a high potential to improve the thermal properties of water, the most common base fluid in heat transfer applications. Therefore, in the current research, the role of carbon nanotube nanoparticles in the water-base fluid has been investigated.

2. NANOFLUID SYNTHESIS TECHNIQUE

In the current work, carbon nanotubes with a carboxyl group functionalized were employed. These tubes had an inner diameter of 5–10 nm, a length of 10–30 m, and a purity of over 98% by weight. Figure 1 displays the nanoparticles' SEM pictures. The most popular technique for determining the overall morphology of multi-walled carbon nanotube samples, quantitative evaluation of sample purity, and nanotube dimensions is scanning electron microscopy (SEM). This technique can be used to determine the morphology and dimensions of MWCNT (in powder form). The shape of the exterior of multi-walled carbon nanotubes can also be determined. According to ASTM D 4541, a scanning electron microscope using a 20 kV electron beam was used to collect data on the features of the sample's surface. Using measurement software, it was established that MWCNTs had an inner diameter of around 5–10 nm, a length of 10–30 micrometers, and an average distance between layers of 0.34 nm.

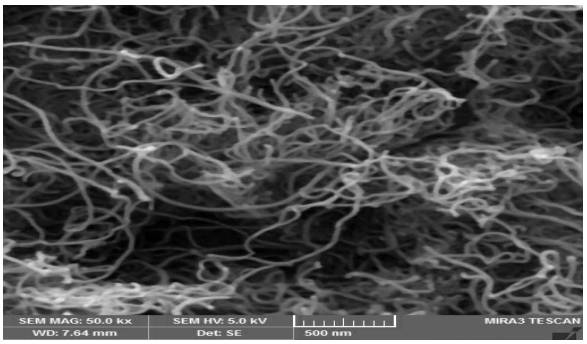

Figure 1 -SEM image of MWCNT

The nanofluid was prepared in a two-step method by adding the specified amount of carbon nanotubes to the aqueous base fluid, placing it on the magnetic stirrer for one hour, and then placing it in an ultrasonic bath for 15 minutes. The 2:1 weight ratio of sodium dodecyl sulfate surfactant was added to the base fluid, placed on a magnetic stirrer at 700 rpm, and finally placed in an ultrasonic bath for one hour, and the water-based carbon nanotube was obtained. In Figure 2, the effect of using an ultrasonic bath in the diffusion and preparation of nanofluids is visible.

Figure 2- Before using ultrasonic bath (a) & Sample after the ultrasonic bath (b)

3. RESULTS

Experiments were done on a double-pipe heat exchanger with an inner tube diameter of 19 mm and an outer tube diameter of 39 mm and a length of 4.5 meters. Thermometers were installed at the entrance of each meter of the outside pipe as well as at the inlet of each pipe to measure fluid temperature. The results were obtained for nanofluids at 0.01 % wt, and the test method was that first pure and hot water were pumped by two pumps with different flow rates, and to check all cases, once cold water was pumped into the outer tube and once into the inner tube, and both counter-current and co-current were examined. The same experiments were done for nanofluids, and the results were compared. To prevent heat loss, the heat exchanger was insulated with glass wool, and the copper heat exchanger was selected. The average temperatures of the hot fluid and the cold fluid in the input and outlet sections were used to calculate the physical parameters of the nanofluid and base fluid. Figure 3 shows the schematic of the apparatus that was used in this research.

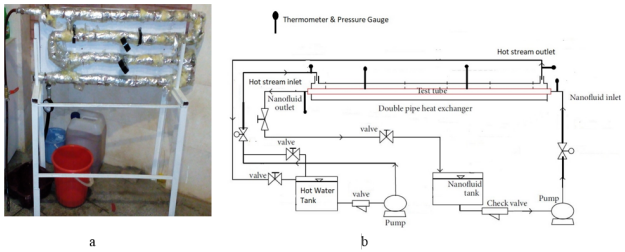

Figure 3- a) Real aparatus b) Schematic of set-up section

First, the thermophysical properties of nanofluid and base fluid, including thermal conductivity and viscosity, have been studied. The density and heat capacity of nanofluid and base fluid were almost the same, so their diagrams were not drawn. In Figure 4.a, the graph of the nanofluid thermal conductivity coefficient versus temperature shows that the samples were tested at three temperatures of 298, 308, and 318 K. It has been demonstrated that when temperatures rose, the thermal conductivity coefficient of nanofluids increased. The increase in both intermolecular collisions and the Brownian motion of the nanoparticles within the base fluid may be to blame for this. The viscosity variations in response to temperature are also depicted in Figure 4.b. These changes are almost linear, with viscosity decreasing with increasing temperature.

Experimental measurements of the viscosity, density, and other physical characteristics of nanofluids have been made and accounted for in the calculations. Plots of the hot and cold fluid pump discharges were made for two cases, four states of the Nusselt number diagram, the overall heat transfer coefficient, the heat transfer coefficient, and the friction factor in terms of Reynolds number.

Figures 5.a to 5.d show the Nusselt number in terms of the Reynolds number. These graphs are plotted for four states, including once considered hot fluid in the inner tube, once in the outer tube, and once flow was co- and counter-current. The mean Nusselt number for nanofluids as well as water increases with increasing Reynolds numbers. This behavior is seen for all nanofluid states, and the highest Nusselt number was 163 that was obtained for the case that the hot fluid was flowing into the outer tube and the flow was counter-current. It can be concluded that when the hot fluid is in the outer tube and the nanofluid is in the inner fluid and the flow is counter-current, it is best to improve the Nusselt number.

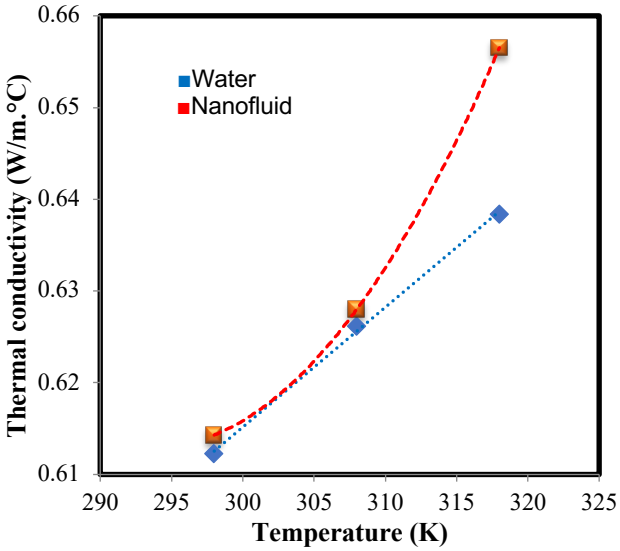

Figure 4.a.- Thermal conductivity coefficient of nanofluids versus temperature

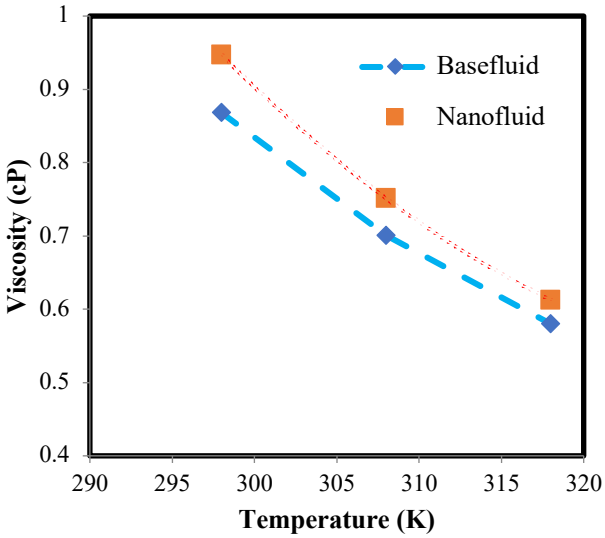

Figure 4.b.- Viscosity of nanofluids versus temperature

The Nusselt number, which measures the ratio of heat transferred through conductors to heat transferred through

displacement at the system's boundary, is a measure of heat transfer, and a rise in the Nusselt number denotes a rise in heat transmission. The heat transfer coefficients of the base fluid and the nanofluid in each of the four states are plotted in Figures 6.a to 6.d. The convective heat transfer coefficient reached its highest value of 5226 W/m2.K when the nanofluid was flowing within the inner tube and the current was going against it.

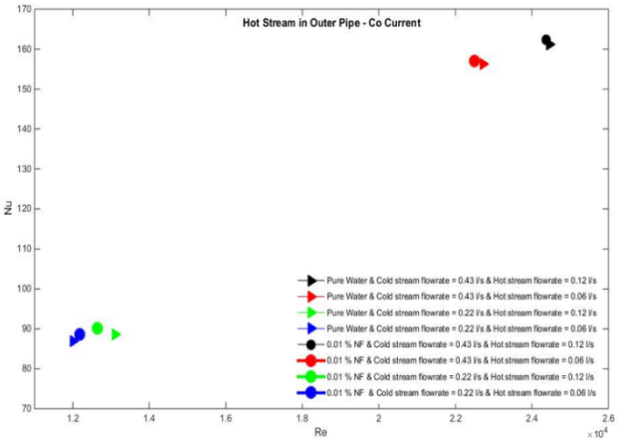

Figure 5.a- Nu vs. Re-Hot Stream in Outer Pipe - Co Current

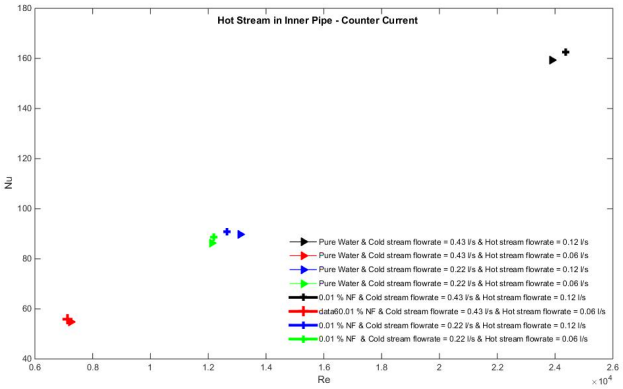

Figure 5.b- Nu vs. Re Hot Stream in Inner Pipe - Counter Current

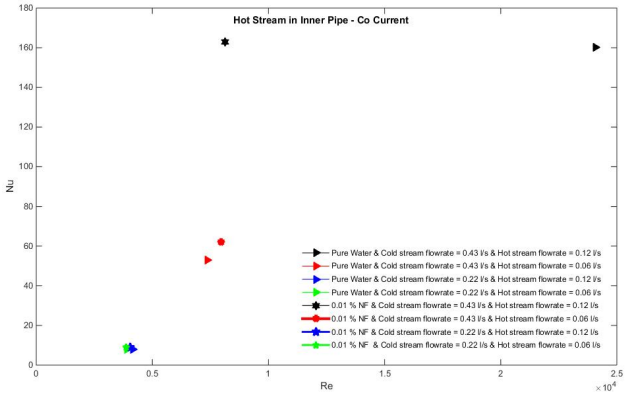

Figure 5.c- Nu vs. Re Hot Stream in Inner Pipe - Co Current

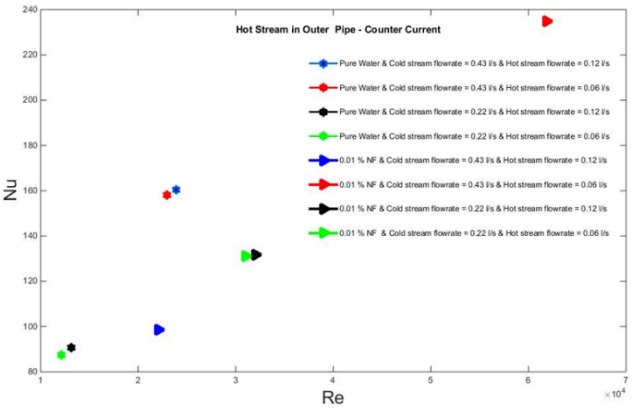

Figure 5.d- Nu vs. Re Hot Stream in Outer Pipe - Counter Current

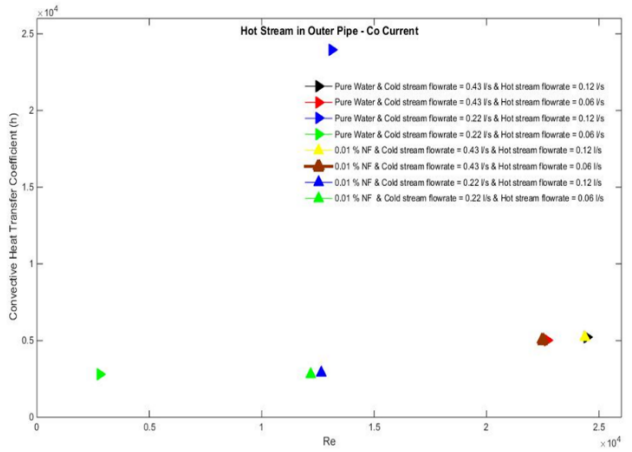

Figure 6.a) h vs. Re Hot Stream in Outer Pipe – Co-Current

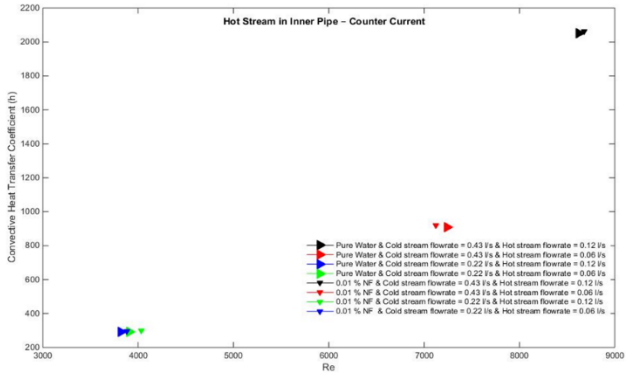

Figure 6.b) h vs. Re Hot Stream in Inner Pipe – Counter-Current

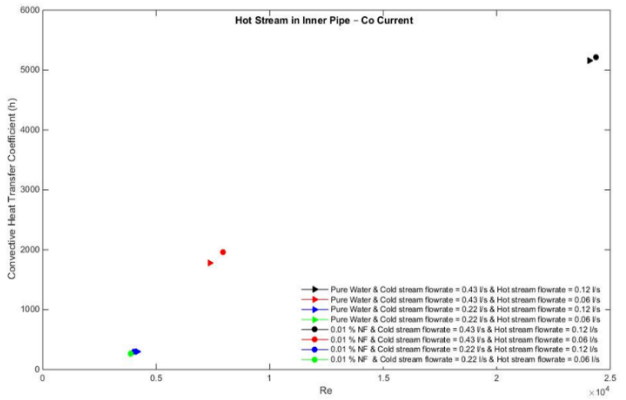

Figure 6.c) h vs. Re Hot Stream in Inner Pipe – Co Current

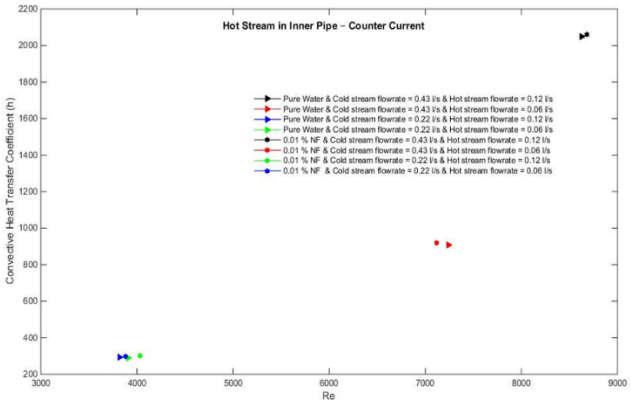

Figure 6.d) h vs. Re Hot Stream in Inner Pipe – Counter Current

The coefficient of heat transfer measured at 5226 W/m2 K, with a hot fluid flow rate of 0.32 kg/s and a cold fluid flow rate of 0.09 kg/s, was maximum whenever the nanofluid had been circulating in the outlet pipe and the movement was counter-current. The rate of heat transfer also rises with growing nanofluid flow and countercurrent, which causes a rise in the coefficient of heat transfer. The heat transfer coefficient (h), which depends on the fluid characteristics, surface roughness, and kind of flow regime, increases as the fluid velocity rises (laminar or turbulence). The Nusselt number is not an appropriate criterion for measuring the increase in heat transfer in nanofluids, so it is recommended to use the convective heat transfer coefficient.

The convective heat transfer coefficient rises as the fluid masses' convective rate rises. On the other hand, the heat transmission will work better if the nanoparticles are evenly dispersed throughout the base fluid, which is consistent with the convective heat transfer coefficient. Fewer nanoparticles are anticipated to boost their transmission efficiency because the number of nanoparticles rises with increased pressure impact as a result of rising transmission costs.

4. CONCLUSION:

In the present study, a nanofluid containing 0.01 wt% carbon nanotubes in a water-based fluid was used, and the method of dispersion of nanoparticles was such that carbon nanotubes were first dispersed in the presence of sodium dodecyl sulfate surfactant. An ultrasonic bath was also used, and the results for the four states were investigated by considering the co-current and counter-current flow for the hot fluid, which was pure water with an inlet temperature of 80 °C, and the nanofluid. In general, the results of this study can be summarized as follows:

- In comparison to pure water, the Reynolds number, the coefficient of heat transfer, and the overall coefficient of heat transfer all increased as the amount of carbon nanotubes increased.
- The nanofluid pressure drop was also investigated, with no significant change in the nanofluid pressure drop relative to the base fluid.

REFERENCE

[1] S.Porgar, L.Vafajoo, H.M.Ali, Investigation of key parameters on nanofluid thermal performance in heat exchangers: A review on recent research, Chemical Engineering & Technology, 2023, https://doi.org/10.1002/ceat.202200527.

[2] M.Hasan, Sh.S.Priam, A.Nur-E Faiaz, A.K.Azad, M.M.Rahman, Influence of thermal conductivity on transient mixed convection in a vented cavity with a hollow cylinder and filled with CNT-water nanofluid, Heliyon, Volume 9, Issue 3, 2023, e13850, ISSN 2405-8440, https://doi.org/10.1016/j.heliyon.2023.e13850.

[3] W.Jin, L.Jiang, L.Han, H.Huang, J.Zhang, M.Guo, Y.Gu, F.Zhi, Zh.Chen, G.Yang, Investigation of thermal conductivity enhancement of water-based graphene and graphene/MXene nanofluids, Journal of Molecular Liquids, Volume 367, Part A, 2022, 120455, ISSN 0167-7322, https://doi.org/10.1016/j.molliq.2022.120455.

[4] S.Porgar, L.Vafajoo, N.Nikkam, Gh.Vakili Nezhaad. Physiochemical studies of functionalized MWCNT/transformer oil nanofluid utilized in a double pipe heat exchanger. Canadian Journal of Chemistry. 99(6): 510-518. https://doi.org/10.1139/cjc-2020-0297

[5] S.Porgar, N.Rahmanian, Investigation of Effect of Aluminium Oxide Nanoparticles on the Thermal Properties of Water-Based Fluids in a Double Tube Heat Exchanger, 2022, Biointerface Research in Applied Chemistry, Volume 12, Issue 2, 2022, 2618 – 2628. [6] S.Pugalenthi, J.Devaraj, J.Kadarkaraithangam, J.Joseph J.Dharmaraj, Improvement in the thermal conductivity and stability of rare-earth metal oxide nanofluids using the stabilizing action of nano CaCO3 in comparison with the stabilizing action of sodium dodecyl sulphate, Journal of Molecular Liquids,Volume 370,2023,121056,ISSN 0167-7322,https://doi.org/10.1016/j.molliq.2022.121056.

[7] K.M.Yashawantha, A.V.Vinod, ANFIS modelling of effective thermal conductivity of ethylene glycol and water nanofluids for low temperature heat transfer application, Thermal Science and Engineering Progress, Volume 24, 2021, 100936, ISSN 2451-9049, https://doi.org/10.1016/j.tsep.2021.100936.

[8] S.Harish, K.Ishikawa, E.Einarsson, S.Aikawa, S.Chiashi, J.Shiomi, S.Maruyama, Enhanced thermal conductivity of ethylene glycol with single-walled carbon nanotube inclusions, Int. J. Heat Mass Transf. 55 (2012) 3885–3890.

[9] A.Aminian "Predicting the effective thermal conductivity of nanofluids for intensification of heat transfer using artificial neural network", Powder Technology 301 (2016) 288–309.

[10] R.Lotfi, A.M.Rashidi, A. Amrollahi, "Experimental Study on the Heat Transfer Enhancement of MWNT Water Nanofluid in a Shell and Tube Heat Exchanger", International Communications in Heat and Mass Transfer, Vol. 39, pp. 108–111, (2012).

[11] M.Pour Jafarqoli, Gh.A.Sheikhzadeh, "Numerical Study of Turbulent Flow of Nano-Liquids Containing

Carbon Nanotubes in a Double-Flow Heat Exchanger with counter Current", Kashan University, 2002).

[12] A.Hosseinian, A.Meghadadi, In vitro study of the effects of nano-fluid multi-walled carbon nanotubes on heat transfer of two-tube heat exchanger with non-metallic shell "isme, 2018.

[13] C.H.Chon, K.D.Kihm, S.P.Lee, S.U.S.Choi, Empirical correlationfinding the role of temperature and particle size for nanofluid (Al2O3) thermal conductivity enhancement, Appl. Phys. Lett. 87 (2005) 153107.

[14] C.H.Li, G.P.Peterson, Experimental investigation of temperature and volume fraction variations on the effective thermal conductivity of nanoparticle suspensions (nanofluids), J.Appl. Phys. 99 (2006) (084314-1-084314-8).

[15] W.Duangthongsuk, S.Wongwises, Measurement of temperature-dependent thermal conductivity and viscosity of TiO2–water nanofluids, Exp. Thermal Fluid Sci.33 (2009) 706–714.

[16] T.P.Teng, Y.H.Hung, T.C.Teng, H.E.Mo, H.G.Hsu, The effect of alumina/water nanofluid particle size on thermal conductivity, Appl. Therm. Eng. 30 (2010) 2213–2218.

[17] M.Ghanbarpour, E.B.Haghigi, R.Khodabandeh, Thermal properties and rheological behavior of water based Al2O3nanofluid as a heat transferfluid, Exp. Thermal Fluid Sci. 53 (2014) 227–235.

[18] M.Hemmat Esfe, S.Saedodin, O.Mahian, S.Wongwises, Heat transfer characteristics and pressure drop of COOH-functionalized DWCNTs/water nanofluid in turbulent flow at low concentrations, Int. J. Heat Mass Transf. 73 (2014) 186–194.

[19] M. Hemmat Esfe, S.Saedodin, O.Mahian, S.Wongwises, Thermophysical properties, heat transfer and pressure drop of COOH-functionalized multi walled carbon nanotubes/water nanofluids, Int.Commun. Heat Mass Transfer 58 (2014) 176–183.

[20] S.Abdulwahab Razuqi, Two-Dimensional Numerical Investigation on Mixed Convection Nanofluids Flow in a Duct having Backward-Facing Step under Laminar Condition, Adv. Nat. Appl. Sci. 11 (2017) 1–10. http://www.aensiweb.com/http://creativecommons.org/licenses/by/4.0/ (accessed June 29, 2020).

[21] V.Arasu, D.Kumar, I.A.Khan, Experimental validation of enhancement in thermal conductivity of titania/water nanofluid by the addition of silver nanoparticles, International Communications in Heat and Mass Transfer 120 (2021) 104910.

[22] S.Akilu, A.T.Baheta, K.V.Sharma, Experimental measurements of thermal conductivity and viscosity of ethylene glycol-based hybrid nanofluid with TiO2-CuO/C inclusions, J.Mol.Liq.246 (2017) 396–405.

[23] S.Porgar, L.Vafajoo, N.Nikkam, Gh.Vakili-Nezhaad, A comprehensive investigation in determination of nanofluids thermophysical properties, Journal of the Indian Chemical Society, Volume 98, Issue 3, 2021, 100037, ISSN 0019-4522, https://doi.org/10.1016/j.jics.2021.100037.

[24] L.Chen, H. Xie, Y. Li, W. Yu, Nanofluids containing carbon nanotubes treated by mechanochemical reaction, Thermochim. Acta 477 (2008) 21–24.

[25] Y.J.Hwang, Y.C.Ahn, H.S.Shin, C.G.Lee, G.T.Kim, H.S.Park, J.K.Lee, Investigation on characteristics of thermal conductivity enhancement of nanofluids, Curr. Appl. Phys. 6 (2006) 1068–1071.

[26] L.Godson, B.Raja, D.Mohan Lal, S.Wongwises, Experimental investigation on the thermal conductivity and viscosity of silver-deionized Water nanofluid, Exp. Heat Transf. 23 (2010) 317–332.

[27] L.Godson, D.Mohan Lal, S.Wongwises, Measurement of thermo physical properties of metallic nanofluids for high temperature applications, Nanoscale Microscale Thermophys. Eng. 14 (2010) 152–173.

[28] H.Xie, H.Lee, W.Youn, M.Choi, Nanofluids containing multiwalled carbon nanotubes and their enhanced thermal conductivities, J.Appl. Phys. 94 (2003) 4967–4971.

[29] M.J.Assael, C.F.Chen, I.Metaxa, W.A.Wakeham, Thermal conductivity of carbon nanotube suspensions in Water, Int. J. Thermophys. 25 (2004) 971–985.

[30] J.Glory, M.Bonetti, M.Helezen, M.M.L.Hermite, C.Reynaud, Thermal and electrical conductivities of Water-based nanofluids prepared with long multiwalled carbon nanotubes, J. Appl. Phys. 103 (2008) 094309.

[31] N.Jha, S.Ramaprabhua, Thermal conductivity studies of metal dispersed multiwalled carbon nanotubes in Water and ethylene glycol based nanofluid, J. Appl. Phys. 106 (2009) 084317.

[32] S.K.Das, N.Putra, P.Thiesen, W.Roetzel, Temperature dependence of thermal conductivity enhancement for nanofluids, J. Heat Transf. 125 (2003) 567–574.

[33] C.H.Li, G.P.Peterson, The effect of particle size on the effective thermal conductivity of Al2O3–Water nanofluids, J. Appl. Phys. 101 (2007) 044312.

[34] M.Beck, Y.Yuan, P.Warrier, A.Teja, The effect of particle size on the thermal conductivity of alumina nanofluids, J.Nanopart. Res. 11 (2009) 1129–1136.

[35] H.A.Mintsa,G. Roy, C.T.Nguyen, D.Doucet, New temperature dependent thermal conductivity data for Water-based nanofluids, Int. J. Therm. Sci. 48 (2009) 363–371.

[36] M.Chandrasekar, S.Suresh, A.Chandra Bose, Experimental investigations and theoretical determination of thermal conductivity and viscosity of Al2O3/Water nanofluid, Exp. Thermal Fluid Sci. 34 (2010) 210–216.

[37] J.Jeong, C.Li, Y.Kwon, J.Lee, S.H.Kim, R.Yun, Particle shape effect on the viscosity and thermal conductivity of ZnO nanofluids, Int. J.Refrig. 36 (2013) 2233–2241.

[38] M.Hemmat Esfe, S.Saedodin, Turbulent forced convection heat transfer and thermophysical properties of

MgO–Water nanofluid with consideration of different nanoparticles diameter, an empirical study, J.Therm. Anal. Calorim.119 (2015) 1205–1213.

[39] M.S.Tahat, A.C.Benim, Experimental Analysis on Thermophysical Properties of Al2O3/CuO Hybrid Nano Fluid with its Effects on Flat Plate Solar Collector, https://doi.org/10.4028/www.scientific.net/DDF.374.148, April 2017.

[40] M.Chopkar, S.Sudarshan, P.K.Das, I.Manna, Effect of Particle Size on Thermal Conductivity of Nanofluid, Metallurgical and Materials Transactions A, Volume 39, Issue 7, pp.1535-1542.

[41] R.Balaga, K. Ramji, T. Subrahmanyam, K. R.Babu, Effect of temperature, total weight concentration and ratio of Fe2O3 and f-MWCNTs on thermal conductivity of water based hybrid nanofluids, Materials Today: Proceedings, Volume 18, Part 7, 2019, Pages 4992-4999, ISSN 2214-7853, https://doi.org/10.1016/j.matpr.2019.07.492.

[42] Yaoting Huang, Chunping Xie, Chuan Li, Yongliang Li, Yulong Ding, Rheological behaviour and aggregation kinetics of EG/water based MCNT nano-suspension for sub-zero temperature cold storage, Energy Procedia, Volume 158, 2019, Pages 4846-4851, ISSN 1876-6102, https://doi.org/10.1016/j.egypro.2019.01.709.

[43] Ahmet Selim Dalkılıç, Gökberk Yalçın, Bedri Onur Küçükyıldırım, Semiha Öztuna, Ayşegül Akdoğan Eker, Chaiwat Jumpholkul, Santiphap Nakkaew, Somchai Wongwises, Experimental study on the thermal conductivity of water-based CNT-SiO2 hybrid nanofluids, International Communications in Heat and Mass Transfer, Volume 99, 2018, Pages 18-25, ISSN 0735-1933, https://doi.org/10.1016/j.icheatmasstransfer.2018.10.002.

[44] M. Chandrasekar, S. Suresh, A. Chandra Bose, Experimental investigations and theoretical determination of thermal conductivity and viscosity of Al2O3/water nanofluid, Experimental Thermal and Fluid Science, Volume 34, Issue 2,2010, Pages 210-216, ISSN 0894-1777, https://doi.org/10.1016/j.expthermflusci.2009.10.022.

[45] S. Porgar, H.F. Oztop, S.Salehfekr, A comprehensive review on thermal conductivity and viscosity of nanofluids and their application in heat exchangers, Journal of Molecular Liquids, Volume 386, 2023, 122213, ISSN 0167-7322, https://doi.org/10.1016/j.molliq.2023.122213.

[46] B.Khatoon, V.K.Choudhary, R.Kumar, M.S.Alam, Sh.K.Pandey, R.Singh, R.Naresh, Enhancement of heat transfer rate in shell & tube heat exchanger using CuO/Al2O3-water based nanofluids, Materials Today: Proceedings, 2022, ISSN 2214-7853, https://doi.org/10.1016/j.matpr.2022.10.258.

[47] A.M. Alklaibi, Kotturu V.V. Chandra Mouli, L. Syam Sundar, Experimental Investigation of Heat Transfer and Effectiveness of Employing Water and Ethylene Glycol Mixture based Fe3O4 Nanofluid in a Shell and Helical Coil Heat Exchanger, Thermal Science and Engineering Progress, 2023, 101739, ISSN 2451-9049, https://doi.org/10.1016/j.tsep.2023.101739.

[48] T.Huq, H.Ch.Ong, B.T.Chew, K.Y.Leong, S.N.Kazi, Review on aqueous graphene nanoplatelet Nanofluids: Preparation, Stability, thermophysical Properties, and applications in heat exchangers and solar thermal collectors, Applied Thermal Engineering, Volume 210, 2022, 118342, ISSN 1359-4311, https://doi.org/10.1016/j.applthermaleng.2022.118342.

[49] Ch.Kamsuwan, X.Wang, P.Piumsomboon, Y.Pratumwal, S.Otarawanna, B.Chalermsinsuwan, Artificial neural network prediction models for nanofluid properties and their applications with heat exchanger design and rating simulation, International Journal of Thermal Sciences, Volume 184, 2023, 107995, ISSN 1290-0729, https://doi.org/10.1016/j.ijthermalsci.2022.107995.

[50] G.Yalçın, S.Öztuna, A.S.Dalkılıç, S.Wongwises, The influence of particle size on the viscosity of water based ZnO nanofluid, Alexandria Engineering Journal, Volume 68, 2023, Pages 561-576, ISSN 1110-0168, https://doi.org/10.1016/j.aej.2022.12.047.

[51] A.B.Çolak, Ö.Açıkgöz, H.Mercan, A.S.Dalkılıç, S.Wongwises, Prediction of heat transfer coefficient, pressure drop, and overall cost of double-pipe heat exchangers using the artificial neural network, Case Studies in Thermal Engineering, Volume 39, 2022, 102391, ISSN 2214-157X, https://doi.org/10.1016/j.csite.2022.102391.

[52] A.Samadzadeh, S.Zeinali Heris, I.Hashim, O.Mahian, An experimental investigation on natural convection of non-covalently functionalized MWCNTs nanofluids: Effects of aspect ratio and inclination angle, International Communications in Heat and Mass Transfer, Volume 111, 2020, 104473, ISSN 0735-1933, https://doi.org/10.1016/j.icheatmasstransfer.2019.104473.

[53] A.Shahsavar, A.H.A.Alwaeli, N.Azimi, Sh.Rostami, K.Sopian, M.Arıcı, P.Estellé, S.Nižetić, A.Kasaeian, H.M.Ali, Zh.Ma, M.Afrand, Exergy studies in water-based and nanofluid-based photovoltaic/thermal collectors: Status and prospects, Renewable and Sustainable Energy Reviews, Volume 168, 2022, 112740, ISSN 1364-0321, https://doi.org/10.1016/j.rser.2022.112740.

[54] V.Y.Rudyak, G.R.Dashapilov, A.V. Minakov, M.I.Pryazhnikov, Comparative characteristics of viscosity and rheology of nanofluids with multi-walled and single-walled carbon nanotubes, Diamond and Related Materials, Volume 132, 2023, 109616, ISSN 0925-9635, https://doi.org/10.1016/j.diamond.2022.109616.

Research Article *Energy, Environment and Storage* (2023) 03-03:105-114

Energy, Environment and Storage

Journal Homepage: www.enenstrg.com

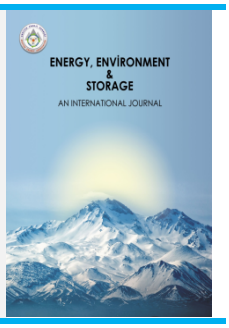

Seasonal Monitoring of Water Quality Parameters and Pesticides at the Altınapa Reservoir Watershed

Betul Aykut-Senel[1], Cihan Ozgur[2], Dilibaier Aibaidula[3], Sehnaz Sule Kaplan-Bekaroglu[1], Filiz Dadaser-Celik[3], Nuray Ates[3*]

[1]*Suleyman Demirel University, Engineering Faculty, Department. of Environmental Engineering, Isparta, Türkiye*

0000-0003-3674-5525, 0000-0003-0917-7219

[2]*Isparta University of Applied Sciences, Sutculer Prof. Dr. Hasan Gurbuz Vocational High School, Isparta, Türkiye*

0000-0001-6085-1585

[3]*Erciyes University, Engineering Faculty, Department of Environmental Engineering, Kayseri, Türkiye*

0000-0002-4611-2978, 0000-0003-3623-7723, 0000-0002-8923-4852

ABSTRACT. Altınapa Reservoir is a reservoir located on the Meram Stream in the Konya Province in Türkiye that supplies drinking water. The Altınapa Reservoir feeds the Konya Drinking Water Treatment Plant with 37.8 million m^3 of water annually and the treated water is delivered by the drinking water network. The aim of this study was to determine the effect of agricultural activities and settlements on water quality in the Altınapa Reservoir Watershed. In the study, major water quality parameters (pH, electrical conductivity, total organic carbon, total nitrogen, nitrite, nitrate, phosphorus, phosphate, and total suspended solids) and pesticides were monitored at four stations (K1, K2, K3, K4) on the sub-streams feeding reservoir. Major water quality parameters were monitored at monthly intervals for 12 months between June 2020 and May 2021, and pesticides were monitored seasonally at 4 seasons (Fall 2019, Winter 2020, Summer 2020, and Spring 2021). A correlation matrix was used to assess the connections between nine indicators of water quality. The annual average conductivity and pH values of the samples taken from four different stations of the Meram Stream were 432 µS/cm and 8.04, respectively. The highest value for total nitrogen was 10.73 mg/L and it was 0.87 mg/L for nitrate. Annual average total organic carbon values were determined as 1.35, 1.69, 1.51, and 1.46 mg/L at K1, K2, K3, and K4 stations, respectively. Specific UV absorbance indicated that organic matters of water are mostly hydrophilic and have low aromatic content. In seasonal pesticide monitoring, 71 different compounds were detected in water samples. The compounds whose concentrations exceeded Turkish Environmental Quality Standards were identified as DDD-op, DDE-p.p', diflufenican, and imidacloprid. Pesticides constitute most of the micropollutants detected in water samples. The highest positive correlation among water quality parameters was obtained between conductivity and nitrate (0.81) and total nitrogen (0.88).

Keywords: Altınapa Reservoir Watershed, Environmental quality standards, Drinking water, Micropollutants, Water Quality.

Article History: Received:01.08.2023; Accepted: 22.08.2023; Available online: 30.09.2023
Doi: https://doi.org/1052924/NILM8823

*Corresponding author: nuraya@erciyes.edu.tr

1. INTRODUCTION

Water quality monitoring is essential for developing water management strategies, identification of pollution sources, and development of effective and economical treatment techniques [1-3]. The quality and quantity of water resources are very important for urban water supply, particularly in regions where water resources are limited [4]. Surface water resources, including lakes, reservoirs, and rivers, constitute a significant portion of drinking water resources. However, the deterioration of surface water quality due to the contamination as a result of human activities causes significant issues worldwide [5]. The World Health Organization (WHO) estimates that water contamination is responsible for 80% of human health problems [6].

Increase in the use of different types of chemicals and toxic substances in urban life, industry, and agriculture leads to the presence of micropollutants and industrial chemicals including pesticides, heavy metals, medicines, pharmaceuticals, personal care products, detergents, and disinfection by-products in water resources, even in treated water [7-9]. Due to bioaccumulation and transfer in the food chain, these micropollutants pose a concern to human health [10], have a negative impact on the aquatic biota, and reduce the efficiency and increase the cost of drinking water treatment [11]. By releasing the Water Framework Directive 2000/60/EC at the beginning of the 2000's, the European Union (EU) came up with a plan to identify priority compounds that pose a high hazard to the aquatic ecosystem. This plan aims to clean up micropollutants in water resources. The European Union's 2008/105/EC water policy directive resulted in the development of a list of 33 priority compounds and substance categories. The efforts led to an update of the water framework policy by the European Parliament and, as a result, identification of a 45-item list of priority items/groups of items [12, 13].

Three substances are recommended for the first watch list of sub-components in the directive 2013/39/EC, along with a number of pesticides (aldrin, dichlorodiphenyl trichloroethane, dicofol, dieldrin, endrin, endosulfan, isodrine, heptachlor, lindane, pentafluorophenol, chlorpyrifos, chlorfenvinphos, dichlorvos, atrazine, simazine, terbutrine, diuron, isoproturon, trifluralin, alacyper), solvents (dichloromethane, dichloroethane, trichloromethane and carbon tetrachloride), perfluorooctane sulfonic acid and its derivatives, polychlorinated biphenyls, polycyclic aromatic hydrocarbons. In addition to nonylphenol and octylphenol, three compounds (diclofenac, 17-alpha-ethinylestradiol (EE2) and 17-beta-estradiol (E2)) were included in the recommendation for the first watch list for sub-components. Additionally, this directive defines several specific pesticides, including acloniphene, bifenox, sibutrin, quinoxifen, organotin compounds (tributyltin), dioxins and dioxin-like compounds, brominated diphenylethers, hexabromocyclododecanes, and di(2-ethylhexyl) phthalate. The directive of 2013/39/EC specify that it is critical to monitor novel pollutants that are not often addressed in monitoring programs but may have ecotoxicological and toxicological consequences, even if the majority of micropollutants has no discharge limits.

In the Surface Water Quality Management Regulation (Türkiye), 250 micropollutants are listed and the Environmental Quality Standards are defined for these micropollutants in rivers, lakes, coastal and transitional waters [14]. Within the scope of the Regulation on the Quality and Treatment of Drinking Water Supply in Türkiye, 99 water quality parameters are monitored at the inlets and outlets of drinking water sources, and water resources are classified according to A1, A2 and A3 categories with distinct guideline values [15]. In addition to the criteria for water quality outlined in this rule, guiding values are also provided for several micropollutants. Selek [16] collected samples from 287 surface water basins nationwide in Türkiye four times a year to conduct a comprehensive site-specific monitoring analysis. In this study, the evaluation of water quality revealed that one water source in the Eastern Black Sea Basin was in A1 water quality, 93 water sources were in A2 water quality, and 193 water sources were in A3 water quality categories. They concluded that despite a pressure regarding micro-contaminants in Türkiye's surface water resources, the issue is more dominating in terms of microbiological quality as well heavy metals from geological formations in certain sites [16]. Canli et al. [17] evaluated water quality in terms of micropollutants in 600 samples collected from Alibeykoy Reservoir (Istanbul), Omerli Reservoir (Istanbul), Sapanca Lake (Sakarya), and the effluent of wastewater treatment plant (Istanbul). It was determined that five most often detected substances in the samples were acetochlor, acetamiprid, thiamethoxam, carbendazim, and terbutryn [17]. Emadian et al. [18] examined 300 samples for 222 organic micropollutants taken from 75 different stations along the Ergene River between August 2017 and May 2018. A total of 165 micropollutants with concentrations ranging from 1.90 ng/L to 1824.55 µg/L were detected.

Yavuz et al. [19] grabbed samples from three major components of the drinking water system, including the raw water sources (the Camlidere and Kesikkopru Reservoirs), the drinking water treatment plant (the Ivedik Water Treatment Plant), and the water distribution network, to evaluate the seasonal fluctuations in biocide levels and their association with general water quality indicators. Triclosan concentrations found in surface water samples were 0.65–11.15 ng/L and 0.8–48.96 ng/L, respectively, for the Camlidere and Kesikköprü Reservoirs. The range of chlorhexidine concentrations was 1.33 to 5.31 ng/L. The results of the treatment plant effluent analysis revealed that the level of all biocides in the distribution network was below the quantification limit. During a hydrological year (February 2017–January 2018), Ustaoglu et al. [20] conducted research at three chosen monitoring stations in the Turnasuyu Basin to determine the impacts of residential pollution and agricultural activities on water quality. The findings demonstrated that Turnasuyu Stream has extremely high-water quality and the trace elements found are not riskily close to the public health threshold.

In recent years, the importance of monitoring and assessing the water quality has increased due to worries based on indicators showing that fresh water has become increasingly scarce. Monitoring of water quality is an effective method to determine the effects of pollution

sources, as well as to ensure the effective use and management of water resources and the maintenance, and also protection of aquatic life [21].

Altınapa Reservoir, located on the Meram Stream in Konya, Türkiye, was built between 1963-1967 by The State Hydraulic Works to provide drinking and utility water, delivers irrigation service to an area of 1,400 hectares and supplies about 38 million m^3 water which is about one-third of Konya's total drinking water demand. Meram Stream, with an annual average flow of approximately 1 m^3/s, is the mainstream feeding the reservoir. The reservoir has an average capacity of 15,000 million m^3 and a surface area of 2.3 km^2. Since the reservoir is a resource for drinking water and other supplies, the reservoir and its basin have been taken under protection and measures against contamination have been adopted.

The aim of this study is to monitor water quality based on major water quality parameters and pesticides and to evaluate water quality at the Altınapa Reservoir Watershed. Besides, the relationships between nine water quality parameters were evaluated by a correlation matrix. In the scope of monitoring at four stations on the sub-streams feeding Altınapa Reservoir pH, electrical conductivity (EC), total organic carbon (TOC), UV absorbance at 254 nm (UV_{254}) wavelength, total nitrogen (TN), nitrite (NO_2^-), nitrate (NO_3^-), total phosphorus (TP), phosphate, total suspended solids (TSS), and pesticides were monitored. Major water quality parameters were monitored monthly for 12 months between June 2020 and May 2021, and pesticides were monitored seasonally for 4 seasons (in months September 2019, January 2020, August 2020, and April 2021). Pesticide contamination was evaluated based on Turkish Environmental Quality Standards (EQS). The associations between water quality parameters were examined by a correlation matrix.

2. MATERIALS AND METHODS

2.1 Sample Collecting and Analytical Methods

2 L water samples were collected at the Altınapa Reservoir Watershed at four monitoring stations (K1, K2, K3, K4) between June 2020 and May 2021 (Figure 1). The water samples were transported within 24 hr to the laboratory in a cooler containing ice cubes, kept at +4°C in a fridge for experimental studies. Table 1 presents the specifics of analysis techniques for water quality parameters. The physicochemical analyses of water samples were conducted according to the Standard Methods [22]. TOC and total nitrogen were determined according to SM 5310 B [36] using a TOC analyzer (TOC-L CPH, Shimadzu). The UV absorbance of water samples at a wavelength of 254 nm were measured using UV-visible spectrophotometer (Hach Lange DR 6000) according to the SM 5910 B method [22]. Nitrite, nitrate, TP, and phosphate were analyzed by Suleyman Demirel University Geothermal Energy Groundwater and Mineral Resources Research and Application Center. Figure 1 shows the watershed boundary and water quality monitoring stations at the Altınapa Reservoir Watershed. Pesticides were analyzed by the Scientific and Technological Research Council of Türkiye (TUBITAK), Marmara Research Center Laboratory. LC-MSMS and GC-MSMS equipment were used for the pesticides analyses, and the limit of quantification values were given as 0.001 g/L.

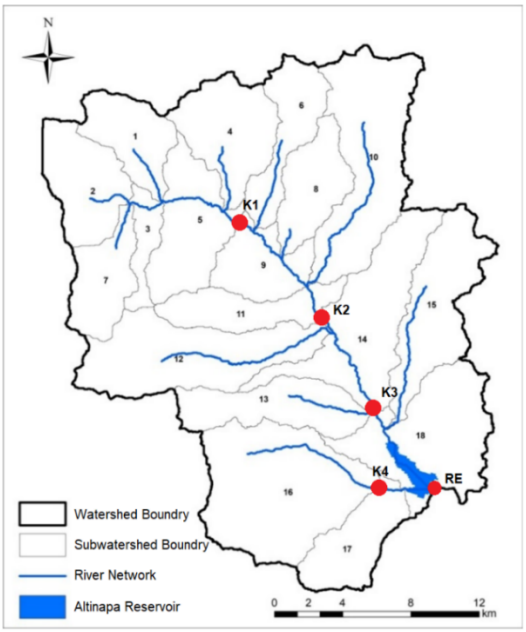

Figure 1. Watershed boundary and water quality monitoring stations at the Altınapa Reservoir Watershed.

Specific UV absorbance (SUVA), which is a normalized parameter, is used to compare various natural organic matter (NOM) properties of different water sources. SUVA values of samples were computed by dividing UV absorbance at a certain wavelength to TOC content. Equation 1 explains the SUVA computation.

$$SUVA_{254} = UV_{254}/TOC * 100 \quad (1)$$

In equation 1, $SUVA_{254}$ (L/mgTOC.m) represents the specific UV absorbance, UV_{254} (cm^{-1}) represents the absorbance at 254 nm wavelength and TOC (mg/L) represents the total organic carbon concentration.

Table 1. Analytical methods and detection limits of water quality parameters

Parameter	Unit	Methods	Equipment	MDL
pH		SM 4500 H+	WTW Multi340i/Set	
EC	µS/cm	SM2510B	WTW Multi340i/Set	
TOC	mg/L	SM5310B	TOC-L CPH Shimadzu	0.1
TN	mg/L	High temperature burning	TOC-L CPH Shimadzu	
UV_{254}	cm^{-1}	SM5910	UV-1700 Shimadzu	±0.005
NO_3-N NO_2-N	mg/L	USEPA Metot 300	Dionex ICS-3000	0.01
$SUVA_{254}$	L/mg TOC.m	UV_{254}/TOC		

4. RESULTS AND DISCUSSIONS

4.1. Water Quality Results

The pH levels of samples ranged from 7.68 to 8.39. Figure 2 displayed seasonal variations of pH values at the monitoring stations and the findings demonstrated that the pH value variations were rather small. During the sampling period, the highest pH value was measured at the K4 monitoring station as 8.39 in September, and the lowest pH value was measured at K1 monitoring stations as 7.68 in January. The pH range of the waters meets the standards in the "Regulation on Water Intended for Human Consumption" established by the Türkiye Republic Ministry of Health [23]. Similar pH ranges were discovered in earlier investigations in Apa Reservoir in Konya [24-26].

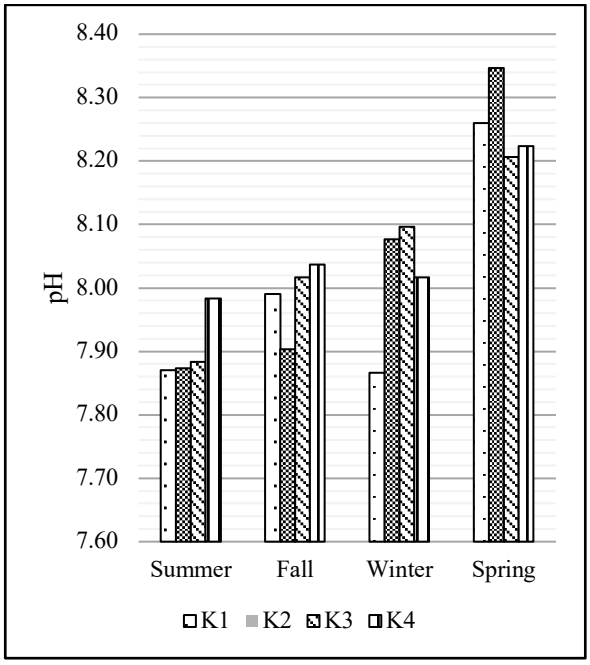

Figure 2. Seasonal average pH values variations at monitoring stations.

Conductivity is a numerical expression of the electric current carrying capacity of an aqueous solution. Conductivity is an indicator parameter that is also used for monitoring pollution in general. The conductivity value of natural rivers and lakes varies between 10-1000 µS/cm. Values above this level indicate that these surface waters are polluted. The conductivity measurement values at the monitoring stations vary between 315 µS/cm and 644 µS/cm (Table 2). The highest conductivity values at the monitoring stations were measured at 644 µS/cm K2 station in August, and the lowest at 315 µS/cm K4 station in August, respectively.

NOM is a heterogeneous mixture containing macro-molecular humic structures, small molecular weight hydrophilic acids, proteins, fats, carboxylic acids, amino acids, carbohydrates, and organic substances such as hydrocarbons, and TOC is an indicator of NOMs [27]. Annual average TOC values were determined as 1.35, 1.69, 1.51 and 1.46 mg/L at K1, K2, K3 and K4 stations, respectively. An increase in the TOC concentration of all monitoring stations was observed in January and February. The increase in TOC values might be attributed to the transport of organic materials to the reservoir by surface runoff due to seasonal precipitation. The natural components of organics are humic acid, fulvic acid, amines, and urea, while synthetic sources include certain detergents, industrial chemicals, pesticides, fertilizers, herbicides, and chlorinated organics [28]. High concentrations of organic matter (TOC>2-3 mg/L) are not desired, especially in drinking water sources. High TOC concentrations in drinking water increase the dose of coagulant, lead to the formation of disinfection by-products, cause microbial growth in the network, as well as cause competition in the removal of micropollutants such as pesticides in treatment processes [29]. Therefore, it is important to monitor TOC values in drinking water sources and to treat them especially before the disinfection process in order to manage water treatment and its distribution in the network in a safe and economical way [30].

Non-specific parameters such as UV absorbance at wavelengths of 254-280 nm are used to characterize NOMs [27, 31]. A strong correlation was found between the aromatic carbon content of the water sample and the UV absorbance. By measuring the UV absorbance of NOM solutions in the range of 254-280 nm, the amount of aromatic compounds (unsaturated double bonds and π-π electron interactions) in water is indirectly determined by the general absorbance value [31, 32]. The highest and lowest UV_{254} absorbance were detected at K3 and K1 stations, and UV_{254} absorbance values were measured as 0.050 cm^{-1} and 0.019 cm^{-1}, respectively. Annual average UV_{254} absorbance values at stations K1, K2, K3 and K4 feeding the reservoir were 0.028, 0.035, 0.035 and 0.030 cm^{-1}, respectively.

As the NOM is a heterogeneous mixture of different organic compounds, the measured SUVA is an average value showing the distribution of chromophores (double bonds and/or aromatic structures) in the NOM. As well, the obtained ratios describe the hydrophilic and hydrophobic properties of NOM in water [31, 33]. In a water sample, $SUVA_{254}$>3.5-4 L/mg-m indicates mainly hydrophobic and especially aromatic material, while water with $SUVA_{254}$<3 L/mg-m indicates mainly hydrophilic material [33, 34]. Figure 3 presented the seasonal variations of the SUVA values of monitoring stations. The $SUVA_{254}$ values calculated in the samples varied on a monthly basis. The highest $SUVA_{254}$ value was observed at 3.80 L/mg-m at the K3 station in November, and the lowest at 1.02 L/mg-m at the K2 station in February. In general, $SUVA_{254}$ is <3 L/mg-m at monitoring stations and is hydrophilic. Although the TOC values are higher in the winter months than the TOC values in the autumn months, the low SUVA values in the winter indicate that organic fractions with low aromatic content are transported to the surface waters with precipitation. On the other hand, low TOC and high SUVA values in autumn indicate that low molecular weight relatively hydrophilic organics degrade with temperature in summer.

Table 2. Water quality parameters at monitoring stations on the Meram Stream

Parameters		Monitoring Station			
		K1	K2	K3	K4
Conductivity (µS/cm)	Annual Average	457	476	449	344
	Minimum	326	325	328	315
	Maximum	544	644	570	380
TSS (mg/L)	Annual Average	5.36	4.00	9.27	2.25
	Minimum	1.00	0.00	0.00	1.00
	Maximum	28.0	23.0	49.0	3.0
UV_{254} (cm^{-1})	Annual Average	0.03	0.04	0.04	0.03
	Minimum	0.02	0.02	0.02	0.02
	Maximum	0.04	0.05	0.05	0.04
TOC (mg/L)	Annual Average	1.35	1.69	1.51	1.46
	Minimum	0.75	1.02	1.09	0.83
	Maximum	2.57	2.55	2.43	2.70
NO_2-N (mg/L)	Annual Average	0.30	0.18	0.12	ND
	Minimum	0.04	0.06	0.09	ND
	Maximum	0.58	0.57	0.14	ND
TP (mg/L)	Annual Average	0.06	0.09	0.06	0.06
	Minimum	0.06	0.09	0.05	0.06
	Maximum	0.06	0.09	0.06	0.06
PO_4 (mg/L)	Annual Average	ND	ND	ND	ND
	Minimum	ND	ND	ND	ND
	Maximum	ND	ND	ND	ND

TN is the sum of total Kjehdahl nitrogen (organic nitrogen and ammonia-N), ammonium-N, nitrate-N, and nitrite-N. The main pollutant sources of TN in water resources are domestic wastewater discharge, fertilizers applied in agricultural activities, and industrial wastewater discharges. Annual average values of TN concentration at monitoring stations of Meram Stream varied in the range of 0.01-4.87 mg/L. The highest TN concentration was measured at the K2 station in August with 10.73 mg/L, and the lowest at K4 station in September with 0.24 mg/L, respectively. Annual mean TN values at the stations K1, K2, K3 and K4 feeding the reservoir were determined as 1.98, 4.81, 3.32, and 0.63 mg/L, respectively. According to the results, there is no serious pollution in the Altınapa Reservoir Watershed in terms of TN. The reason might be attributed to that Altınapa Reservoir Watershed is a relatively closed and small basin, only agricultural activities are carried out in the basin. There are 5-6 small settlements and there is no serious wastewater flow from these areas and there is no industrial activity.

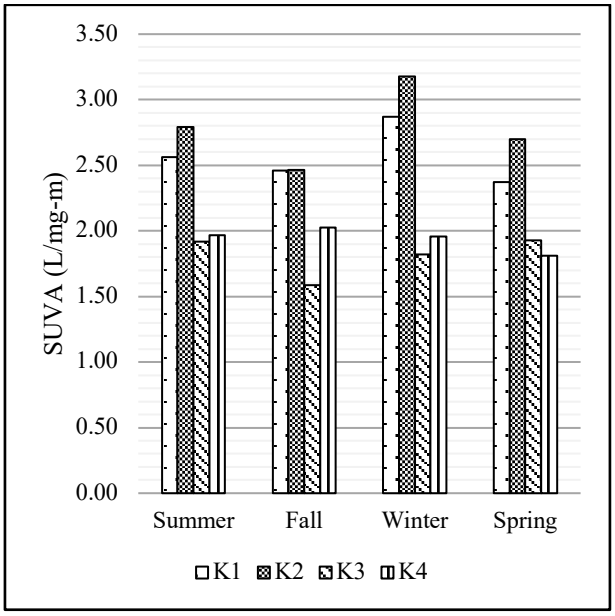

Figure 3. Seasonal average SUVA variations at the monitoring stations.

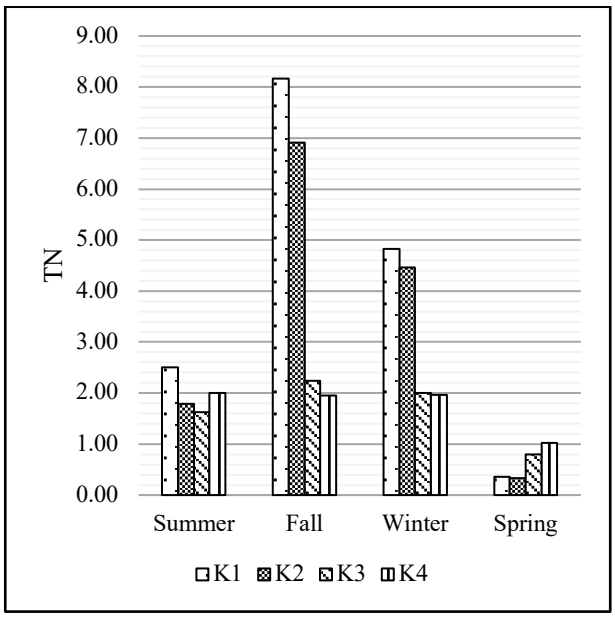

Figure 4. Seasonal average TN variations at the monitoring stations.

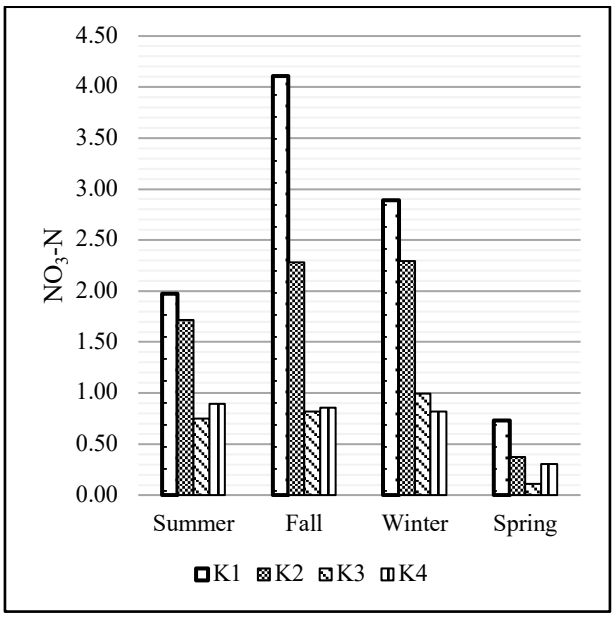

Figure 5. Seasonal average nitrate variations at the monitoring stations.

The annual average nitrate concentration was determined as 1.33, 2.02, 1.82 and 0.43 mg/L in K1, K2, K3 and K4, respectively (Figure 5). The highest nitrate concentration was observed at the K2 station with 4.87 mg/L in August and at the K3 station with 4.75 mg/L in September, while the lowest was detected at the K4 station with 0.01 mg/L in April. The nitrate concentration increase at some stations is thought to be due to agricultural activities or wastewater discharges close to the sampling stations. On the other hand, the highest nitrite concentration was measured at the K1 station in April with 0.58 mg/L. The maximum nitrite content was recorded at the K1 station in April during the monitoring period with 0.58 mg/L. However, it was found to be below the detection limit (<DL) of 0.01 mg/L at all stations in the annual monitoring in June, July, December, January, February, March and May.

The highest TSS value at the monitoring stations was 49 mg/L, and the lowest was 1 mg/L in April at the K4 station. However, TSS could not be found between August 2020 and February 2021 at the K4 station. The TSS values of K1, K2, and K3 stations also showed an increase in April. The severe rains and increased surface runoff are believed to be the reasons for this increase.

Fertilizers, animal and human waste, and garden waste all contain TP. There is no atmospheric (gaseous) form of TP. Due to the lack of atmospheric phosphorus cycling and the scarcity of phosphorus natural sources, phosphorus is frequently a limiting component in water systems [35]. Algae blooms in lakes and reservoirs are caused by TP, which comprises both dissolved and particulate forms of phosphorus. Except for August, the highest TP concentration of 0.09 mg/L was recorded at K2. However, since TP remained below the detection limit at all stations except August and September, the values in Table 2 include August and September.

Pesticides were monitored for 4 seasons in the months September 2019, January 2020, August 2020, and April 2021. The results of pesticides analyses were presented in Table 3. 71 different micropollutants including pesticides were detected. Pesticides detected in the reservoir effluent and/or at least at two monitoring stations were selected and presented in Table 3. The data belonging to the spring period is not shown in table, because any of compounds except acetamiprid could not be detected at least at two stations. Acetamiprid, aldrin, BHC-alpha, bromopropylate, ethoprophos, permethrin, piperonyl butoxide, and terbutryn were found in almost every station as well as reservoir effluents. In addition, acetamiprid, permethrin, piperonyl butoxide, and terbutryn were detected at least in two seasons. Moreover, the levels of DDD-op, DDE-p.p', diflufenican, and imidacloprid were higher than Türkiye's EQS.

Because they are carcinogenic, mutagenic, and teratogenic, pesticides have negative effects on both human health and aquatic life. Furthermore, because of their capacity to bioaccumulate in organism tissues and spread to higher species, they are extremely poisonous. To avoid pesticide infiltration and pesticide pollution in water resources, it is necessary to regulate agricultural activities and pesticide applications. Controlling pesticides at the source, handling them safely, managing waste pesticides and empty containers, setting up catchments to delay and slow runoff, building vegetated waterways and buffer strips, planning irrigation, and applying pesticides on schedule are the fundamental precautions that can be used to prevent pesticide pollution.

Table 3. Pesticides identified at the Altınapa Reservoir Watershed and their concentrations at monitoring stations

Pesticides	Type of Pesticides	EQS[a] (µg/L)	Autumn 2019 (µg/L)					Winter 2020 (µg/L)					Summer 2020 (µg/L)				
			K1	K2	K3	K4	RE[b]	K1	K2	K3	K4	RE[b]	K1	K2	K3	K4	RE[b]
Acetamiprid	Insecticide	42	0.0020	0.0058									0.0007		0.0011		0.0005
Aldrin	Insecticide	0.01											0.0007	0.0007	0.0054		0.0011
Azoxystrobin	Fungicide	0.20	0.0005	0.0007													
BHC-alpha	Insecticide	-											0.0023	0.0014	0.0015	0.0003	0.0003
Bromopropylate	Acaricide	0.12										0.074	0.0075	0.0006	0.0208	0.0000	0.0036
DDD-op	Insecticide	0.025						0.017	**0.065**		**0.058**	**0.061**					
DDE-p.p'	Insecticide	0.02											0.0098	0.0025	**0.0372**	0.0022	
Diflufenican	Herbicide	0.010							**0.044**			**0.070**					
Ethoprophos	Nematicide, insecticide	0.21	0.0311	0.0278		0.1410	0.0198										
Imidacloprid	Insecticide	0.14	0.0543	**0.3577**													
Metalaxyl	Fungicide	17	0.0169	0.0123													
Metrafenone	Fungicide	12							0.937			0.038					
Permethrin	Insecticide	0.12						0.011	0.036	0.012	0.039	0.084	0.0010		0.0179		0.0021
Piperonyl butoxide	Pesticide synergist	3.3						0.011	0.041		0.046	0.059	0.0254		0.1337		
Prometryne	Herbicide	0.3	0.0022	0.0027													
Tebuconazole	Fungicide	23	0.0289	0.0463													
Terbuthylazine	Herbicide	0.2	0.0061	0.0054													
Terbutryn	Herbicide	0.065	0.0091	0.0183	0.0073	0.0045	0.0071						0.0036	0.0024	0.0282	0.0026	0.0020
Tolclofos Methyl	Fungicide	1.2											0.0005		0.0024		

[a]EQS: Environmental Quality Standards [42]

[b]RE: Reservoir Effluent

4.2. Compositional Relations of Water Quality Parameters

A correlation matrix of nine parameters, namely, pH, conductivity, TSS, UV absorbance, TOC, TN, SUVA, nitrite, nitrate, was constructed and was shown in Table 4. Nitrate exhibited a significant positive correlation with TN (0.91) and conductivity (0.88). Similarly, a significant positive linear correlation with TN and conductivity (0.81) was detected. There is often a relationship between the conductivity of water and the total nitrogen and nitrate concentrations in the water. Conductivity is a measure of the water's ability to conduct an electrical current, which is influenced by the presence of dissolved ions in the water samples [36]. Nitrate is a common ion found in water that can contribute to the conductivity of the water [37]. Therefore, as the concentration of nitrate increases, the conductivity of the water tends to increase. Similarly, TN includes various forms of nitrogen, including nitrate [37]. As the concentration of TN increases, the concentration of nitrate in the water may also increase, leading to a corresponding increase in conductivity [38].

It is worth noting that the relationship between conductivity and nitrogen/nitrate concentrations can vary depending on other factors that may be present in the water, such as dissolved organic matter and other ions. Therefore, while conductivity can be a useful indicator of nitrogen/nitrate levels in water, it is important to also measure these nutrients directly to fully understand water quality. The UV_{254}. parameter showed moderate positive correlation with TOC (0.40), TN (0.52), and nitrate (0.34). TSS had moderate positive correlation with UV_{254}. (0.39) and TOC (0.31) and this can be explained by suspended solids in water that can come from a variety of sources, including natural and anthropogenic (human-made) sources [39].

Table 4. Correlation matrix of nine parameters of water quality

	pH	EC	SS	UV_{254}	TOC	TN	SUVA	Nitrite	Nitrate
pH	1								
EC	-0.67	1							
TSS	-0.23	-0.20	1						
U	-0.03	0.16	0.39	1					
TOC	0.12	-0.49	0.31	0.40	1				
TN	-0.51	0.81	0.01	0.52	-0.04	1			
SUVA	-0.15	0.61	-0.02	0.32	-0.73	0.38	1		
Nitrite	0.58	-0.75	0.23	0.21	0.59	-0.57	-0.66	1	
Nitrate	-0.56	0.88	0.03	0.34	-0.36	0.91	0.59	-0.62	1

Some natural sources of suspended solids include erosion of soil and rock, organic matter from decaying plants and animals, and algae blooms [40]. Anthropogenic sources of suspended solids include urban and agricultural runoff, wastewater discharge, construction activities, and mining activities [41]. Suspended solids can have harmful effects on aquatic ecosystems and human health if they are present in high concentrations [42]. Therefore, it is important to properly manage and reduce the sources of suspended solids in water sources. This can include implementing erosion control measures, reducing fertilizer and pesticide use, properly disposing of wastewater, and minimizing soil disturbance during construction activities.

5. CONCLUSIONS

In the Altınapa Reservoir Watershed, a total of 6018 people live in six little settlements. Agricultural activities and animal husbandry practices as well as wastewater discharges have impacts on the water quality of Altınapa Reservoir and the streams in the basin. In this study, the water quality of Meram Stream, which feeds the Altınapa Reservoir, was monitored in terms of major water quality parameters and pesticides for 1 year in the 2020-2021 period.

All water samples had pH values between 7.8 and 8.4 and conductivity values between 315 and 644 µS/cm. The TOC, nitrogen, and phosphorus species were used to evaluate the organic load in the basin. The continuous inflow of organic matter into the reservoir and the degradation of waste organics accumulated in the sediment over time resulted in a higher organic load at reservoir effluent than Meram Stream. The values of UV_{254} and SUVA of the water samples indicated that the organic compounds in the water source are hydrophilic and aliphatic. In contrast to the TOC values, the TN concentration was found to be lower at the reservoir effluent than at the waters from monitoring stations on Meram Stream. While nitrite was not found in all water samples, nitrate levels ranged from 0.01 to 4.87 mg/L throughout the year. Except for August and September 2020, total phosphorus and phosphate were not detected in the water samples. TSS levels in all samples were observed to be in the range of 2-98 mg/L.

The pesticide screenings revealed a total of 71 pesticides at various stations and seasons, although their concentrations were not higher than the EQSs. 8 of these pesticides were insecticides, 5 of them were fungicides, 4 of them were herbicides, 1 of them was an acaricide and 1 of them was a pesticide synergist.

Significant positive linear associations between conductivity and nitrate and TN were observed. Similar to that, there was a strong positive linear association between nitrate and TN.

Acknowledgments

This study was supported by the Scientific and Technological Research Council of Türkiye (Project No: 118Y402).

REFERENCES

[1] E.T. Aisien, E. Gbegbaje-Das II and F.A. Aisien. Water quality assessment of river Ethiope in the Niger-delta coast of Nigeria. Electronic Journal of Environmental, Agricultural & Food Chemistry. 9 (11), 1739-1745, 2010.

[2] O.A.A. Eletta. Water quality monitoring and assessment in a developing country. Water Quality Monitoring and Assessment, IntechOpen.**:** 481-494, 2012.

[3] J.O. Ighalo and A.G. Adeniyi. A comprehensive review of water quality monitoring and assessment in Nigeria. Chemosphere. 260, 2020.

[4] C.J. Vorosmarty, P.B. McIntyre, M.O. Gessner, D. Dudgeon, A. Prusevich, P. Green, S. Glidden, S.E. Bunn, C.A. Sullivan, C.R. Liermann and P.M. Davies. Global threats to human water security and river biodiversity Nature. 468 (7321), 334-334, 2010.

[5] R. Reservoiro and P. Icka. Evaluation of Water Quality Index for Drinking Water. Pol J Environ Stud. 22 (4), 1045-1051, 2013.

[6] Y.M. Zhang, J. Chen, L.Q. Wang, Y.L. Zhao, P. Ou and W.L. Shi. Establishing a method to assess comprehensive effect of gradient variation human health risk to metal speciation in groundwater. Environ Pollut. 241, 887-899, 2018.

[7] S.T. Glassmeyer, E.T. Furlong, D.W. Kolpin, A.L. Batt, R. Benson, J.S. Boone, O. Conerly, M.J. Donohue, D.N. King, M.S. Kostich, H.E. Mash, S.L. Pfaller, K.M. Schenck, J.E. Simmons, E.A. Varughese, S.J. Vesper, E.N. Villegas and V.S. Wilson. Nationwide reconnaissance of contaminants of emerging concern in source and treated drinking waters of the United States. Sci Total Environ. 581, 909-922, 2017.

[8] R. Troger, P. Klockner, L. Ahrens and K. Wiberg. Micropollutants in drinking water from source to tap - Method development and application of a multiresidue screening method. Sci Total Environ. 627, 1404-1432, 2018.

[9] P.A. Neale, C. Feliers, L. Glauch, M. König, C. Lecarpentier, R. Schlichting, S. Thibert and B.I. Escher. Application of in vitro bioassays for water quality monitoring in three drinking water treatment plants using different treatment processes including biological treatment, nanofiltration and ozonation coupled with disinfection. Environmental Science: Water Research & Technology. 6 (9), 2444-2453, 2020.

[10] R. Miniero, V. Abate, G. Brambilla, E. Davoli, E. De Felip, S.P. De Filippis, E. Dellatte, S. De Luca, R. Fanelli, E. Fattore, F. Ferri, I. Fochi, A.R. Fulgenzi, N. Iacovella, A.L. Iamiceli, D. Lucchetti, P. Melotti, I. Moret, R. Piazza, A. Roncarati, A. Ubaldi, S. Zambon and A. Di Domenico. Persistent toxic substances in Mediterranean aquatic species. Sci Total Environ. 494, 18-27, 2014.

[11] C. Teodosiu, A.F. Gilca, G. Barjoveanu and S. Fiore. Emerging pollutants removal through advanced drinking water treatment: A review on processes and environmental performances assessment. J Clean Prod. 197, 1210-1221, 2018.

[12] EU (2013). Directive 2013/39/EC of the European Parliament and of the Council of 12 August 2013 Amending Directives 2000/60/EC and 2008/105/EC as Regards Priority Substances in the Field of Water Policy Text with EEA Relevance Off J L. E. Union, European Union. 226, pp. 1-17.

[13] A.R. Ribeiro, O.C. Nunes, M.F.R. Pereira and A.M.T. Silva. An overview on the advanced oxidation processes applied for the treatment of water pollutants defined in the recently launched Directive 2013/39/EU. Environ Int. 75, 33-51, 2015.

[14] MoFWW (2015). Ministry of Forest and Water Works (MoFWW). Surface Water Quality Management. Ankara, Turkey, Official Gazette. 29327.

[15] MoAF (2019). Ministry Of Agriculture and Forestry (MoAF). Regulation on the Quality and Treatment of Drinking Water Supply. Ankara, Turkey, Official Gazette. 30823.

[16] B. Selek. Assessment of Surface Drinking Water Resources of Turkey in Terms of Water Quality Standards. J Water Chem Techno+. 42 (5), 415-426, 2020.

[17] O. Canli, E.O. Olgun, B. Guzel and M. Kaplan. Sensitive and accurate determination of 168 micropollutants including pharmaceuticals and pesticides in surface water and wastewater samples with direct injection using jet stream ESI LC-MS/MS. Int J Environ an Ch, 2022.

[18] S.M. Emadian, F.O. Sefiloglu, I.A. Balcioglu and U. Tezel. Identification of core micropollutants of Ergene River and their categorization based on spatiotemporal distribution. Sci Total Environ. 758, 2021.

[19] M. Yavuz, M. Oggioni, U. Yetis and F.B. Dilek. Biocides in drinking water system of Ankara, Turkey. Desalin Water Treat. 53 (12), 3253-3262, 2015.

[20] F. Ustaoglu, Y. Tepe and B. Tas. Assessment of stream quality and health risk in a subtropical Turkey river system: A combined approach using statistical analysis and water quality index. Ecol Indic. 113, 2020.

[21] R.O. Strobl and P.D. Robillard. Network design for water quality monitoring of surface freshwaters: A review. J Environ Manage. 87 (4), 639-648, 2008.

[22] APHA/AWWA/WEF (2012). Standard Methods for the Examination of Water and Wastewater, 20th Edition. APHA, AWWA and WEF. Washington, DC, American Public Health Association.

[23] THOM. Turkish Ministry of Health (TMOH), Regulation Concerning Water Intended for Human Consumption, Official Gazette, No. 25730, Ankara, Turkey (2005).

[24] R. Mert, S. Bulut and K. Solak. Investigation of some physical and chemical properties of Apa Reservoir Lake (Konya). Afyon Kocatepe University Journal of Science and Engineering. 2, 1-10, 2008.

[25] B.Y. Öztürk and C. Akköz. Investigation of water quality of Apa Reservoir Lake (Çumra-Konya) and according to the evaluation of PCA. Biodicon. 7 (2), 136-147, 2014.
[26] M. Diri. Monitoring Alteration of The Konya Closed Basin's Surface Water Quality. MSc Thesis (In Turkish), Necmettin Erbakan University, 2018.
[27] M. Kitis, T. Karanfil, J.E. Kilduff and A. Wigton. The reactivity of natural organic matter to disinfection byproducts formation and its relation to specific ultraviolet absorbance. Water Sci Technol. 43 (2), 9-16, 2001.
[28] R.A. Al Dwairi, K.M. Ibrahim and H.N. Khoury. Potential use of faujasite-phillipsite and phillipsite-chabazite tuff in purification of treated effluent from domestic wastewater treatment plants. Environ Earth Sci. 71 (12), 5071-5078, 2014.
[29] A. Matilainen, M. Vepsalainen and M. Sillanpaa. Natural organic matter removal by coagulation during drinking water treatment: A review. Adv Colloid Interfac. 159 (2), 189-197, 2010.
[30] Y. Hashempour, M. Nasseri, A. Mohseni-Bandpei, S. Motesaddi and M. Eslamizadeh. Assessing vulnerability to climate change for total organic carbon in a system of drinking water supply. Sustain Cities Soc. 53, 101904, 2020.
[31] N. Ates, M. Kitis and U. Yetis. Formation of chlorination by-products in low-SUVA surface waters: Correlations with SUVA and differential UV spectroscopy. Abstr Pap Am Chem S. 233, 416-416, 2007.
[32] S. Faixo, N. Gehin, S. Balayssac, V. Gilard, S. Mazeghrane, M. Haddad, G. Gaval, E. Paul and J.C. Garrigues. Current trends and advances in analytical techniques for the characterization and quantification of biologically recalcitrant organic species in sludge and wastewater: A review. Anal Chim Acta. 1152, 2021.
[33] J.K. Edzwald and J.E. Tobiason. Enhanced coagulation: US requirements and a broader view. Water Sci Technol. 40 (9), 63-70, 1999.
[34] S. Lee and J. Park. Identification of Dissolved Organic Matter Origin Using Molecular Level Analysis Methods. Water-Sui. 14 (9), 2022.
[35] S.P. Gorde and M.V. Jadhav. Assessment of water quality parameters: a review. International Journal of Engineering Research and Applications 3(36), 2029-2035, 2013.
[36] A. Marandi, M. Polikarpus and A. Joeleht. A new approach for describing the relationship between electrical conductivity and major anion concentration in natural waters. Appl Geochem. 38, 103-109, 2013.
[37] C.L. Tang, Z.Q. Zhang and X.N. Sun. Effect of common ions on nitrate removal by zero-valent iron from alkaline soil. J Hazard Mater. 231, 114-119, 2012.
[38] M.A. Sanchez-Monedero, A. Roig, C. Paredes and M.P. Bernal. Nitrogen transformation during organic waste composting by the Rutgers system and its effects on pH, EC and maturity of the composting mixtures. Bioresource Technol. 78 (3), 301-308, 2001.
[39] N. Akhtar, M.I.S. Ishak, S.A. Bhawani and K. Umar. Various Natural and Anthropogenic Factors Responsible for Water Quality Degradation: A Review. Water-Sui. 13 (19), 2021.
[40] R. Bhateria and D. Jain. Water quality assessment of lake water: a review. Sust Wat Resour Man. 2 (2), 161-173, 2016.
[41] N. Khatri and S. Tyagi. Influences of natural and anthropogenic factors on surface and groundwater quality in rural and urban areas. Front Life Sci. 8 (1), 23-39, 2015.
[42] G.S. Bilotta and R.E. Brazier. Understanding the influence of suspended solids on water quality and aquatic biota. Water Res. 42 (12), 2849-2861, 2008.

Energy, Environment and Storage

Journal Homepage: www.enenstrg.com

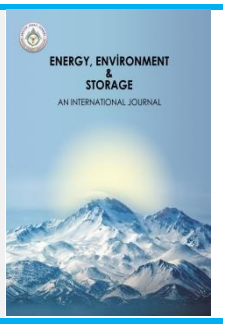

NUMERICAL INVESTIGATION OF NATURAL CONVECTION IN A RECTANGULAR CAVITY BY CFD CODES

Evrim ÖZRAHAT[1*], Mehmet TOPRAK[2], Sebahattin ÜNALAN [3]

[1]*Kayseri University Bünyan Vocational School, https://orcid.org/0000-0002-6912-9633*

[2]*Erciyes University, Institute of Sciences, https://orcid.org/0009-0008-1396-2416*

[3]*Erciyes University, Engineering Faculty, https://orcid.org/0000-0002-5605-2614*

ABSTRACT. In this study natural convection in air-filled rectangular cavity is studied numerically by two commercial CFD codes. Numerical simulations are carried out for air and water for different aspect ratios and wall temperatures. Calculations are compared with experimental correlations in the literature and with each other. Calculation time and mesh number are the main parameters considered in this study. According to the numerical results SIMCENTER FLOEFD is an effective CFD code as ANSYS FLUENT and gives accurate results for this type of problems.

Keywords: Natural Convection, Conjugate Heat transfer, CFD Codes, Rectangular cavity.

Article History: Received 20.09.2023; Accepted:29.09.2023; Available online:30.09.2023
Doi: https://doi.org/1052924/EFIJ8822

1. INTRODUCTION

Natural convection in a cavity occurs in many living areas Heating cooling in a room or heat transfer in a double pane window or heat transfer in an air-filled brick can be examples of natural convection in daily life. So, researchers are interested in understanding this phenomenon. Frederick [1], carried out a numerical study of two-dimensional natural convection of air in rectangular, differentially heated cavities. For three Rayleigh numbers the aspect ratio S was varied. It was found that heat transfer between the active walls has a maximum at each Rayleigh number, which is located at values of S between 1 and 2. The aspect ratio for which the maximum heat transfer occurs is determined by the process of transition from a shallow cavity regime to a slender cavity regime.

Manz [2] investigated heat transfer by the natural convection of air layers within vertical, rectangular cavities with aspect ratios (A) of 20, 40 and 80 in relation to applications in building facade elements, such as insulating glazing units, double-skin facades, doors, etc. using a computational fluid dynamics (CFD) code. Boundary conditions were assumed to be isothermal hot and cold wall, and zero heat flux at bottom and top cavity surfaces. Rayleigh numbers were between 1000 and 10^6, i.e., flow was either laminar or turbulent, and a conduction, transition or boundary layer regime was applied. His study improved the starting position for future applications of the code to more complex cases of facade elements, where less or even no experimental data are available in literature. Ganguli at all [3], performed independent CFD simulations in order to predict the variation in heat transfer coefficient setup by natural convection for various tall slender vertical geometries with varying gap widths and temperature differences covering the ranges reported in the literature. A good agreement of Nusselt number (±10%) has been found between the CFD predictions and the literature data. Bahlaoui at all [4], reported numerical results of mixed convection and surface radiation within a horizontal ventilated cavity heated from below and provided with an adiabatic thin partition on the heated surface. Air, a radiatively transparent medium, is considered to be the cooling fluid. Mahdavi at all [5], studied laminar natural convection in a rectangular cavity with three different heat transfer fluids: water, ethylene glycol (EG)–water and air experimentally and numerically. The enclosure has a uniform aspect ratio (AR). The EG–water mixture is madeup of 60% EG and 40% water. The main experiments aimedto reach proper thermal boundary conditions for the two differentially heated vertical walls of the cavity. Early experiments revealed that it is hard for the heated and cooled walls to reach a uniform temperature when the cavity is filled with water or EG–water, while a uniform distribution of temperature was achieved when it is simplyfilled with air. Commercial computational fluid dynamics (CFD) software, ANSYS-FLUENT 15, simulated the entiresetup to include two special heat exchangers and the cavitybetween them to investigate all the transport phenomena. The simulation results were in good agreement with

*Corresponding author: evrimozrahat@kayseri.edu.tr

measured data. Cianfrini at all [6], studied natural convection in air-filled rectangular cavities inclined with respect to gravity, so that the heated wall is facing upwards, numerically under the assumption of two-dimensional laminar flow. A computational code based on the SIMPLE-C algorithm is used for the solution of the system of the mass, momentum and energy transfer governing equations. Simulations are performed for height-to-width aspect ratios of the enclosure from 0.25 to 8, Rayleigh numbers based on the length of the heated and cooled walls from 10^2 to 10^7, and tilting angles of the enclosure from 0° to 75°. The existence of an optimal tilting angle is confirmed for any investigated configuration, at a location that increases as the Rayleigh number is decreased, and the height-to-width aspect ratio of the cavity are increased, unless the value of the Rayleigh number is that corresponding to the onset of convection or just higher. Dimensionless correlating equations are developed to predict the optimal tilting angle and the heat transfer performance of the enclosure. Prasopchingchana [7] investigated the effects of cavity aspect ratios and cavity inclination angles to natural convection in a rectangular cavity numerically. Investigation is performed at the Rayleigh number (Ra) equal to 10^4, the cavity aspect ratios from 1 to 50 and the cavity inclination angles from 0 to 180°. Consequently, Heat transfer enhancement or decreasing due to the effects is exposed. In addition, streamline contours in the rectangular cavity are illustrated. Multi-cellular flow figuring on the appropriate conditions is exhibited. A new correlation of the average Nusselt number, the cavity aspect ratio and the cavity inclination angle are formulated at Ra equal to 10^4. Hernández-Castillo at all [8], studied natural convection coupled with radiation numerically in a tall rectangular parallel piped cavity filled with air and constant differentially heated opposite vertical walls. This type of tall cavity is found in walls built with hollow blocks.

Three-dimensional steady state numerical simulations are performed. Numerical models for pure natural convection and natural convection coupled with radiation are validated with experimental results. For pure natural convection, a Nu_c correlation as a function of Ra_W is obtained. A simplified calculation of the total heat transfer, Nu_t, is proposed. Sondur and Mescher [9] explored natural convection of air in a tall rectangular cavity by solutions of the fully compressible transient Navier–Stokes equations in two-dimensional form, without the Boussinesq approximation. A temperature difference is imposed on the two vertical side walls, each isothermal, with the two horizontal boundaries adiabatic. Thermo-physical properties of air, including density, viscosity, thermal conductivity and specific heat, are all variable with temperature. Contrary to the conclusions in most previous numerical studies invoking the Boussinesq approximation, this study finds the instability of the conduction regime to be a traveling wave drifting downward in the cavity. The wave-drift speed is a strong function of the dimensionless wall temperature difference, e, defined as the temperature difference between the vertical walls divided by twice the mean wall temperature. Wave-drift speeds and wave numbers are calculated over a range of e less than 0.5 and Rayleigh numbers less than 9000. The dimensionless temperature difference e is also found to have significant effects on local heat transfer and transient flow structure inside the cavity.

Parallel to the literature findings this study performs numerical analyses with two commercial CFD codes. Also includes the comparison with experimental data from the literature.

2. NUMERICAL MODEL

The 3D rectangular cavity filled with air has 100x100x400 mm dimensions as seen in Figure 1. Boundary conditions were assumed to be isothermal hot and cold wall, and zero heat flux at bottom and top cavity surfaces. Two opposite walls are determined as constant temperature boundary condition at 273 and 283 K. The filling fluid air is assumed as incompressible ideal gas and its thermophysical properties are given in Table 1. The simulation is done for Rayleigh number 10^6 corresponding to the 273 K and 283 K wall temperatures. Gravity is taking into account with boussinesq approximation. Simulations are done both with ANSYS FLUENT [10] and SIMCENTER FLOEFD [11]. For all computations same computer (Intel core i7 4 GPU) is used. Convergence criterion is 10-6 for all parameters. It should be noted that this cavity das an aspect ratio (H/L) equal to 4.

Fig. 1. Rectangular cavity filled with air

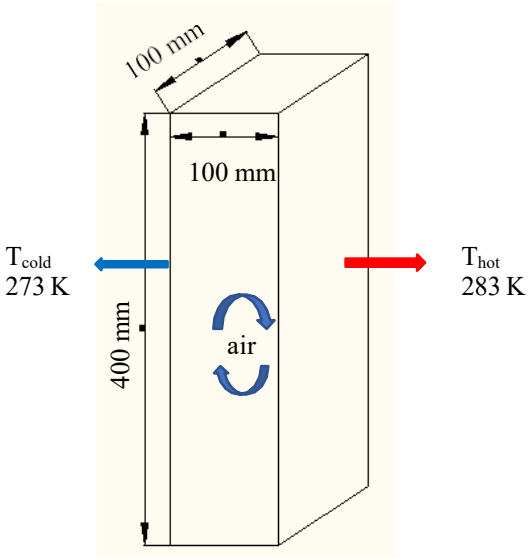

Table 1 Thermophysical properties of air

	A	B	C	D	E
k	62500	422	2:26	0,096	
cp	256000	425	10:08	0,107	
nü	500000	437	18:57	0,109	

For the calculation of Nusselt number inside the cavity following correlation is used [12]:

$$Nu_L = 0,22\left(\frac{Pr}{0,2+Pr^{Ra_L}}\right)^{0,28}\left(\frac{H}{L}\right)^{-1/4} \quad (1)$$

$$2 < \frac{H}{L} < 10$$

$$Pr < 10^5$$

$$10^3 < Ra_L < 10^{10}$$

3. NUMERICAL RESULTS

Both for the mesh independency and comparative study 3 models determined with increasing mesh size (Model-1, Model-2, Model-3 in Table 2). Calculations are done with the same computer with same GPU. Temperature contours inside the cavity at x-y plane at steady state are given in Figure 2 and Figure 3 for both FLUENT and FLOEFD respectively.

Fig. 2. Temperature contours at xy plane inside the cavity (FLUENT)

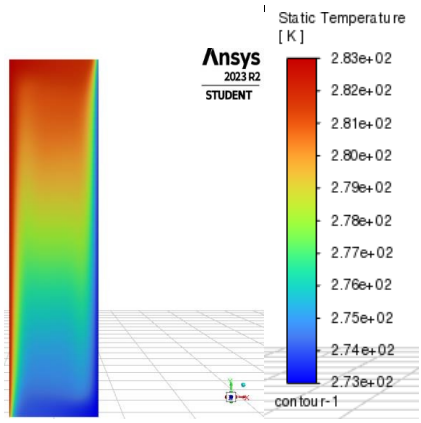

Fig. 3. Temperature contours at xy plane inside the cavity (FLOEFD)

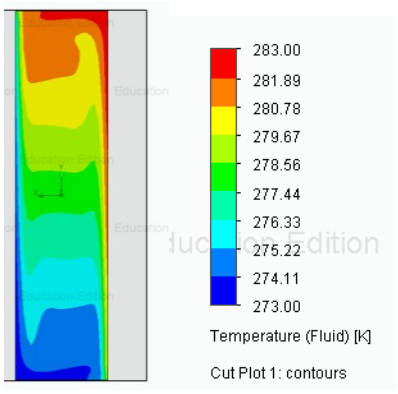

Temperature of the fluid rises when flowing up near the hot wall and declines flowing down the cold wall as expected. Comparison of the models with different parameters are summarized in Table 2. Increasing the mesh size increased the calculation time and iteration number for both codes. Velocity value differs in a negligible level between the Model-2- to Model-3 as 0,2%. For Model 1 calculation time of the two codes is very close. For model 2 calculation time is nearly same too. However, for more mesh numbers (Model-3) calculation time differs significantly.

Table 2 Comparison of numerical simulation results

Ra= 10^6	Ref [12]	ANSYS FLUENT	SIMCENTER FLOEFD
Nusselt Number	7,019	7,541	7,311
Deviation (%)		7,429	4,160

In addition, an important parameter Nusselt number for the air-filled cavity is calculated by equation 1 for Model-3 for both numerical codes and experimental study from the literature [12]. The results are summarized in Table 3. Error values are also calculated and given in Table 3. According to the table numerical results from FLUENT deviates by 7 percent from the experimental value. Numerical results from FLOEFD deviates by 4 percent from the experimental value. These results are proving the acceptability of CFD codes in numerical simulations.

Table 3 Comparison of Nusselt Numbers

Ra= 10^6	Ref[12]	ANSYS FLUENT	SIMCENTER FLOEFD
Nusselt Number	7,019	7,541	7,311
Deviation (%)		7,429	4,160

4. CONCLUSIONS

CFD codes are effective ways for the analyses of natural convection in cavities. Both codes used in this study are acceptable for accurate results. According to the simulation results, results from FLUENT deviates by 7 percent from the experimental value. Numerical results from FLOEFD deviates by 4 percent from the experimental value. These results are proving the acceptability of CFD codes in numerical simulations.

REFERENCES

[1] R. L. FREDERICK, On the aspect ratio for which the heat transfer in differentially heated cavities is maximum. International communications in heat and masstransfer, 26.4: 549-558, 1999.

[2] H. MANZ, Numerical simulation of heat transfer by natural convection in cavities of facade elements. Energy and buildings, 35.3: 305-311, 2003.

[3] A.A. GANGULI, A. B. PANDIT, J.B. JOSHI, CFD simulation of heat transfer in a two-dimensional vertical enclosure. Chemical Engineering Research and Design, 87.5: 711-727,2009.

[4] A. BAHLAOUI, A. RAJI, M. HASNAOUI, M. NAIMI, T. MAKAYSSI., M. LAMSAADI (2009). Mixed convection cooling combined with surface radiation in a partitioned rectangular cavity. Energy Conversion and Management, 50(3), 626-635, 2009.

[5] M. MAHDAVI et al. Experimental and numerical study of the thermal and hydrodynamic characteristics of laminar natural convective flow inside a rectangular cavity with water, ethylene glycol–water and air. Experimental Thermal and Fluid Science, 78: 50-64, 2016.

[6] C. CIANFRINI, et al. Effects of the aspect ratio on the optimal tilting angle for maximum convection heat transfer across air-filled rectangular enclosures differentially heated at sides. Journal of Thermal Science, 26: 245-254, 2017.

[7] U. PRASOPCHINGCHANA, U. Numerical study of natural convection in a rectangular cavity with variation of cavity aspect ratios and cavity inclination angles. In: IOP Conference Series: Materials Science and Engineering. IOP Publishing. p. 012044, 2019.

[8] P. HERNÁNDEZ-CASTILLO, P., J.A. CASTILLO, G. HUELSZ, Heat transfer by natural convection and radiationin three dimensional differentially heated tall cavities. Case Studies in Thermal Engineering, 40: 102529, 2022.

[9] S. SONDUR, A.M. MESCHER, Non-Boussinesq effects on natural convection airflows simulated in a tall rectangular cavity. Numerical Heat Transfer, Part A: Applications, 84.4: 297-314, 2023.

[10] ANSYS FLUENT 2023 STUDENT VERSION https://www.ansys.com/academic/students

[11] SIMCENTER FLOEFD https://resources.sw.siemens.com/en-US/download-computational-fluid-dynamics-simcenter-solid-edge-student

[12] F. Incropera, W. Dewitt, Fundamentals of Heat and Mass Transfer, Wiley, 2004.

Energy, Environment and Storage

Journal Homepage: www.enenstrg.com

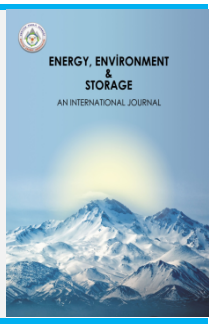

Investigation of Deep Eutectic Solvent Based Super Dielectric Electrolytes for Supercapacitors

Ekrem Akif Yigit[1,3], Yahya Erkan Akansu[2,3*]

[1] *Department of Electronics and Automation, Nigde Omer Halisdemir University, Türkiye*

[2] *Department of Mechanical Engineering, Nigde Omer Halisdemir University, Türkiye*

[3] *Faradx Energy Technologies, Nigde Teknopark, Nigde, Türkiye*

ABSTRACT. This study investigates a new type of electrolyte based on deep eutectic solvents. Choline chloride based deep eutectic solvents were prepared and they were used as base ionic solvents for super dielectric theory. Deep eutectic solvent was mixed with a non-conducting material such as fumed silica, alumina. The mixture shows a super dielectric behavior which is used as electrolyte for electrochemical double layer capacitors also known as supercapacitor. The supercapacitor cells were composed of an electrode, a paper-based separator and this super dielectric electrolyte. The electrode of commercial standard supercapacitor is used first as an electrode. Second an electrode slurry was prepared in order to make custom electrode. Then the performance of both cells was investigated. The specific capacitances of cells were measured and the amount of increase at the capacitances was evaluated. The results showed that up to 14-fold increase of the specific capacitances of the commercial supercapacitor have been achieved. Also, up to 12-fold increase of the specific capacitances of our custom-made cells have been achieved. The charge discharge characteristics and ESR values of the cells confirms that the cells show outperforming properties. Deep eutectic solvents based super dielectric electrolytes are very promising electrolytes for high energy density supercapacitors.

Keywords: *Super Dielectric, Supercapacitor, Equivalent Series Resistance (ESR)*

Article History: Received:18.07.2023; Accepted:28.09.2023; Available online: 30.09.2023
Doi: https://doi.org/1052924/MSKH9311

1. INTRODUCTION

The needs of energy storage systems are increasing rapidly nowadays because of developing mobile systems, electrical vehicles and renewable energy system such as solar and wind power generation facilities. The major energy storage systems still use lead acid and lithium-ion batteries. The problem of existing battery systems such as highly cost, short life, safety and difficult production processes increase the needs of promising energy storage systems. One of the possible alternatives of current battery system is electrochemical double layer capacitors [1,2].

Electrochemical double layer capacitors (EDLCs), also known as supercapacitors or ultracapacitors are the most promising energy storage technology [3]. In EDLCs the charge is electrostatically stored at the electrode and electrolyte interface. These devices can be charged and discharged within seconds. They can give high power (up to 10 kW) and a high cycle life (>500,000). Now, the commercial EDLCs contain activated carbon as active material and electrolytes based on quaternary ammonium salt dissolved in organic solvents (acetonitrile (ACN) or propylene carbonate (PC)). The cell voltage of these EDLCs are 2.3 V and 2.7 V. In order to use EDLCs in today applications, their energy storage capacities need to be improved. The specific energy of EDLCs is defined by the equation E=1/ 2CU2, where C and U are the capacitance and operative voltage of the EDLC, respectively [4-6].

Traditional electrolytes for EDLCs can be generally divided into aqueous, organic, IL and solid- or quasi-solid types [7,8]. The working voltage of a EDLCs is determined by the decomposition of an electrolyte on the electrode surface at high potential. The working voltage of a EDLCs can be raised from 2,3 V to 2.7 V using organic electrolytes instead of aqueous electrolytes. The common working voltage of commercial EDLCs with organic electrolytes is 2.7 V. Because the energy density of a EDLCs is directly proportional to the squared working voltage, the research is focused on developing

*Corresponding author: akansu@ohu.edu.tr

electrolytes with high conductivity, good chemical and thermal stability, and wider electrochemical window. An organic electrolyte is composed of an organic solvent and a supporting electrolyte [9]. The organic solvent must have low volatility, good electrochemical stability and large dielectric constant.

In recent years, as a new type of green electrolyte, Ionic Liquids (IL) has been widely used in EDLCs. IL is featured with wide electrochemical window, relatively high conductivity and ion mobility. Deep Eutectic Solvents (DES) are also a new type of green electrolyte which has wide electrochemical windows as alternative of ILs. DES can be produced cost effectively and easily. Super dielectric materials are also newly proposed subject and getting more interest recently. Their dielectric constant can be between 106-1012 [10].

In the present study, we synthesized a novel deep eutectic solvent-based super dielectric electrolytes and used on both standard commercial and custom-made supercapacitor electrodes to demonstrate its effect. As an outstanding result, the synthesized super dielectric electrolyte exhibited the specific capacitance of up to 14-fold increase for standard commercial supercapacitor electrodes and 12-fold increase for custom made supercapacitor electrodes**.**

2. EXPERIMENTAL

The chemicals choline chloride (ChCl), urea, monoethylene glycol, glycerin, malonic acid, boron nitride and alumina were purchased from Sigma Aldrich, Germany. Fumed silica, xylitol and carboxymethyl cellulose (CMC) were purchased from Introgen, Türkiye and the activated carbon and Styrene-butadiene rubber (SBR) were obtained from Nanografi, Türkiye. The commercial supercapacitors were purchased from Greencap, South Korea. All chemicals were used without further purification.

2.1 Preparation of Deep Eutectic Solvents (DES)

Deep eutectic solvents (DESs) are new class of ionic liquid (IL) because they share a lot of characteristics and properties with ILs [11-15]. DESs contain large, nonsymmetrical ions. They have low lattice energy and low melting points. They are usually obtained by the complexation of a quaternary ammonium salt with a metal salt or hydrogen bond donor. Different type of DESs can be made by using suitable chemicals [16].

The following DESs were prepared by mixing at magnetic stirrer at 80 C about 1 hour. Then they were slowly cooled to room temperature. The molar ratios were used in order to make deep eutectic solvents as $\boldsymbol{ChCl + Urea}$ (1:2); $\boldsymbol{ChCl + Glycerin}$ (1:2); $\boldsymbol{Chcl + MEG}$ (1:2); $\boldsymbol{ChCl + Malonic\ acid}$ (1:2); $\boldsymbol{ChCl + Xylitol}$ (1:2). These are well known DESs and their characterization is available at scientific literature [12-14]. Our interest is to see the super dielectric properties of DESs when they mixed with non-conducting powders.

The electro chemical voltage window of these DESs is given Table 1. The supercapacitor cells are charged according to this table. This EPWs were accepted as a cell voltage but, the real stable cell voltages were below these voltages because of water content in the DESs. DESs contain water since the chemicals that we use are not anhydrous. If the chemicals are anhydrous and the electrolyte is injected in controlled atmosphere, EPWs will be at Table 1. We did not use a controlled atmosphere to see the performance of DESs at open atmosphere.

Table 1: The EAL, ECL and EPWs of ChCl Based DESs [17-19]**.**

DESs	E_{AL} (V)	E_{CL} (V)	EPWs (V)
ChCl + glycerol	–2.21	1.38	3.59
ChCl + urea	–2.75	1.54	4.29
ChCl + MEG	–2.35	1.26	3.61
ChCl+malonic acid	–2.55	1.70	4.25
ChCl+xylitol	–2.67	1.66	4.33

2.2 Preparation of Super Dielectric Electrolyte

Super Dielectric Materials subject is a new theory that can be verified by experimental studies [20-22]. The super dielectric theory was first discovered by Prof. Jonathan Phillips and his friends.

According to theory, any porous, non-conducting material with a liquid containing a high concentration of ionic species will potentially be a Super Dielectric Material (SDM). The dielectric constant of SDM can be measured by making a parallel plate capacitor. The dielectric constant can be obtained from the time constant and this standard equation:

$$\boldsymbol{C = \varepsilon_0\ \varepsilon_R\ A/d}$$

where ε_0 is the permittivity of free space ($8.85 \times 10{-}12$ F/m) and ε_R is the dielectric constant. The area of the plate surface is A and the distance between the two electrode surfaces is d. The measured dielectric constant is between $\boldsymbol{5 \times 109 - 1.2 \times 1011}$ [23].

Different type electrostatic capacitors (EC) were made by super dielectric materials that have energy density greater than 200 J. cm3 [24,25].

According to Super Dielectric Materials theory, the electrolyte is needed to mix with any non-conducting nano powder. Our deep eutectic solvents were mixed with fumed silica for one sample, mixed with boron nitride for second sample. The produced electrolyte has gel like properties. This electrolyte is our new electrolyte for EDLCs. Five different types of DESs and three different types of non-conducting powders were used in order to make 15 different types of super dielectric electrolyte. Table 2. shows these super dielectric electrolytes (Fig. 1).

Table 2. Our new super dielectric electrolytes

DESs	Non conducting powder
ChCl+glycerol	Fumed Silica
ChCl+urea	Fumed Silica
ChCl+MEG	Fumed Silica
ChCl+malonic acid	Fumed Silica
ChCl+xylitol	Fumed Silica
ChCl+glycerol	Boron Nitride
ChCl+urea	Boron Nitride
ChCl+MEG	Boron Nitride
ChCl+malonic acid	Boron Nitride
ChCl+xylitol	Boron Nitride
ChCl+glycerol	Alumina
ChCl+urea	Alumina
ChCl+MEG	Alumina
ChCl+malonic acid	Alumina
ChCl+xylitol	Alumina

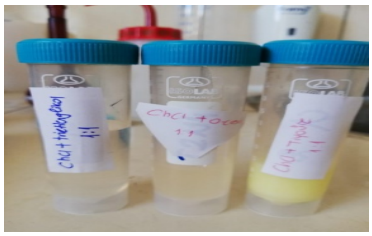

Fig. 1 - Some samples of prepared DESs

2.3. *Fabrication of EDLC cells*

EDLC cells were prepared 2 different methods. First a commercial supercapacitor cell used. Second an electrode was made by electrode slurry.

2.3.1. Using Commercial Cell Electrode

A commercial 2,7V, 500 F supercapacitor as shown in Fig. 2 was disassembled, and its electrode and paper type separator in Fig. 3 were used to fabricate of supercapacitor

Fig. 2 - Disassembled standard commercial supercapacitor

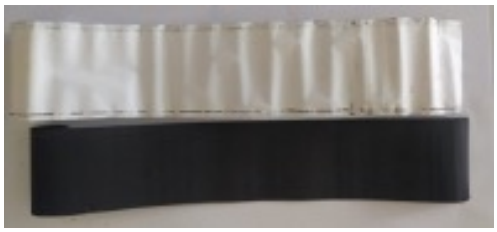

Fig. 3 - The electrode and separator taken from disassembled standard commercial supercapacitor.

First, before disassembling process, its real capacity was measured by ZTE electronic load via PC. Its real capacity was between 380-430 F. The size of the electrode of the cell were measured. It is 4.5 cm x 77 cm. Then the specific capacity was calculated, and it was found 0,32 F/cm2 as expected. In order to compare our results with the commercial cell easily, the electrode was cut 1 cm x 2 cm sizes and a new cell was constructed by using this electrode by using 1 cm x 1 cm of the electrode as shown in Fig. 4.

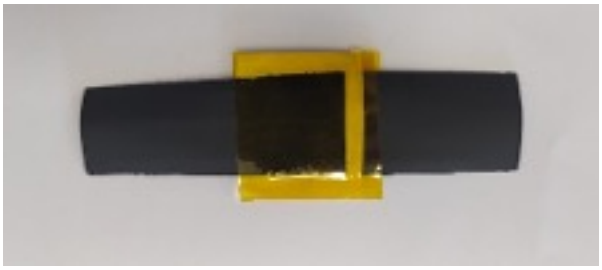

Fig.4 - The finished cell

Then, our deep eutectic solvent based super dielectric electrolyte was injected on two electrode and the paper separator were used and the cell were constructed. Then the cell insulated by Kapton tape. Fig. 5 shows our cell structure used in our measurements.

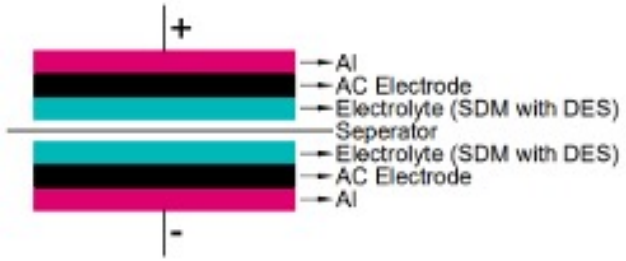

Fig. 5 - Cell structure of the supercapacitor

3. MAKING CUSTOM ELECTRODE:

3.1. Preparation Electrode Slurry

Three items are necessary for making a conductive ink. These are a solvent (water, ethanol, DMF etc.), a binder (water-based adhesive, etc.) and an active ingredient (activated carbon, graphene, a conductive material (carbon black, Super-P etc.) We used the same and common formula that is used at commercial supercapacitors. It is 80% Activated Carbon +10% Conducting Material + %10 Binder. We used activated carbon as active ingredient, graphite powders as conductive material and CMC+SBR mixture as binder. First, 0.25g of CMC added to 50 ml DI water and stirred at magnetic stirrer at 70 C about 1 hour then 0.25g of SBR added slowly into this solution and stirred about 1 hour at 70 C. 8,5g of activated carbon was mixed with 1 g of graphite powder. Then this mixture added to binder (CMC-SBR). The mixture was stirred at

vacuum mixer about 4 hours. Then the electrode slurry was obtained (Fig. 6). The viscosity of the slurry was measured with a digital viscosity meter. The viscosity was adjusted between 4000-5000 cpt by adding more DI water and vacuum mixing.

Fig 6- Electrode slurry and its visual testing on paper.

3.2. Coating Slurry

Copper or aluminium strips were cut to the desired scale. The surface of strip was cleaned with ethanol. The prepared electrode slurry was coated by Dr. Blade on a special Al foil (Fig 7). The coating thickness is 100 □m. Then allowed to dry in an oven at 50 °C about 5 hours.

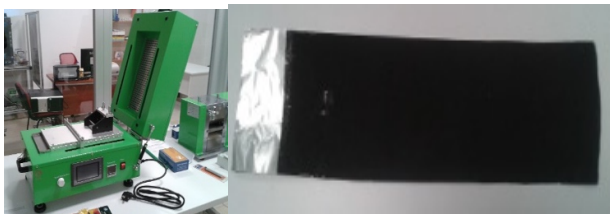

Fig. 7 - Film coating machine with drying oven (TOB-VFC-150) and coated electrode.

3.3. Calendaring Electrode

The coated electrode was processed at hot roll press (Fig. 8). The thickness of active material was reduced to 65 μm. After this process the surface of the electrode became smooth and perfect. Then the electrode was vacuum dried at 60 C about 2 hours in order to remove the water content. Then the electrode was cut by a mechanical blade under hydraulic press.

Fig. 8 - Hot roll press machine (TOB-JS100L) and prepared electrode.

3.4. Making Cells

To make a supercapacitor, the cut electrodes were stacked with a NKK 4030 type separator then our electrolyte was added. The cell was insulated by a Captone tape. One of made supercapacitors is shown in Fig. 9. In order to understand the standard cell capacity of our electrode, 3M KOH solution was used as electrolyte first. Then, its specific capacitance was measured. It is 0.4 F/cm^2

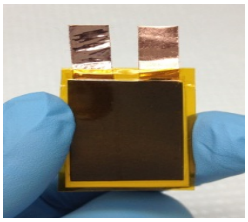

Fig. 9 - Finished Cell

3.5. Instrumentation

The ESR of the cell were measured by MESR-100 model digital ESR meter, 100 kHz in circuit test. The capacity of the cell was measured by charging and discharging the cell. The cell was charged by a DC power supply up to cell voltage of our electrolyte and the cell were discharged by ZTE electronic load via PC under constant current. According to C=Dt*I/DV equation, the cell capacity was calculated. This process was repeated several times. It showed that, the cells are EDLCs but its discharge voltage characteristic is a little bit different. According to SDM theory, the discharge voltage is effective below 1V. Fig. 10 shows a discharge graph of ChCl + MEG + Boron Nitride Sample.

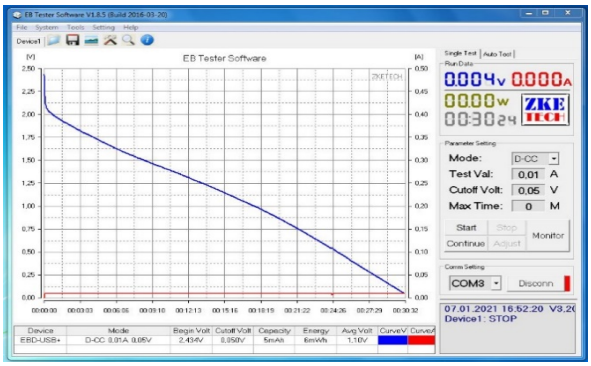

Fig. 10 - ChCl + MEG + Fumed Silica Cell.

The calculated Cell capacity is about 8,77 F for 2 cm^2 cell. The specific capacitance is 4,39 F/cm^2

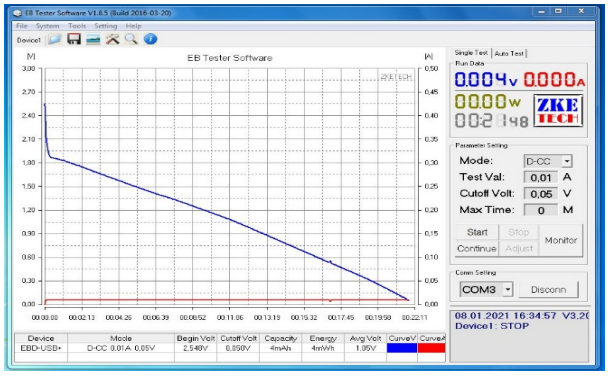

Fig. 11 - *ChCl + MEG + Boron Nitride* Cell.

The calculated cell capacity is 7,07 F for 2 cm2 cell. The specific capacitance is 3,54 F/cm2 for commercial supercapacitor electrode cell (Table 3). The best one is ChCl-MEG- Fumed Silica cell, it has about 14-fold increased capacity over KOH electrolyte. Table 4 shows specific capacity of custom-made supercapacitor cells. The best one is ChCl-MEG cell, it has about 12-fold increased capacity over KOH electrolyte. ChCl-MEG shows the best performance because of low viscosity and high conductivity of MEG.

Table 3. Specific capacity of commercial supercapacitor electrode made cells.

Electrolyte Type	Specific Capacitance (F/cm2)
ChCl+glycerol - Fumed Silica	2,90
ChCl+urea - Fumed Silica	3,11
ChCl+MEG - Fumed Silica	3,54
ChCl+malonic acid - Fumed Silica	2,59
ChCl+xylitol - Fumed Silica	2.33
ChCl+glycerol - Boron Nitride	2.03
ChCl+urea - Boron Nitride	2,09
ChCl+MEG - Boron Nitride	3,25
ChCl+malonic acid - Boron Nitride	2.17
ChCl+xylitol - Boron Nitride	1,78
ChCl+glycerol - Alumina	2.07
ChCl+urea - Alumina	1.98
ChCl+MEG - Alumina	2,60
ChCl+malonic acid - Alumina	1.55
ChCl+xylitol - Alumina	1.67

Table 4. Specific capacity of Custom-made supercapacitor cells

Electrolyte Type	Specific Capacitance (F/cm2)
ChCl+glycerol - Fumed Silica	3,64
ChCl+urea -Fumed Silica	3,21
ChCl+MEG- Fumed Silica	4,27
ChCl+glycerol -Boron Nitride	3.73
ChCl+urea -Boron Nitride	3,69
ChCl+MEG -Boron Nitride	4,77

4. RESULTS AND DISCUSSION

ESR values of the cell were measured with a digital ESR meter. CV measurements were taken with a cyclic voltmeter device.

4.1. Electrochemical properties of EDLCs cells

ESR Values of Some Capacitors

470 uF 16 V standard capacitor 11 mΩ

10F 2.7 V supercapacitor 30 mΩ

ESR value of commercial supercapacitor cell is 30 mΩ

Table 5. ESR values of same samples (commercial cell electrode)

DESs - Non conducting powder	ESR(Ohm)
ChCl+glycerol - Fumed Silica	44,6
ChCl+urea - Fumed Silica	34,2
ChCl+MEG - Fumed Silica	18,6
ChCl+malonic acid - Fumed Silica	36,4
ChCl+xylitol - Fumed Silica	46,1
ChCl+glycerol - Boron Nitride	43,2
ChCl+urea - Boron Nitride	33,7
ChCl+MEG - Boron Nitride	16,4
ChCl+malonic acid - Boron Nitride	34,5
ChCl+xylitol - Boron Nitride	48,7
ChCl+glycerol - Alumina	45,0
ChCl+urea - Alumina	37,4
ChCl+MEG - Alumina	22,2
ChCl+malonic acid - Alumina	33,9
ChCl+xylitol - Alumina	45,1

As seen Table 5, ChCl + MEG samples have lower ESR because of the viscosity. Therefore, ChCl + MEG based electrolytes were studied. In order to understand our cell shows a real EDLC characteristics, a CV measurement weas made. Fig. 12 shows that our cell shows a EDLC characteristics.

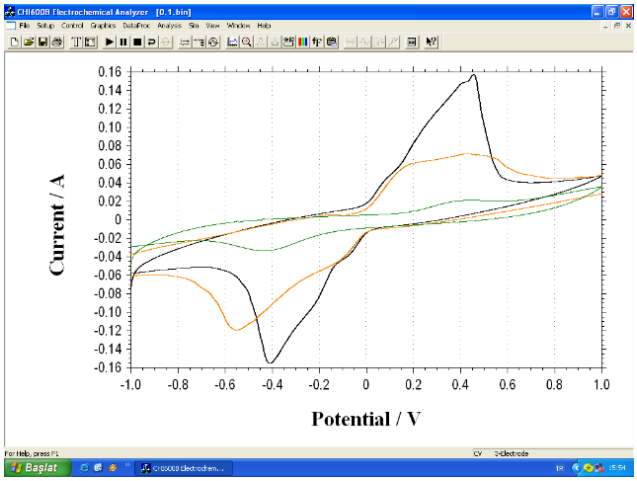

Fig. 12 - A sample from CV measurement of our cells (on commercial supercapacitor electrode) (8 Black: ChCl + MEG with Fumed Silica, Red: ChCl + glycerol with Fumed Silica, Green: ChCl + urea with Fumed Silica).

Nyquist plots of ChCl-MEG type DES electrolyte - fumed silica cell is shown in Fig.13. It shows the behaviour of an ideal capacitor at straight line parallel to the imaginary axis.

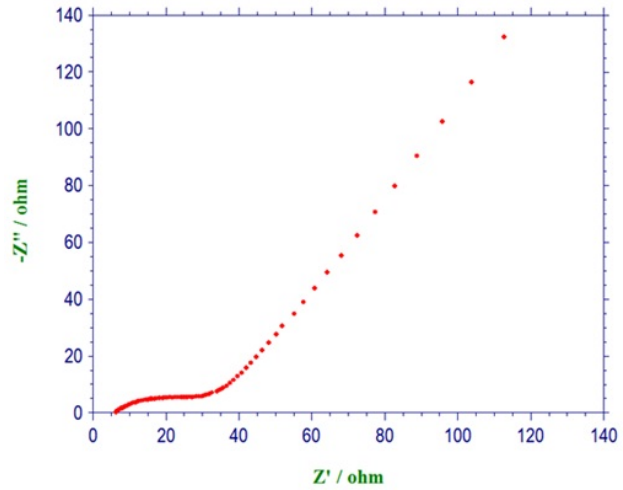

Fig. 13 - Nyquist plots of ChCl-MEG -Fumed silica electrolyte cell (on commercial supercapacitor electrode).

5. CONCLUSIONS

The commercial supercapacitor cells have 0,32 F/cm2 specific capacitance and it gives 4,7 Wh/kg energy density.

Our ***ChCl + MEG + Fumed Silica cell*** (on commercial supercapacitor electrode) showed 4,54 F/cm2 specific capacitance and it is about 14 fold increase and ChCl +MEG +Boron Nitride cell (on custom made supercapacitor electrode) showed 3,54 F/cm2 and it is about 12 fold increase. The capacity increase comes from high dielectric constant of ChCl-MEG and non-conducting powder mixture.

The energy densities will be less than 12-14-fold since the electrolyte volume is bigger than the standard electrolytes. The electrolyte contains fumed silica and boron nitride. They increase the volume of the cells.

Deep eutectic solvent based super dielectric electrolyte works both commercial supercapacitor cells electrode and custom made cells electrode. But ESR values are very big because of high viscosity and content of nonconducting powders in electrolyte.

ChCl + Glycerol and ChCl + Urea showed worse ESR because of viscosity. By adding other chemicals to DESs, ESR can be lowered.

CV plot and Nyquist plot confirm the capacitive behaviour of the cells.

Specific capacitance increases with lower viscosity. ChCl-MEG gives the highest specific capacitance because of low viscosity and high ionic conductivity.

Deep eutectic solvent based super dielectric electrolytes are very promising for making high energy density supercapacitors at their usage in hydrogen energy systems.

Acknowledgements

This study is supported by KOSGEB Research & Development and Innovation Support Program (Project No:1723948).

REFERENCES

[1] Mondal S, Rana U, Malik S. Reduced graphene oxide/Fe3O4/ polyaniline nanostructures as electrode materials for an allsolid- state hybrid supercapacitor. J. Physical Chemistry C 2017; 121:7573-7583. https://doi: 10.1021/acs.jpcc.6b10978

[2] Dalvand, S., Khoushab, Z., Mousavi-Khoshdel, S. M., Ghafuri, H., Zand, H. R. E., & Omidvar, M. (2023). Graphene oxide@ Fe3o4@ Tungstate modified ionic liquid as a novel electrode material for high-performance supercapacitor. International Journal of Hydrogen Energy, 48(27), 10098-10107. https://doi.org/10.1016/j.ijhydene.2022.12.026

[3] Libich J, Máca J, Vondrák J, Čech O, Sedlaříková M. Supercapacitors: Properties and applications. Journal of Energy Storage 2018; 17:224-227. https://doi.org/10.1016/j.carbon.2022.08.091

[4] Hashim MAB, Sa'adu L, Dasuki KA. Supercapacitors based on activated carbon and polymer electrolyte. International Journal of Sustainable Energy and Environmental Research 2012;1(1):1-6.

[5] Horn M, MacLeod J, Liu M, Webb J, Motta N. Supercapacitors: a new source of power for electric cars?. Economic Analysis and Policy 2019; 61:93-103. https://doi.org/10.1016/j.eap.2018.08.003

[6] Ye W, Wang H, Ning J, Zhong Y, Hu Y. New types of hybrid electrolytes for supercapacitors. Journal of Energy Chemistry 2021;57:219-232. https://doi.org/10.1016/j.jechem.2020.09.016

[7] Mirzaeian M, Abbas Q, Ogwu A, Hall P, Goldin M, Mirzaeian M, Jirandehi HF. Electrode and electrolyte materials for electrochemical capacitors. International Journal of Hydrogen Energy 2017;42(40):25565-25587. https://doi.org/10.1016/j.ijhydene.2017.04.241

[8] Obreja VV, Dinescu A, Obreja AC. Activated carbon based electrodes in commercial supercapacitors and their performance. Int. Rev. Electr. Eng 2010;5(1):272-281.

[9] Yanik MO, Yigit EA, Akansu YE, Sahmetlioglu E. Magnetic conductive polymer-graphene nanocomposites-based supercapacitors for energy storage. Energy, 2017;138:883-889. https://doi.org/10.1016/j.energy.2017.07.022

[10] Fromille S, Phillips J. Super dielectric materials. Materials 2014;7(12):8197-8212. https://doi.org/10.3390/ma7128197

[11] Kowsari E. High-performance supercapacitors based on ionic liquids and a graphene nanostructure. In Ionic Liquids-Current State of the Art 2015; IntechOpen. http://dx.doi.org/10.5772/59201

[12] Garcia G, Aparicio S, Ullah R, Atilhan M. Deep eutectic solvents: physicochemical properties and gas separation applications. Energy & Fuels 2015;29(4):2616-2644. https://doi.org/10.1021/ef5028873

[13] Smith EL, Abbott AP, K. Ryder S | Chem. Rev. Deep eutectic solvents (DESs) and their applications. Chemical reviews 2014;114(21):11060-11082. dx.doi.org/10.1021/cr300162p

[14] Li, G., Yang, H., Zuo, D., Xu, J., & Zhang, H. (2021). Deep eutectic solvent-based supramolecular gel polymer electrolytes for high-performance electrochemical double layer capacitors. International Journal of Hydrogen Energy, 46(24), 13044-13049. https://doi.org/10.1016/j.ijhydene.2021.01.158

[15] Puttaswamy R, Mondal C, Mondal D, Ghosh D. An account on the deep eutectic solvents-based electrolytes for rechargeable batteries and supercapacitors. Sustainable Materials and Technologies 2022;33:e00477. https://doi.org/10.1016/j.susmat.2022.e00477

[16] Gurkan B, Squire H, Pentzer E. Metal-free deep eutectic solvents: Preparation, physical properties, and significance. The Journal of Physical Chemistry Letters 2019;10(24):7956-7964. https://doi.org/10.1021/acs.jpclett.9b01980

[17] Ong SP, Andreussi O, Wu Y, Marzari N, Ceder G. Electrochemical windows of room-temperature ionic liquids from molecular dynamics and density functional theory calculations. Chemistry of Materials 2011;23(11):2979-2986. https://doi.org/10.1021/cm200679y

[18] Kadhom MA, Abdullah GH, Al-Bayati N. Studying two series of ternary deep eutectic solvents (choline chloride–urea–glycerol) and (choline chloride–malic acid–glycerol), synthesis and characterizations. Arabian Journal for Science and Engineering 2017;42(4):1579-1589. https://doi.org/10.1007/s13369-017-2431-4

[19] Li Q, Jiang J, Li G, Zhao W, Zhao X, Mu T. The electrochemical stability of ionic liquids and deep eutectic solvents. Science China Chemistry 2016; 59:571-577. https://doi.org/10.1007/s11426-016-5566-3

[20] Fromille S, Phillips J. Super dielectric materials. Materials 2014;7(12):8197-8212. https://doi.org/10.3390/ma7128197

[21] Cortes FJQ, Phillips J. Novel materials with effective super dielectric constants for energy storage. Journal of Electronic Materials, 2015;44:1367-1376. https://doi.org/10.1007/s11664-015-3641-8

[22] Zhong M, Tang QF, Zhu YW, Chen XY, Zhang ZJ. An alternative electrolyte of deep eutectic solvent by choline chloride and ethylene glycol for wide temperature range supercapacitors. Journal of Power Sources, 2020;452:227847. https://doi.org/10.1016/j.jpowsour.2020.227847

[23] Phillips J. Novel superdielectric materials: aqueous salt solution saturated fabric. Materials 2016;9(11): 918. https://doi.org/10.3390/ma9110918

[24] Cortes FJQ, Phillips J. Tube-super dielectric materials: Electrostatic capacitors with energy density greater than 200 J· cm− 3. Materials 2015;8(9):6208-6227. https://doi.org/10.3390/ma8095301

[25] Gandy J, Cortes FJQ, Phillips J. Testing the tube super-dielectric material hypothesis: Increased energy density using NaCl. Journal of Electronic Materials 2016; 45:5499-5506. https://doi.org/10.1007/s11664-016-4843-4

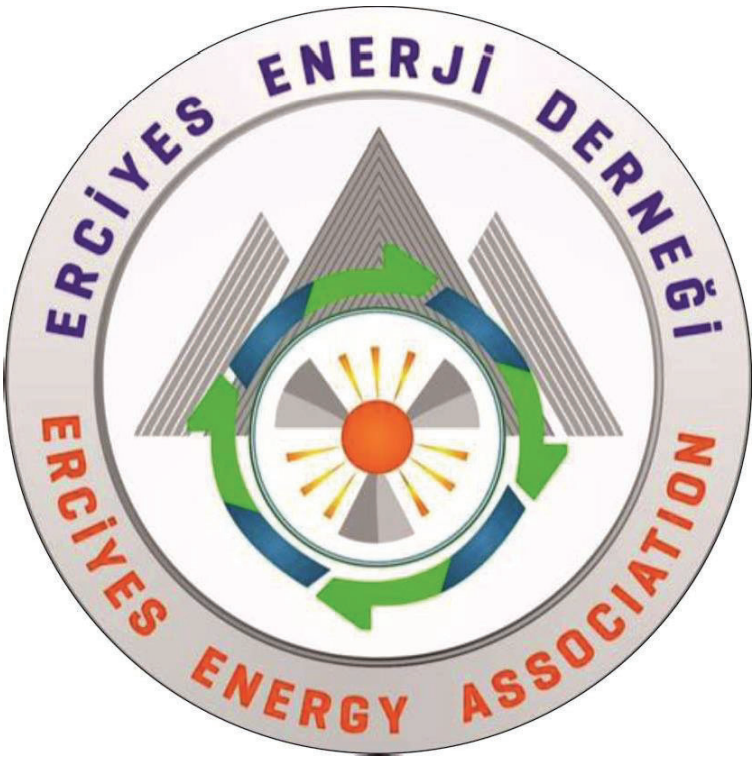

Founded in 2016, our association is open to everyone who is interested in energy and devoted to sustainability.

ERCIYES ENERGY ASSOCIATION